# Fluorescence-guided cancer surgery

using clinical available and innovative tumor-specific contrast agents

Quirijn Tummers

Fluorescence-guided cancer surgery

using clinical available and innovative tumor-specific contrast agents

Quirijn Tummers

Fluorescence-guided cancer surgery

using clinical available and innovative tumor-specific contrast agents

Proefschrift

ter verkrijging van
de graad van Doctor aan de Universiteit Leiden,
op gezag van Rector Magnificus prof. mr. C.J.J.M. Stolker,
volgens besluit van het College voor Promoties
te verdedigen op woensdag 11 oktober 2017
klokke 15:00 uur

door

Quirijn Robert Johannes Guillaume Tummers

geboren te Leiden
in 1986

TABLE OF CONTENTS

Chapter 1

GENERAL INTRODUCTION
AND THESIS OUTLINE

Over the past decades multiple preoperative imaging modalities have become available that have the ability to non-invasively detect tumors, improve accuracy of staging and preoperative planning, and can identify sentinel lymph nodes (SLN) of various tumor types or vital structures[1;2].

However, during surgery, translation of these preoperative obtained images can be challenging due to altering in body position and tissue manipulation by the surgeon. Therefore surgeons mainly have to rely on their eyes and hands to identify structures that need to be resected or spared. Distinction between malignant and healthy tissue based on inspection and palpation can often be very difficult. Therefore, incomplete resections (R1) still occur in a significant number of cancer patients. In breast cancer for example, the number of patients with positive resection margins ranges from 11% to 46% after resection of the primary tumor[3]. Because complete resections are the cornerstone of curative cancer surgery, this leads to unfavorable patient outcomes, resulting in additional surgical procedures, delays in adjuvant treatment, increased morbidity rates and increased healthcare costs, and most likely decreased quality of life.

Next to imaging solitary tumors, improving the detection of metastasized disease could also improve patient outcomes. In metastasized ovarian cancer for example, identification of malignant lesions can improve staging procedures and facilitate treatment decisions between primary surgery and systemic therapy. Moreover, it can increase the number of optimal debulking procedures resulting in prolonged survival[4-6]. In metastasized uveal melanoma, intraoperative identification of hepatic metastases can assist in selecting patients that will benefit from resection, and expedite adjuvant systemic therapies for patients with miliary disease[7-9].

Moreover, minimally invasive procedures are increasingly applied in daily clinical practice, limiting the possibility to palpate tissue and making the visual inspection more important for identification of malignant tissue and normal structures. Therefore, there is a clear unmet need for imaging modalities that facilitate the detection of cancer tissue and vital structures in real time during the surgical procedure.

Fluorescence imaging
Fluorescence imaging is an innovative optical imaging technique that can assist in the intraoperative identification of tumor tissue, SLNs, and vital

structures[10]. This technique, like medical imaging techniques in general, is based on the ability to create a contrast ratio between the tissue of interest and its surrounding normal tissue.
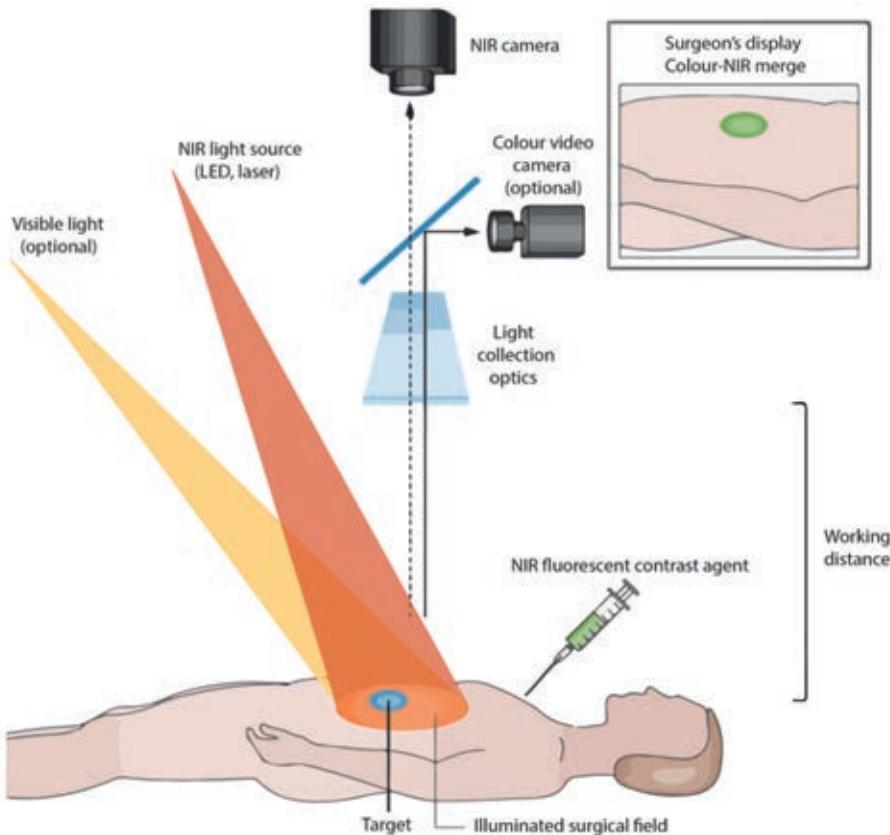
Figure 1. NIR fluorescence imaging

NIR fluorescent contrast agents are administered intravenously. During surgery, the agent is visualized using a NIR fluorescent imaging system of the desired form factor (above the surgical field for open surgery or encased within minimal invasive surgery). All systems must have adequate NIR excitation light, collection optics, filter sets and a camera sensitive to NIR fluorescent emission light. An optimal imaging system includes simultaneous visible (white) light illumination of the surgical field, which can be merged with the generated NIR fluorescence images. The surgeon's display can be one of several form factors, including a standard computer monitor, goggles or a wall projector. Abbreviations: LED, light emitting diode; NIR, near-infrared. Illustration and caption are depicted from Vahrmeijer et al., Nat Rev 2013[10].

Fluorescence can be captured by a specialized imaging system and made visible for the human eye in real-time. Advantages of this technology include high sensitivity and high resolution. Depending on the wavelength of the

emission light, penetration into tissue can be micrometers in the visible light spectrum (400 – 600nm), up to several millimeters to a centimeter in the near-infrared (NIR) light spectrum (700 – 900nm)[11;12].

For intraoperative fluorescence imaging, both an imaging system and fluorescent contrast agent are needed. Moreover, the combination of imaging device and optical properties of the fluorophore is of paramount importance for successful intraoperative imaging. The imaging system contains an excitation light source and a detection device to capture emitted fluorescence from the exited fluorophores. Several imaging systems, either investigational or commercially available, have been developed over the past years for intraoperative fluorescence imaging[13]. As fluorescence imaging is gaining more attention, systems optimized for open surgery[14-19] and endoscopic surgery[20-23] are available at present.

With respect to fluorescent contrast agents, there are only a few that have become clinically available over the past decades. These include fluorescein[24], methylene blue (MB)[25], 5-aminolevulinic acid (5-ALA)[26] and indocyanine green[27]. Although some of these contrast agents possess properties to specifically accumulate inside or around tumors, they are not ligand- targeted contrast agents. This limits the clinical applicability of these compounds for a broad application.

Tumor imaging
For intraoperative tumor imaging, accumulation of a contrast agent in or around the tumor is essential to differentiate between tumors and surrounding normal structures. Several mechanisms are described that could facilitate this. Ideally, a contrast agent solely binds cancer specific proteins, while getting excreted from the rest of the body. Development of this kind of contrast agents is an expensive, time-consuming process and requires specific knowledge, experience in drug-development and an advanced infrastructure. Therefore, it is important to exploit clinically available contrast agents, such as ICG and MB whenever possible. As these contrast agents are not linked to tumor-targeted ligands, other mechanisms such as the enhanced permeability and retention (EPR) effect[28;29], difference in vascular pattern[30-32], disturbed excretion profiles[33] and favorable biodistribution of compounds with comparable biophysical properties[34] can be explored.

For several indications, these mechanisms may be sufficient for tumor imaging[33;35-38]. However, there are many more indications that require tailor-made tumor-specific fluorescent ligands. These ligands can either be monoclonal antibodies, antibody fragments, such as single-chain (scFv) or fab fragments, small peptides or structure-inherent targeting fluorophores[39-42]. If these ligands target proteins that are only present on cancer cells, and not on healthy tissue, they could facilitate optimal contrast ratios during imaging. Hanahan and Weinberg elaborated on these hallmarks of cancer, comprising of biological capabilities acquired during the multistep development of human tumors[43]. Over the past years multiple tumor-specific agents targeting these hallmarks are developed and validated in various animal models. However, only a few compounds have currently been introduced in clinical studies[44-48]. This underlines the difficulty of bringing tumor-specific contrast agents to the clinic.

In conclusion, the objective of this thesis is to explore surgical indications where clinically available contrast agents can be used to improve tumor imaging and cancer surgery. Besides, newly developed tumor-specific contrast agents will be investigated in patients and healthy subjects, to assess their tolerability, pharmacokinetics and pharmacodynamics, and to determine their ability to visualize tumor tissue.

THESIS OUTLINE

This thesis is divided in two parts; **Part 1** focuses on the exploration of clinically available NIR fluorescent contrast agents for tumor imaging. **Part 2** describes the first in human introduction of newly developed tumor-specific fluorescence contrast agents in both healthy subjects and subsequently patients.

Chapter 2 describes the intraoperative use of indocyanine green (ICG) absorbed to nanocolloid for the detection of sentinel lymph nodes in gastric cancer. **Chapter 3** describes the successful detection of breast cancer tissue using methylene blue (MB) at different time points. **Chapter 4** shows the identification of hepatic uveal melanoma metastases during laparoscopic liver surgery using ICG. **Chapter 5** demonstrates the intraoperative distinction between normal pituitary gland and pituitary adenoma based on differences in vascular perfusion patterns during endoscopic transsphenoidal surgery

using a low-dose of ICG. **Chapter 6** shows the intraoperative detection of a paraganglioma and otherwise undetectable local metastases using MB. **Chapter 7** reports the detection of parathyroid adenomas and normal parathyroid glands using MB and **Chapter 8** described the intraoperative identification of ovarian cancer metastases using enhanced permeability and retention of ICG.

Chapter 9 reports the identification of ovarian cancer metastases and primary breast cancer using the tumor-specific folate receptor alpha (FRα) targeting agent EC17. **Chapter 10** describes the successful clinical translation of a new tumor-specific contrast agent in the near-infrared spectrum targeting the FRα in healthy subjects and patients.

In **Chapter 11,** all results are summarized and the future perspectives are discussed.

REFERENCES

1. Frangioni JV. New technologies for human cancer imaging. *J Clin Oncol* 2008;26:4012-4021.

2. Weissleder R, Pittet MJ. Imaging in the era of molecular oncology. *Nature* 2008;452:580-589.

3. Thill M, Baumann K, Barinoff J. Intraoperative assessment of margins in breast conservative surgery--still in use? *J Surg Oncol* 2014;110:15-20.

4. Bristow RE, Tomacruz RS, Armstrong DK, Trimble EL, Montz FJ. Survival effect of maximal cytoreductive surgery for advanced ovarian carcinoma during the platinum era: a meta-analysis. *J Clin Oncol* 2002;20:1248-1259.

5. Griffiths CT. Surgical resection of tumor bulk in the primary treatment of ovarian carcinoma. *Natl Cancer Inst Monogr* 1975;42:101-104.

6. Hoskins WJ, McGuire WP, Brady MF et al. The effect of diameter of largest residual disease on survival after primary cytoreductive surgery in patients with suboptimal residual epithelial ovarian carcinoma. *Am J Obstet Gynecol* 1994;170:974-979.

7. Frenkel S, Nir I, Hendler K et al. Long-term survival of uveal melanoma patients after surgery for liver metastases. *Br J Ophthalmol* 2009;93:1042-1046.

8. Hsueh EC, Essner R, Foshag LJ, Ye X, Wang HJ, Morton DL. Prolonged survival after complete resection of metastases from intraocular melanoma. *Cancer* 2004;100:122-129.

9. Vahrmeijer AL, van de Velde CJ, Hartgrink HH, Tollenaar RA. Treatment of melanoma metastases confined to the liver and future perspectives. *Dig Surg* 2008;25:467-472.

10. Vahrmeijer AL, Hutteman M, van der Vorst JR, van de Velde CJ, Frangioni JV. Image-guided cancer surgery using near-infrared fluorescence. *Nat Rev Clin Oncol* 2013.

11. Chance B. Near-infrared images using continuous, phase-modulated, and pulsed light with quantitation of blood and blood oxygenation. *Ann N Y Acad Sci* 1998;838:29-45.

12. Frangioni JV. In vivo near-infrared fluorescence imaging. *Curr Opin Chem Biol* 2003;7:626-634.

13. Zhu B, Sevick-Muraca EM. A review of performance of near-infrared fluorescence imaging devices used in clinical studies. *Br J Radiol* 2015;88:20140547.

14. Mieog JS, Troyan SL, Hutteman M et al. Toward optimization of imaging system and lymphatic tracer for near-infrared fluorescent sentinel lymph node mapping in breast cancer. *Ann Surg Oncol* 2011;18:2483-2491.

15. van Driel PB, van de Giessen M, Boonstra MC et al. Characterization and Evaluation of the Artemis Camera for Fluorescence-Guided Cancer Surgery. *Mol Imaging Biol* 2014.

16. Crane LM, Themelis G, Pleijhuis RG et al. Intraoperative multispectral fluorescence imaging for the detection of the sentinel lymph node in cervical cancer: a novel concept. *Mol Imaging Biol* 2011;13:1043-1049.

17. Gotoh K, Yamada T, Ishikawa O et al. A novel image-guided surgery of hepatocellular carcinoma by indocyanine green fluorescence imaging navigation. *J Surg Oncol* 2009;100:75-79.

18. Hirche C, Engel H, Kolios L et al. An experimental study to evaluate the fluobeam 800 imaging system for fluorescence-guided lymphatic imaging and sentinel node biopsy. *Surg Innov* 2013;20:516-523.

19. Yamauchi K, Nagafuji H, Nakamura T, Sato T, Kohno N. Feasibility of ICG fluorescence-guided sentinel lymph node biopsy in animal models using the HyperEye Medical System. *Ann Surg Oncol* 2011;18:2042-2047.

20. Moroga T, Yamashita S, Tokuishi K et al. Thoracoscopic segmentectomy with intraoperative evaluation of sentinel nodes for stage I non-small cell lung cancer. *Ann Thorac Cardiovasc Surg* 2012;18:89-94.

21. Spinoglio G, Priora F, Bianchi PP et al. Real-time near-infrared (NIR) fluorescent cholangiography in single-site robotic cholecystectomy (SSRC): a single-institutional prospective study. *Surg Endosc* 2013;27:2156-2162.

22. van der Poel HG, Buckle T, Brouwer OR, Valdes Olmos RA, van Leeuwen FW. Intraoperative Laparoscopic Fluorescence Guidance to the Sentinel Lymph Node in Prostate Cancer Patients: Clinical Proof of Concept of an Integrated Functional Imaging Approach Using a Multimodal Tracer. *Eur Urol* 2011;60:826-33.

23. Yamashita S, Tokuishi K, Anami K et al. Video-assisted thoracoscopic indocyanine green fluorescence imaging system shows sentinel lymph nodes in non-small-cell lung cancer. *J Thorac Cardiovasc Surg* 2011;141:141-144.

24. Moore GE, Peyton WT. The clinical use of fluorescein in neurosurgery; the localization of brain tumors. *J Neurosurg* 1948;5:392-398.

25. van der Vorst JR, Vahrmeijer AL, Hutteman M et al. Near-infrared fluorescence imaging of a solitary fibrous tumor of the pancreas using methylene blue. *World J Gastrointest Surg* 2012;4:180-184.

26. Stummer W, Stocker S, Wagner S et al. Intraoperative detection of malignant gliomas by 5-aminolevulinic acid-induced porphyrin fluorescence. *Neurosurgery* 1998;42:518-525.

27. Schaafsma BE, Mieog JS, Hutteman M et al. The clinical use of indocyanine green as a near-infrared fluorescent contrast agent for image-guided oncologic surgery. *J Surg Oncol* 2011;104:323-332.

28. Maeda H, Wu J, Sawa T, Matsumura Y, Hori K. Tumor vascular permeability and the EPR effect in macromolecular therapeutics: a review. *J Control Release* 2000;65:271-284.

29. Matsumura Y, Maeda H. A new concept for macromolecular therapeutics in cancer chemotherapy: mechanism of tumoritropic accumulation of proteins and the antitumor agent smancs. *Cancer Res* 1986;46:6387-6392.

30. Heijblom M, Klaase JM, van den Engh FM, van Leeuwen TG, Steenbergen W, Manohar S. Imaging tumor vascularization for detection and diagnosis of breast cancer. *Technol Cancer Res Treat* 2011;10:607-623.

31. Jugenburg M, Kovacs K, Stefaneanu L, Scheithauer BW. Vasculature in Nontumorous Hypophyses, Pituitary Adenomas, and Carcinomas: A Quantitative Morphologic Study. *Endocr Pathol* 1995;6:115-124.

32. Padhani AR, Dzik-Jurasz A. Perfusion MR imaging of extracranial tumor angiogenesis. *Top Magn Reson Imaging* 2004;15:41-57.

33. Ishizawa T, Fukushima N, Shibahara J et al. Real-time identification of liver cancers by using indocyanine green fluorescent imaging. *Cancer* 2009;115:2491-2504.

34. Winer JH, Choi HS, Gibbs-Strauss SL, Ashitate Y, Colson YL, Frangioni JV. Intraoperative Localization of Insulinoma and Normal Pancreas Using Invisible Near-Infrared Fluorescent Light. *Ann Surg Oncol* 2009.

35. Kosaka N, Mitsunaga M, Longmire MR, Choyke PL, Kobayashi H. Near infrared fluorescence-guided real-time endoscopic detection of peritoneal ovarian cancer nodules using intravenously injected indocyanine green. *Int J Cancer* 2011;129:1671-1677.

36. Litvack ZN, Zada G, Laws ER, Jr. Indocyanine green fluorescence endoscopy for visual differentiation of pituitary tumor from surrounding structures. *J Neurosurg* 2012;116:935-941.

37. van der Vorst JR, Schaafsma BE, Hutteman M et al. Near-infrared fluorescence-guided resection of colorectal liver metastases. *Cancer* 2013;119:3411-3418.

38. van der Vorst JR, Schaafsma BE, Verbeek FP et al. Intraoperative near-infrared fluorescence imaging of parathyroid adenomas with use of low-dose methylene blue. *Head Neck* 2013.

39. Altintas I, Kok RJ, Schiffelers RM. Targeting epidermal growth factor receptor in tumors: from conventional monoclonal antibodies via heavy chain-only antibodies to nanobodies. *Eur J Pharm Sci* 2012;45:399-407.

40. Choi HS, Gibbs SL, Lee JH et al. Targeted zwitterionic near-infrared fluorophores for improved optical imaging. *Nat Biotechnol* 2013;31:148-153.

41. Hyun H, Park MH, Owens EA et al. Structure-inherent targeting of near-infrared fluorophores for parathyroid and thyroid gland imaging. *Nat Med* 2015;21:192-197.

42. Oliveira S, Heukers R, Sornkom J, Kok RJ, van Bergen En Henegouwen PM. Targeting tumors with nanobodies for cancer imaging and therapy. *J Control Release* 2013;172:607-617.

43. Hanahan D, Weinberg RA. The hallmarks of cancer. *Cell* 2000;100:57-70.

44. van Dam GM, Crane LM, Themelis G et al. Intraoperative tumor-specific fluorescence imaging in ovarian cancer by folate receptor-alpha targeting: first in-human results. *Nat Med* 2011;Sep 18;17(10):1315-9.

45. Burggraaf J, Kamerling IM, Gordon PB et al. Detection of colorectal polyps in humans using an intravenously administered fluorescent peptide targeted against c-Met. *Nat Med* 2015.

46. Rosenthal EL, Warram JM, de BE et al. Safety and Tumor Specificity of Cetuximab-IRDye800 for Surgical Navigation in Head and Neck Cancer. *Clin Cancer Res* 2015;21:3658-3666.

47. Lamberts LE, Koch M, de jong JS et al. Tumor-specific uptake of fluorescent bevacizumab-IRDye800CW microdosing in patients with primary breast cancer: a phase I feasibility study. *Clin Cancer Res* 2016.

48. Whitley MJ, Cardona DM, Lazarides AL et al. A mouse-human phase 1 co-clinical trial of a protease-activated fluorescent probe for imaging cancer. *Sci Transl Med* 2016;8:320ra4.
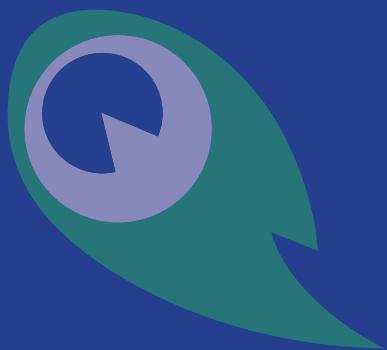
Part I

Exploring clinical available fluorescent contrast agents in cancer surgery

Chapter 2

Near-infrared fluorescence sentinel lymph node detection in gastric cancer: a pilot study

Quirijn R.J.G. Tummers[*1], Leonora S.F. Boogerd[*1], Wobbe O. de Steur[1], Floris P.R. Verbeek[1], Martin C. Boonstra[1], Henricus J.M. Handgraaf[1], John V. Frangioni[2,3], Cornelis J.H. van de Velde[1], Henk H. Hartgrink[1] and Alexander L. Vahrmeijer[1]

* Q.R.J.G. Tummers and L.S.F. Boogerd share first authorship.

[1] Department of Surgery, Leiden University Medical Center
[2] Department of Radiology, [3]Division of Hematology/Oncology, Department of Medicine, Beth Israel Deaconess Medical Center, Boston, USA

ABSTRACT

Aim: To investigate feasibility and accuracy of near-infrared fluorescence imaging using indocyanine green:nanocolloid for sentinel lymph node (SLN) detection in gastric cancer.

Methods: A prospective, single-institution, phase I feasibility trial was conducted. Patients suffering from gastric cancer and planned for gastrectomy were included. During surgery, a subserosal injection of 1.6mL ICG:Nanocoll was administered around the tumor. NIR fluorescence imaging of the abdominal cavity was performed using the Mini-FLARE™ NIR fluorescence imaging system. Lymphatic pathways and SLNs were visualized. Of every detected SLN, the corresponding lymph node station, signal-to-background ratio and histopathological diagnosis was determined. Patients underwent standard-of-care gastrectomy. Detected SLNs outside the standard dissection planes were also resected and evaluated.

Results: Twenty-six patients were enrolled. Four patients were excluded because distant metastases were found during surgery or due to technical failure of the injection. In 21 of the remaining 22 patients, at least 1 SLN was detected by NIR fluorescence (mean 3.1 SLNs; range 1-6). In 8 of the 21 patients, tumor-positive LNs were found. Overall accuracy of the technique was 90% (70-99%; 95% CI), which decreased by higher pT-stage (100%, 100%, 100%, 90%, 0% for respectively Tx, T1, T2, T3, T4 tumors). All NIR-negative SLNs were completely effaced by tumor. Mean fluorescence signal-to-background ratio of SLNs was 4.4 (range 1.4-19.8). In 8 of the 21 patients, SLNs outside the standard resection plane were identified, that contained malignant cells in 2 patients.

Conclusions: This study shows successful use of ICG:Nanocoll as lymphatic tracer for SLN detection in gastric cancer. Moreover, tumor-containing LNs outside the standard dissection planes were identified.

INTRODUCTION

Gastric cancer is still one of the most frequent causes of cancer deaths worldwide with an incidence rate varying between countries[1;2]. The highest estimated mortality rates are in Eastern Asia (24 per 100,000 in men, 9.8 per 100,000 in women), the lowest in North America (2.8 and 1.5, respectively)[3].

Surgical resection of the tumor is the only curative treatment option. Depending on the size, infiltration depth, and location of the tumor, surgery can be performed endoscopically, or by partial or total gastrectomy. In addition to resection of the affected part of the stomach, a lymph node (LN) dissection is typically performed. This can either be done by extensive lymphadenectomy or by a sentinel lymph node (SLN) procedure, depending on T status and size of the tumor. Nodal involvement in gastric cancer occurs in only 2-18% when the depth of cancer invasion is limited to the mucosal or submucosal layer (T1), and in about 50% when tumors invade the subserosal layer (T2)[4]. In patients with tumor-negative lymph nodes, a SLN procedure could avoid the risk of morbidity and mortality of an unnecessary lymphadenectomy. Additionally, in patients who are undergoing a partial or total gastrectomy combined with lymphadenectomy, identification of potentially involved LNs outside the standard plane of resection is possible by detecting the SLN. In this way, also in tumors with higher T stages, one can find the true first tumor draining LN(s), and not leaving them *in situ*. As the lymphatic drainage route of gastric cancer is generally multidirectional and complicated[5], intraoperative assistance in identification of potentially involved lymph nodes could improve gastric cancer treatment.

SLN detection in gastric cancer was first described by Kitagawa et al.[6] Since then, multiple studies were performed. A prospective multicenter trial in 433 patients with T1 or T2 stadium tumors showed an accuracy rate of 99% for identification of metastasis in SLNs with the use of a dual tracer consisting of radiolabeled tin colloid and blue dye[7].

Near-infrared (NIR) fluorescence imaging is an innovative technique to visualize tumors, vital structures, lymphatic channels, and LNs[8]. Soltesz et al.[9] in a preclinical setting and Kusano et al.[10] in a clinical setting were the first to report the SLN procedure in gastric cancer using NIR fluorescence imaging. Since then, multiple studies confirmed the feasibility of this technique for both open and laparoscopic surgery[11-15]. All clinical studies reported to date

utilized indocyanine green (ICG) as the lymphatic tracer. However, the use of ICG resulted in detection of more fluorescent lymph nodes per patient than expected due to migration through the SLN to second tier nodes. Consequently, resection and pathological assessment of multiple nodes was still needed. Adsorption of ICG to a nanocolloid (ICG:Nanocoll) increases its hydrodynamic diameter, which may result in better retention of the lymphatic tracer in the SLN, and thereby staining less second-tier nodes. This results in intraoperative identification of true SLNs, and avoids analyzing non-SLNs during pathological assessment for tumor-status of the SLN. This principle was already successfully described for breast cancer[16] and skin melanoma[17].

The aim of this study was to investigate feasibility of ICG adsorbed to nanocolloid as a lymphatic tracer for the intraoperative detection of the SLN in gastric cancer patients with different pT stages, and to determine the prognostic utility of the detected SLN.

MATERIALS AND METHODS

Tracer preparation
ICG:Nanocoll was prepared by diluting 25mg ICG (Pulsion Medical Systems, Munich, Germany) in 5ml water and diluting 0.5mg Nanocoll (GE Healthcare, Eindhoven, the Netherlands) in 3ml saline. Portions of these solutions were mixed to obtain 1.6ml ICG:Nanocoll containing 0.05mg ICG and 0.1mg Nanocoll. Preparation was performed in the operating room, following preparation instructions of the institutional pharmacist.

Clinical trial
The trial was approved by the Medical Ethics Committee of the Leiden University Medical Center and was performed in accordance with the ethical standards of the Helsinki Declaration of 1975. Registration within the Netherlands Trial Register was performed (NTR4280).

Twenty-six patients with different T stages of gastric cancer, planned for a partial or total gastrectomy, were included between February 2013 and March 2015. Patients underwent standard-of-care preoperative imaging using a Computed Tomography (CT) scan. No standard endoscopic ultrasound or staging laparoscopy was performed. All procedures were performed by surgeons with broad experience in gastric cancer surgery.

After opening of the abdominal cavity the tumor was exposed without causing damage to lymphatic vessels around the tumor as much as possible. When no metastasized disease was found, 1.6ml ICG:Nanocoll was administered subserosally in 4 quadrants around the tumor. Directly after injection NIR fluorescence images of lymphatic pathways were acquired using the Mini-FLARE™ NIR fluorescence imaging system[18]. Fluorescence imaging was performed on multiple time points during surgery. A SLN was defined as fluorescent hotspot that appeared after injection of the tracer. When multiple fluorescent hotspots appeared in the same LN basin all fluorescent LNs were defined as SLNs. The anatomical location of the fluorescent hotspots was determined using the lymph node stations as defined by the Japanese Research Society for the Study of Gastric Cancer[19]. Patients underwent a standard-of-care partial or total gastrectomy with modified D2 resection, consisting of resection of the peri-gastric LNs and LN station 7,8 and 9. After resection, the specimen was analyzed *ex vivo* using the FLARE™ NIR fluorescence imaging system at the Pathology Department. The marked fluorescent hotspots were resected from the specimen, transected, fixed in formalin and embedded in paraffin for routine hematoxylin and eosin staining, and analyzed for tumor status.

The *in vivo* signal-to-background ratio (SBR) of the SLN was calculated by dividing the fluorescence intensity of the SLN by the fluorescence intensity of the directly surrounding fatty tissue. Accuracy rate was defined by the number of patients in which tumor-negative SLNs were found when no tumor-positive lymph nodes were found in the entire specimen and the number of patients in which tumor-positive SLNs were found when tumor-positive lymph nodes were found in the whole specimen divided by the total number of patients. Accuracy rate was expressed as percentage with a 95% confidence interval. A false-negative patient was defined as a patient in whom tumor-negative SLNs were found, while tumor-positive LNs were found in the resection specimen.

Confidence intervals for the binomial proportions were calculated using exact binomial confidence intervals. Numerical data were summarized with median (range).

Intraoperative near-infrared fluorescence imaging
Intraoperative imaging procedures were performed using the Mini-Fluorescence-Assisted Resection and Exploration (Mini-FLARE™) image-guided surgery system, as described earlier[18]. Briefly, the system consists of

2 wavelength isolated light sources: a "white" light source, generating 26,600 lx of 400 to 650 nm light, and a "near-infrared" light source, generating 1.08 mW/ca^me of ≈760 nm light. Color video and NIR fluorescence images are simultaneously acquired and displayed in real time using custom optics and software that separate the color video and NIR fluorescence images. A pseudo-colored (lime green) merged image of the color video and NIR fluorescence images is also displayed. The imaging head is attached to a flexible gooseneck arm, which permits positioning of the imaging head at extreme angles virtually anywhere over the surgical field. For intraoperative use, the imaging head and imaging system pole stand are wrapped in a sterile shield and drape (Medical Technique Inc., Tucson, AZ).

RESULTS

Patient characteristics

Twenty-six patients with gastric cancer undergoing partial or total gastrectomy were included in this study (Table 1). Median age was 64 years (range 30–82) and 19 patients were male. T-stadium of tumors were pTx, pT1, pT2, pT3, and pT4 in respectively 2, 5, 5, 10, and 4 patients. Median tumor size was 31 mm (range 10 – 90). Tumors were located in the cardia in 8, corpus in 6 and antrum in 12 patients. Eleven patients underwent a total gastrectomy, 14 patients underwent a partial gastrectomy and in 1 patient no resection was performed due to metastasized disease. Twenty-three patients received neoadjuvant chemotherapy consisting of Epirubicine, Oxaliplatin and Capecitabine or Epirubicine, Cisplatine and Capecitabine.

Sentinel lymph node detection

Three patients (#3, #12, and #16) did not receive an injection of ICG:Nanocoll because metastatic disease was found during surgery. In 1 patient (#8), ICG:Nanocoll was injected through the wall of the stomach. After this technical failure, this patient was excluded for further analysis.

Table 1. Patient and tumor characteristics

Characteristic	Median	Range
Age	64	30 - 82
Tumor size (in mm)	35	10 – 90
	N (n = 26)	**%**
Gender		
M	19	73
F	7	27
Tumor location		
Cardia	8	31
Corpus	6	23
Antrum	12	46
Tumor pT stage		
pTx	2	8
pT1	5	19
pT2	5	19
pT3	10	39
pT4	4	15
Type of resection		
Total gastrectomy	11	42
Partial gastrectomy	14	54
No resection	1	4
Preoperative CTx	23	88

Table 2 shows the characteristics of the intraoperatively detected SLNs in each patient. In 21 of the remaining 22 patients (95%, 77–100 95% CI interval), at least 1 SLN was found during surgery (mean of 3.1 SLNs per patient; range 1-6). SLNs were identified as bright fluorescent spots in the surrounding tissue of the stomach. Figure 1A shows a bright fluorescent spot, which was found histologically to be a tumor-negative lymph node. Figure 1B shows an example of a tumor-positive lymph node and visualization of lymphatic vessels running from the injection site to the lymph node. The mean SBR of the SLNs was 4.4 (range 1.4–19.8). In total, 533 LNs were identified in the resection specimens by the pathologist, resulting in a mean number of 24 resected LNs (range 11 - 44) per patient.

Table 2. Characteristics of detected SLNs

Patient no.	T stage	Tumor location	Pre-operative CTx	Number of detected SLNs	Location of detected SLNs by LN St	Mean SBR of SLNs	Tumor status in SLNs	SLN Identification accurate?	SLN outside Standard dissection plane?
1	1	M	No	3	3	5.4	Neg	Yes	No
2	4	M	Yes	3	3; 3 and 6	1.9	Pos	No	No
3	4	D	Yes	*No tracer injected because of metastasized disease.*					
4	1	D	Yes	3	4; 6 and 6	4.3	Neg	Yes	No
5	2	U	Yes	4	3; 3; 4 and 4	3.9	Neg	Yes	No
6	3	M	Yes	3	4; 4 and 7	5.3	Neg	Yes	No
7	1	M	No	4	3; 3; 6 and 6	3.1	Neg	Yes	No
8	2	U	Yes	*Technical failure of tracer administration*					
9	3	U	Yes	2	1 and 1	8.7	Neg	Yes	No
10	3	D	No	3	6; 6 and 12	4.7	Pos	No	Yes
11	3	D	Yes	4	5; 6 and 12	4.9	Pos	Yes	Yes
12	4	U	Yes	*No tracer injected because of metastasized disease.*					
13	2	U	Yes	3	1; 7 and 9	3.5	Neg	Yes	No
14	2	D	Yes	4	6 and 12	5.1	Pos	Yes	Yes
15	2	M	Yes	0	N/A	N/A	N/A	N/A	No
16	4	M	Yes	*No tracer injected because of metastasized disease.*					
17	3	U	Yes	2	8 and 12	2.6	Neg	Yes	Yes
18	3	D	Yes	2	5 and 6	11.4	Neg	Yes	No
19	x	D	Yes	2	3 and 3	3.6	Neg	Yes	No
20	x	D	Yes	2	3 and 14	3.6	Neg	Yes	Yes
21	3	M	Yes	5	3; 3; outside standard planes of 9 (3x)	2.8	Pos	Yes	Yes
22	3	D	Yes	4	3; 6; 6 and 14	3.1	Pos	Yes	Yes
23	3	U	Yes	1	1	6.2	Pos	Yes	No
24	3	D	Yes	6	3; 3; 6; 6; 6 and 11	4.0	Pos	Yes	Yes
25	1	D	Yes	4	3; 3; 4 and 6	4.6	Neg	Yes	No
26	1	D	Yes	4	5; 6; 6 and 6	5.6	Neg	Yes	No

Abbreviations: CTx, Chemotherapy; D, antrum of stomach; LN, Lymph Node; M, corpus of stomach; N/A, Not Applicable; SBR, Signal-to-Background Ratio; SLN, Sentinel Lymph Node; St, Lymph node station according to Japanese Research Society for the Study of Gastric Cancer; U, cardia of stomach;
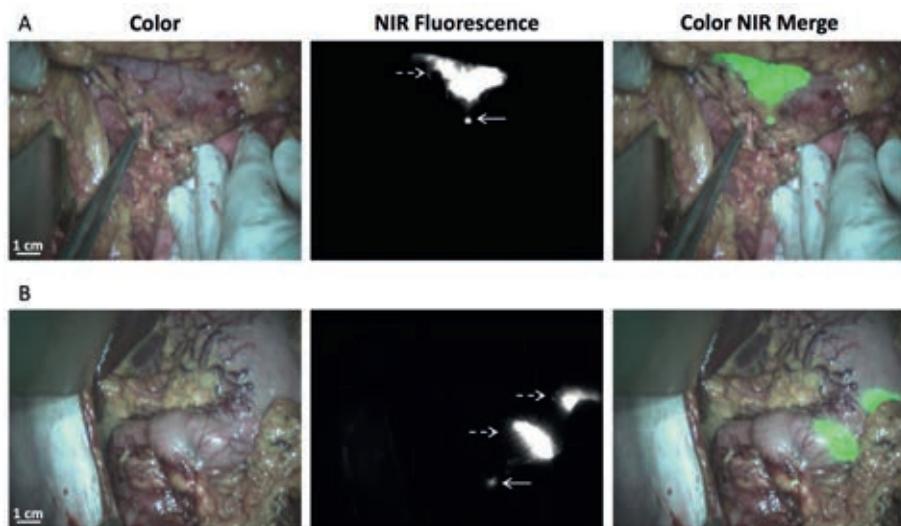
Figure 1. Identification of SLNs using NIR fluorescence imaging

A. Identification of SLN (arrow) 15 min after injection of ICG:Nanocoll using NIR fluorescence imaging. The injection site around the tumor is indicated by a dashed arrow. **B.** Patient with tumor-positive lymph node (indicated by arrow). Injection sites and fluorescent SLN are clearly detected. Lymphatic vessels are also visible between the injection site and SLN. The SLN is marked using sutures.

In 19 out of 21 patients, an accurate SLN was found. The overall accuracy of the SLN procedure was 90% (70 – 99 95% CI) and a higher pT-stadium was associated with a lower accuracy rate. Accuracy rates for pTx, pT1, pT2, pT3, and pT4 were respectively 100, 100, 100, 90, and 0%.

Histological analysis of the SLNs showed lymph node metastases in 8 out of 21 patients. In 6 patients, the SLNs that were identified using NIR fluorescence imaging were tumor-positive (true positive). In the other 2 patients, tumor-positive lymph nodes were not identified using NIR fluorescence imaging (false-negative). One false-negative patient (#2) had a T4 tumor. The tumor positive lymph nodes (3 out of 33 LNs) in this patient were found in the peripancreatic fatty tissue and in lymph node station 3, where a SLN was also detected. The second false-negative patient (#10) had a T3 tumor. Four out of 11 LNs that contained tumor cells were not detected by NIR fluorescence imaging. Of particular importance, all 7 tumor-positive LNs that were not detected by NIR fluorescence imaging were completely effaced by tumor tissue and no lymphatic tissue could be identified.

In 8 patients, SLNs outside the standard resection plane were identified. In 4 patients these were located in the hepatoduodenal ligament (LN station

12), in 2 patients near the border of the pancreas (LN station 14), in 1 patient outside the standard plane near LN station 9 and in 1 patient in LN station 11. In 2 patients, the extra-detected lymph nodes outside the standard plane of resection contained tumor cells (#21 and #22)(Figure 2).

No adverse events regarding the use of ICG:Nanocoll or NIR fluorescence imaging were encountered.
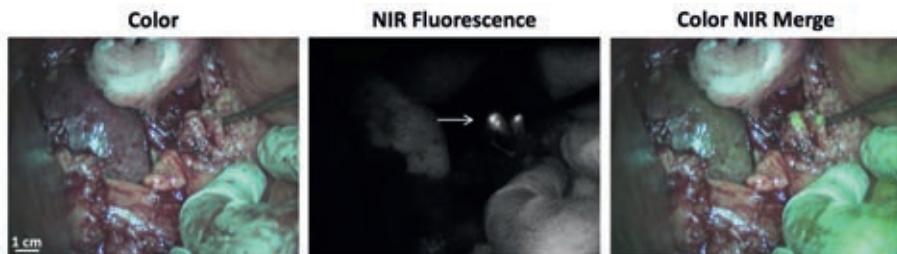
Figure 2. Identification of tumor-positive SLNs outside the standard dissection planes

Identification of tumor-positive SLNs (arrow) outside the standard resection specimen in patient #21. LNs are identified after gastrectomy and located outside the standard dissection plane near LN station 9.

DISCUSSION

The current feasibility study demonstrates that the SLN detection in gastric cancer, using ICG adsorbed to nanocolloid as the lymphatic tracer, is feasible and safe. In 21 out of 22 patients at least 1 SLN was identified, and in 19 out of 21 patients an accurate SLN was found.

In fewer than 50 percent of patients with a T1 or T2 tumor, lymph nodes show tumor involvement. In these patients, the SLN procedure has the potential to avoid an unnecessary lymphadenectomy, and its associated potential morbidity and mortality. Kitagawa et al reported an accuracy of nodal evaluation for metastasis of 99 percent[7], underlining the clinical applicability of the technique in this selected patient group. The SLN procedure in gastric cancer was validated for previously untreated cT1-T2 tumors with a diameter of less than 4 mm. However, in the Western world patients often present with a higher T stadium, and are often pretreated with chemotherapy. In these patients who need an extensive lymphadenectomy, the described technique could assist in identifying potentially involved lymph nodes located outside the standard plane of resection. Moreover, morbidity and mortality rates

increase when a more extended lymph node dissection is performed[20]. A more targeted and personalized treatment, including identification and dissection of truly or potentially involved lymph nodes, could result in improved gastric cancer treatment. Therefore, in both early gastric cancer and in resectable cases of advanced gastric cancer, accurate identification of true SLNs is of great importance.

Many different lymphatic tracers have been reported for SLN identification. The largest prospective multicenter trial until now used a combination of blue dye and radiolabeled tin colloids[7]. However, both tracers have disadvantages. Blue dye could alter the surgical field by dark staining, and only permits identification of superficially located lymph nodes. Moreover, in previous studies comparing radiolabeled colloids, blue dye, and NIR fluorescence for SLN detection in breast cancer patients, only 84 - 88 percent of the identified SLNs stained blue compared to 100 percent that were NIR fluorescent[16;21]. For the SLN procedure in skin melanoma blue dye staining was successful in only 73 percent[22]. Radiolabeled colloids only permit acoustic guidance during SLN identification, but no visual guidance. Besides, radioactive isotopes are scarce in many areas of the world. NIR fluorescence imaging could overcome these limitations as it only needs an imaging system and fluorescent tracer, and allows real-time optical identification of lymph nodes in up to ≈ 6 mm of tissue, for example in visceral dense fat tissue[8].

Since Kusano et al.[10] reported the first SLN procedure in gastric cancer using NIR fluorescence imaging, multiple studies confirmed the feasibility of this technique for both open and laparoscopic surgery[11-15]. All reported studies to date used ICG alone as lymphatic tracer, which resulted in detection of many fluorescent lymph nodes per patient. For example, Tajima et al.[14] reported a mean number of 7.2 ± 7 SLN per patient and Fujita et al.[11] a mean number of 9.3 ± 6.4 SLN per patient when using ICG as lymphatic tracer. This was possibly due to migration through the SLN to second tier nodes, and resection and pathological assessment of multiple nodes was still needed.

By combining ICG with nanocolloid, its hydrodynamic diameter increases from ≤ 1 nm (ICG) to 20 - 80 nm (ICG:Nanocoll). It has been shown that the hydrodynamic diameter of a lymphatic tracer has a major impact on the lymphatic migration and accumulation in lymph nodes. Molecules with a hydrodynamic diameter less than approximately 10 nm (for example ICG) have the potential to migrate through the SLN to second tier nodes, while

larger molecules with a hydrodynamic diameter of <100 nm (ICG:Nanocoll) are retained in the SLN[23]. In the current study, a mean number of 3.1 SLN per patient was found. This lower number of detected SLNs is in accordance with our hypothesis that better retention in SLNs is obtained when a lymphatic tracer with a higher hydrodynamic diameter is used. This highly improves the clinical applicability of SLN detection using NIR fluorescence imaging in gastric cancer.

Although the number of patients was limited in the current study, an excellent accuracy rate was obtained in lower pT stages, in which the clinical value of a SLN procedure is becoming more and more accepted. These data are consistent with previous studies where the SLN procedure was performed for T1 and T2 tumors. However, even for advanced gastric cancer, identifying the first draining lymph nodes can be of added value. In the current study, LNs from 8 patients were identified outside the standard resection margin using NIR fluorescence imaging; they would otherwise not have been resected. In 2 patients, the extra-detected LNs outside the standard plane of resection contained tumor cells. These LNs were only resected because NIR fluorescence imaging identified them. Larger studies are needed to determine the additional value of the described technique in advanced gastric cancer.

In 2 patients, tumor-positive LNs were not identified using NIR fluorescence imaging. One explanation for the false positivity of these LNs might be the fact that these tumors were relatively large, respectively 60 and 45mm diameter, and consequently, adequate injection of the tracer in four quadrants around the tumor might be hampered. However, other fluorescent LNs that that did contain tumor cells, were found in tumors with a median size of 52mm (range 27 – 90). Moreover, all 7 of these LNs were completely effaced by tumor tissue. Such LNs lose function, lymph doesn't flow in or out, and no lymphatic tissue is present to trap the fluorescent tracer. Subsequently, these tumor-positive LNs can't be identified, a principle that counts for the SLN procedure in all solid cancers. In one of these patients however, the identified SLN was found in the same LN basin as one of the tumor-involved LNs. This underlines the theory that whenever SLNs are visualized, the entire lymph node basin should be resected instead of only the SLN by lymph node picking, because it is shown that most of the metastatic non-SLNs are positioned in the same basin as the detected SLNs[24;25].

A well-known difficulty in SLN mapping in gastric cancer is the presence of skip metastasis: involvement of extra-perigastric lymph nodes without

the detection of perigastric lymph node metastasis. The incidence of skip metastasis among patients with gastric cancer and metastasis is reported to be as high as 11%[26]. The described technique could assist in identifying these potentially involved extra-perigastric lymph nodes.

One of the limitations of this study is the administration technique, which is performed during surgery in the subserosal layer of the gastric wall. Opening the abdominal cavity, and exposing the affected part of the stomach could damage lymphatic vessels. This potentially hampers lymphatic flow to SLNs and was overcome as much as possible by avoiding dissections near the primary tumor. Besides, injecting the tracer in the submucosal layer seems more appropriate in case of tumor invasion limited to the mucosa or submucosa. However, it is shown that subserosal injection leads to drainage of the tracer to the same lymph nodes as submucosal injection, because of communication through vertical connections of lymphatic vessels in the gastric wall[27]. These limitations could be overcome by submucosal endoscopic administration of the lymphatic tracer before surgery. One of the additional advantages of this administration technique is that it allows visual tumor demarcation during surgery through the stomach wall, which assists in intraoperative tumor identification, and determination of resection margins. Especially in patients who experience good response on neoadjuvant chemotherapy this could be of added value.

Another limitation of the current feasibility study is that no true SLN procedure was performed, but instead intraoperative detection of SLNs. However, all fluorescent hotspots that were detected during surgery were directly marked using sutures. After the surgical procedure, they were mapped from the specimen for pathological assessment. By doing this, the same LNs were analyzed as if they would have been resected directly during surgery, and feasibility of ICG:Nanocoll as lymphatic tracer could still be showed.

Finally, pathological assessment of the LNs consisted of standard-of-care transection and hematoxylin and eosin staining. Multiple transections and additional keratin staining could possibly have resulted in the detection of tumor-tissue in the SLNs of the 2 false-negative patients, and thereby increasing accuracy rate. However, small tumor deposits in the detected SLNs were unlikely to be present as the tumor-positive LNs in the specimen were completely effaced by tumor.

In conclusion, this is the first study using ICG combined with nanocolloid as lymphatic tracer for the detection of the SLN in gastric cancer patients by NIR fluorescence imaging. In T1 and T2 gastric tumors, an excellent accuracy was observed. Moreover, this technique allowed identification of tumor-positive lymph nodes outside the standard dissection planes.

ACKNOWLEDGEMENTS

REFERENCES

1. Bray F, Jemal A, Grey N, Ferlay J, Forman D. Global cancer transitions according to the Human Development Index (2008-2030): a population-based study. *Lancet Oncol* 2012;13:790-801.

2. Hartgrink HH, Jansen EP, van Grieken NC, van de Velde CJ. Gastric cancer. *Lancet* 2009;374:477-490.

3. World Health Organization. GLOBOCAN 2012: Estimated cancer incidence, mortality and prevalance worldwide in 2012. Accessed 30th June 2014. 30-7-2014.

4. Sasako M, McCulloch P, Kinoshita T, Maruyama K. New method to evaluate the therapeutic value of lymph node dissection for gastric cancer. *Br J Surg* 1995;82:346-351.

5. Tokunaga M, Ohyama S, Hiki N et al. Investigation of the lymphatic stream of the stomach in gastric cancer with solitary lymph node metastasis. *World J Surg* 2009;33:1235-1239.

6. Kitagawa Y, Fujii H, Mukai M, Kubota T, Otani Y, Kitajima M. Radio-guided sentinel node detection for gastric cancer. *Br J Surg* 2002;89:604-608.

7. Kitagawa Y, Takeuchi H, Takagi Y et al. Sentinel node mapping for gastric cancer: a prospective multicenter trial in Japan. *J Clin Oncol* 2013;31:3704-3710.

8. Vahrmeijer AL, Hutteman M, van der Vorst JR, van de Velde CJ, Frangioni JV. Image-guided cancer surgery using near-infrared fluorescence. *Nat Rev Clin Oncol* 2013.

9. Soltesz EG, Kim S, Kim SW et al. Sentinel lymph node mapping of the gastrointestinal tract by using invisible light. *Ann Surg Oncol* 2006;13:386-396.

10. Kusano M, Tajima Y, Yamazaki K, Kato M, Watanabe M, Miwa M. Sentinel node mapping guided by indocyanine green fluorescence imaging: a new method for sentinel node navigation surgery in gastrointestinal cancer. *Dig Surg* 2008;25.

11. Fujita T, Seshimo A, Kameoka S. Detection of sentinel nodes in gastric cancer by indocyanine green fluorescence imaging. *Hepatogastroenterology* 2012;59:2213-2216.

12. Miyashiro I, Miyoshi N, Hiratsuka M et al. Detection of sentinel node in gastric cancer surgery by indocyanine green fluorescence imaging: comparison with infrared imaging. *Ann Surg Oncol* 2008;15.

13. Miyashiro I, Kishi K, Yano M et al. Laparoscopic detection of sentinel node in gastric cancer surgery by indocyanine green fluorescence imaging. *Surg Endosc* 2011;25:1672-1676.

14. Tajima Y, Yamazaki K, Masuda Y et al. Sentinel node mapping guided by indocyanine green fluorescence imaging in gastric cancer. *Ann Surg* 2009;249:58-62.

15. Tajima Y, Murakami M, Yamazaki K et al. Sentinel node mapping guided by indocyanine green fluorescence imaging during laparoscopic surgery in gastric cancer. *Ann Surg Oncol* 2010;17:1787-1793.

16. Schaafsma BE, Verbeek FP, Rietbergen DD et al. Clinical trial of combined radio- and fluorescence-guided sentinel lymph node biopsy in breast cancer. *Br J Surg* 2013;100:1037-1044.

17. Brouwer OR, Klop WM, Buckle T et al. Feasibility of Sentinel Node Biopsy in Head and Neck Melanoma Using a Hybrid Radioactive and Fluorescent Tracer. *Ann Surg Oncol* 2011;19:1988-1994.

18. Mieog JS, Troyan SL, Hutteman M et al. Towards Optimization of Imaging System and Lymphatic Tracer for Near-Infrared Fluorescent Sentinel Lymph Node Mapping in Breast Cancer. *Ann Surg Oncol* 2011;18:2483-2491.

19. Kajitani T. The general rules for the gastric cancer study in surgery and pathology. Part I. Clinical classification. *Jpn J Surg* 1981;11:127-139.

20. Giuliani A, Miccini M, Basso L. Extent of lymphadenectomy and perioperative therapies: two open issues in gastric cancer. *World J Gastroenterol* 2014;20:3889-3904.

21. van der Vorst JR, Schaafsma BE, Verbeek FP et al. Randomized comparison of near-infrared fluorescence imaging using indocyanine green and 99(m) technetium with or without patent blue for the sentinel lymph node procedure in breast cancer patients. *Ann Surg Oncol* 2012;19:4104-4111.

22. van der Vorst JR, Schaafsma BE, Verbeek FP et al. Dose Optimization for Near-Infrared Fluorescence Sentinel Lymph Node Mapping in Melanoma Patients. *Br J Dermatol* 2012.

23. van Leeuwen AC, Buckle T, Bendle G et al. Tracer-cocktail injections for combined pre- and intraoperative multimodal imaging of lymph nodes in a spontaneous mouse prostate tumor model. *J Biomed Opt* 2011;16:016004.

24. Ajisaka H, Miwa K. Micrometastases in sentinel nodes of gastric cancer. *Br J Cancer* 2003;89:676-680.

25. Miyashiro I. What is the problem in clinical application of sentinel node concept to gastric cancer surgery? *J Gastric Cancer* 2012;12:7-12.

26. Maruyama K, Gunven P, Okabayashi K, Sasako M, Kinoshita T. Lymph node metastases of gastric cancer. General pattern in 1931 patients. *Ann Surg* 1989;210:596-602.

27. Yaguchi Y, Ichikura T, Ono S et al. How should tracers be injected to detect for sentinel nodes in gastric cancer--submucosally from inside or subserosally from outside of the stomach? *J Exp Clin Cancer Res* 2008;27:79.

Chapter 3

Real-time intraoperative detection of breast cancer using near-infrared fluorescence imaging and Methylene Blue

Quirijn R.J.G. Tummers[1*], Floris P.R. Verbeek[1*], Boudewijn E. Schaafsma[1],
Martin C. Boonstra[1], Joost R. van der Vorst[1], Gerrit-Jan Liefers[1],
Cornelis J.H. van de Velde[1], John V. Frangioni[2,3] and Alexander L. Vahrmeijer[1]

* Q.R.J.G. Tummers and F.P.R. Verbeek share first authorship.

[1] Department of Surgery, Leiden University Medical Center
[2] Department of Radiology, [3] Division of Hematology/Oncology, Department of Medicine,
Beth Israel Deaconess Medical Center, Boston, USA

ABSTRACT

Background: Despite recent developments in preoperative breast cancer imaging, intraoperative localization of tumor tissue can be challenging, resulting in tumor-positive resection margins during breast conserving surgery. Based on certain physicochemical similarities between Technetium(^{99m}Tc)-sestamibi (MIBI), an SPECT radiodiagnostic with a sensitivity of 83-90% to detect breast cancer preoperatively, and the near-infrared (NIR) fluorophore Methylene Blue (MB), we hypothesized that MB might detect breast cancer intraoperatively using NIR fluorescence imaging.

Methods: Twenty-four patients with breast cancer, planned for surgical resection, were included. Patients were divided in 2 administration groups, which differed with respect to the timing of MB administration. N = 12 patients per group were administered 1.0 mg/kg MB intravenously either immediately or 3 h before surgery. The mini-FLARE imaging system was used to identify the NIR fluorescent signal during surgery and on post-resected specimens transferred to the pathology department. Results were confirmed by NIR fluorescence microscopy.

Results: 20/24 (83%) of breast tumors (carcinoma in N=21 and ductal carcinoma *in situ* in N=3) were identified in the resected specimen using NIR fluorescence imaging. Patients with non-detectable tumors were significantly older. No significant relation to receptor status or tumor grade was seen. Overall tumor-to-background ratio (TBR) was 2.4 ± 0.8. There was no significant difference between TBR and background signal between administration groups. In 2/4 patients with positive resection margins, breast cancer tissue identified in the wound bed during surgery would have changed surgical management. Histology confirmed the concordance of fluorescence signal and tumor tissue.

Conclusions: This feasibility study demonstrated an overall breast cancer identification rate using MB of 83%, with real-time intraoperative guidance having the potential to alter patient management.

INTRODUCTION

Breast cancer is the most common malignancy in women worldwide and is a leading cause of cancer-related mortality[1]. More than 1.2 million cases are diagnosed every year, affecting 10–12% of the female population and accounting for 500,000 deaths per year worldwide.

In early breast cancer, breast conserving surgery (BCS) is the preferred standard of care. Despite preoperative imaging modalities such as CT and MRI, intraoperative identification of breast cancer tissue can be challenging. Previous studies reported that the incidence of tumor cells at or near the cut edge of the surgical specimen ranged from 5% to 82%, with the majority of studies indicating positive resection margins in 20%–40% of patients after resection of the primary tumor[2]. Positive margins may lead to additional surgical procedures, delays in adjuvant treatment, increased morbidity, poor aesthetic results, and increased healthcare costs. Therefore, there is an urgent need for new technology to identify breast cancer tissue intraoperatively.

Technetium(^{99m}Tc)-sestamibi (MIBI) is a lipophilic cation used for preoperative, non-invasive identification of malignant tissue via SPECT imaging[3]. Using ^{99m}Tc-MIBI, preoperative identification of breast cancer is possible in approximately 83-90% of patients[3-5]. Based on the lipophilic, cationic structure of Methylene Blue (MB), and the fact that like ^{99m}Tc-MIBI, MB can function as a perfusion tracer *in vivo*[6;7], we hypothesized that it too might be able to detect breast tumors. Importantly, MB is a clinically available tracer that can be used at relatively low dose (0.5-1 mg/kg) as a fluorescent tracer during NIR fluorescence imaging. NIR fluorescence imaging is a promising technique to assist in the intraoperative identification of sentinel lymph nodes, tumors, and vital structures[8].

During ^{99m}Tc-MIBI SPECT imaging, early (within 30 min after tracer administration) and delayed (3 h post tracer administration) imaging is performed in succession[5;9]. The reason for this is to differentiate more accurately between malignant and benign lesions because it is presumed that tracer uptake in malignant lesions might persist, whereas clearance from benign lesions would be more rapid. Delayed imaging could thereby result in higher tumor-to-background ratios (TBRs) from lower background signal.

The aim of this study was to determine the feasibility of using MB as an NIR fluorescent tracer for the identification of breast tumor intraoperatively, and to compare early and delayed imaging protocols.

METHODS

Patients

Breast cancer patients planning to undergo breast surgery were eligible for participation in the trial. Patients planned for either breast conserving surgery (BCS) or modified radical mastectomy (MRM) were included. Consent was performed at the department of Surgery. Exclusion criteria were pregnancy or lactation, and various contraindications to MB including the use of serotonin reuptake inhibitors, serotonin and noradrenalin reuptake inhibitors and/or tricyclic antidepressants, severe renal failure, a G6PD-deficiency or a known allergy to MB. All patients gave informed consent and were anonymized.

Clinical trial

This clinical trial was approved by the Medical Ethics Committee of the Leiden University Medical Center and was performed in accordance with the ethical standards of the Helsinki Declaration of 1975.

Patients were divided in 2 administration groups, which differed with respect to the timing of MB administration. 12 patients per group were administered 1.0 mg/kg MB intravenously over 5 min either immediately before surgery, or 3 h before surgery. Distribution between groups was based on the logistics of the operating room time on a particular day. Patients scheduled to be first on the day's surgical program were administered MB immediately before surgery (early imaging). Patients scheduled later in the day were administered MB 3 h before surgery (delayed imaging).

The mini-FLARE imaging system was used to identify the fluorescent signal during surgery and on post-resected specimens transferred to the Pathology department. During surgery, images were obtained from the surgical field, resected specimen, and wound bed after resection. When fluorescent signal was observed, the operating surgeon could decide whether to resect the fluorescent tissue or not, based on clinical judgment of the tissue. The resected specimen was sliced at the pathology department, where images from the bisected tumor were obtained. When possible, snap frozen tissue was collected for fluorescence microscopy images.

Intraoperative near-infrared fluorescence imaging system (Mini-FLARE)
Imaging procedures were performed using the Mini-Fluorescence-Assisted Resection and Exploration (Mini-FLARE) image-guided surgery system, as described earlier[10]. Briefly, the system consists of 2 wavelength isolated light sources: a "white" light source, generating 26,600 lx of 400–650 nm light, and a "near-infrared" light source, generating 1.08 mW/ca^{me} of $\approx$ 670 nm light. Color video and NIR fluorescence images are simultaneously acquired and displayed in real time using custom optics and software that separate the color video and NIR fluorescence images. A pseudo-colored (lime green) merged image of the color video and NIR fluorescence images is also displayed. The imaging head is attached to a flexible gooseneck arm, which permits positioning of the imaging head at extreme angles virtually anywhere over the surgical field. For intraoperative use, the imaging head and imaging system pole stand are wrapped in a sterile shield and drape (Medical Technique Inc., Tucson, AZ).

***Ex vivo* imaging and fluorescence microscopy of resected lesion**
After slicing of the resected lesion at the Pathology department, fluorescence imaging was again performed with the mini-FLARE imaging system. Fluorescence microscopy images were obtained with the Odyssey Infrared Imaging System (LI-COR, USA).

Statistical analysis
For statistical analysis, SPSS statistical software package (Version 20.0, Chicago, IL) was used. Graphs were generated using GraphPad Prism Software (Version 5.01, La Jolla, CA). TBRs were calculated by dividing the fluorescent signal of the tumor by fluorescent signal of surrounding tissue. Patient age and body mass index (BMI) were reported in median and range and TBR was reported in mean and standard deviation. To compare patient characteristics, independent samples t-test and chi-square tests were used. To compare TBR and background signal between dose groups, independent samples t-test was used. $P < 0.05$ was considered significant.

RESULTS

A total of 24 patients were included in this study. Patient and tumor characteristics are detailed in Table 1. Mean patient age was 60 years (range 44 - 82 years); 21 patients were planned for BCS, 3 patients received an MRM. Histopathological analysis showed 14 patients with infiltrating ductal adenocarcinoma, 4 patients with infiltrating lobular adenocarcinoma, 3 patients with ductal carcinoma *in situ*, 1 patient with a primary mucoepidermoid carcinoma, 1 patient with a mucinous adenocarcinoma, and in 1 patient, no tumor was found in the resected specimen even though a preoperative biopsy showed infiltrating adenocarcinoma. Although patients were not assigned to a specific administration group by randomization, groups were comparable as no significant differences in patient or tumor characteristics were found (Table 1). All patients received preoperative ultrasound, and 9 patients also underwent preoperative MRI scan.

In 20 out of 24 patients (83%), breast tumors (carcinoma in N=21 and ductal carcinoma *in situ* in N=3) were identified in the resection specimen with NIR fluorescence imaging after bisection in the Pathology department. Tumors were identified as a bright fluorescent spot in the sliced specimen (Figure 1).

Table 2 shows patient and tumor characteristics related to detectability of the tumor. Patients with non-detectable tumors were significantly older (mean age 68 years old versus 58 years old; P=0.03). Both infiltrating ductal type adenocarcinoma and infiltrating lobular type adenocarcinoma were detectable. In patients with mucinous adenocarcinoma or primary mucoepidermoid carcinoma, no fluorescent tumor was found. No significant relation was found regarding receptor status or tumor grade.

Table 1. Patient and tumor characteristics

| Characteristic	Total N=24 Mean	Range	Early Imaging N=12 Mean	Range	Delayed Imaging N=12 Mean	Range	P
Age	60	(44-82)	59	(44-82)	60	(46-71)	0.97
Body mass index	24	(19-37)	24	(19-37)	27	(22-37)	0.16
Pathological tumor size (mm)	15	(6-33)	14	(7-27)	16	(6-33)	0.58
	N	%	N	%	N	%	
Clinical Stage							0.22
Stage 0	3	13	3	25	0	0	
Stage 1A	13	54	7	58	6	50	
Stage 1B	1	4	0	0	1	9	
Stage 2A	4	17	2	17	2	17	
Stage 2B	2	8	0	0	2	17	
Stage 3C	1	4	0	0	1	9	
Type of operation							0.54
Mastectomy	3	13	1	9	2	17	
Wide local excision	21	87	11	92	10	84	
Histological type							0.22
Infiltrating ductal type adenocarcinoma	15	63	6	50	9	75	
Infiltrating lobular type adenocarcinoma	4	17	2	17	2	17	
Mucinous adenocarcinoma	1	4			1	9	
Primary mucoepidermoid carcinoma	1	4	1	4			
Ductal carcinoma *in situ*	3	12	3	25			
Receptor status							
ER positive	19	79	8	67	11	92	0.83
PR positive	11	46	6	50	5	42	0.26
HER2/NEU positive	1	4	0	0	1	9	0.38
Triple Negative	2	8	1	9	1	9	0.95
Histological grade (Bloom-Richardon)							0.34
I	5	21	1	9	4	34	
II	9	38	5	42	4	34	
III	4	16	2	17	2	17	
No grading possible	6	25	4	34	2	17	
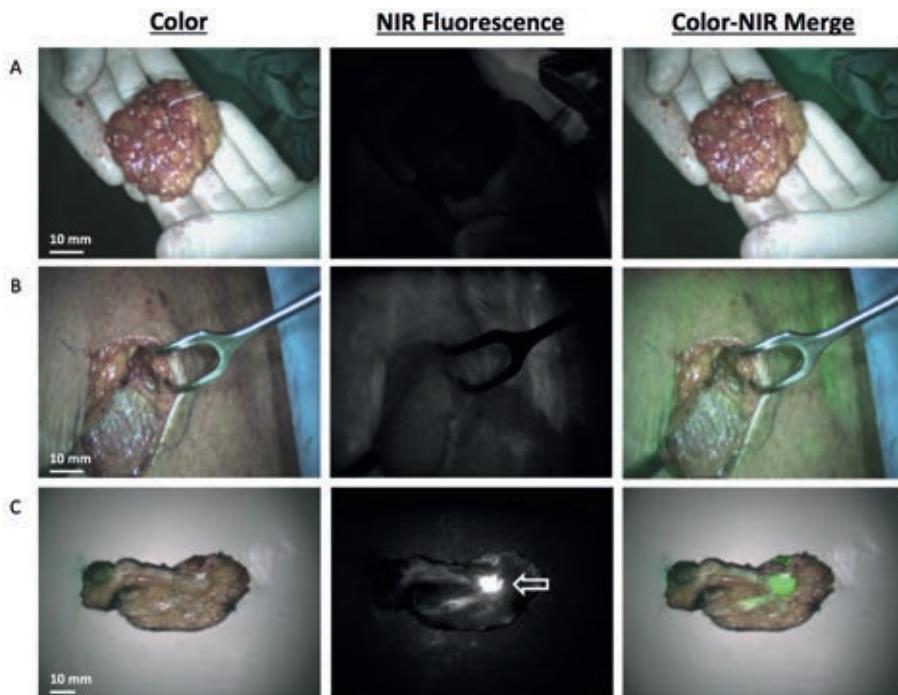
Figure 1. NIR fluorescence imaging of a tumor resection with negative margins

A. Resected specimen after wide local excision. No fluorescent signal was seen at resection margins. **B.** Inspection of wound bed after resection. No fluorescent signal was seen at resection margins. **C.** Sliced resection specimen at Pathology department. A clear fluorescent spot (arrow) was seen at the location of the tumor. Tumor was an infiltrating ductal adenocarcinoma, grade 2, ER+ PR+ Her2/neu-.

The overall TBR was 2.4 ± 0.8 (Figure 2A). There was no significant difference between administration groups in TBR (2.5 ± 0.9 vs. 2.3 ± 0.5; P=0.50) or background signal in arbitrary units (333 ± 215 vs. 262 ± 134; $P = 0.37$, data not shown) in the sliced specimens.

Four patients (17%) were found to have positive resection margins. In case 1, tumor tissue was identified both on the surface of the resected specimen (Figure 3A) and intraoperatively in the wound bed using NIR fluorescence imaging (Figure 3B). Direct re-resection was performed, and histopathological analysis confirmed that the fluorescent resected tissue was tumor (data not shown). Both primary resected and re-resected tumor tissue was an infiltrating lobular adenocarcinoma, grade 2, ER+ PR- Her2/neu -.

In case 2, no fluorescent tumor signal was seen on the surface of the resected specimen. In the bisected specimen, no fluorescent signal was seen at location

Table 2. Patient and tumor characteristics related to detectability

Characteristic	Detectable N=20 Mean	Range	Not Detectable N=4 Mean	Range
Age	58	(44-71)	68	(56-82)
Body mass index	26	(19-37)	24	(22-26)
Pathological tumor size (mm)	16	(6-33)	10	(7-12)
	N	%	N	%
Clinical Stage				
Stage 0	2	8	1	4
Stage 1A	10	42	3	13
Stage 1B	1	4	0	0
Stage 2A	4	17	0	0
Stage 2B	2	8	0	0
Stage 3C	1	4	0	0
Histological type				
Infiltrating ductal type adenocarcinoma	14	59	1	4
Infiltrating lobular type adenocarcinoma	4	17	0	0
Mucinous adenocarcinoma	0	0	1	4
Primary mucoepidermoid carcinoma	0	0	1	4
Ductal carcinoma *in situ*	2	8	1	4
Receptor status				
ER positive	17	71	2	8
PR positive	9	38	2	8
HER2/NEU positive	1	4	0	0
Triple Negative	2	4	0	0
Histological grade (Bloom-Richardon)				
I	4	17	1	4
II	9	37	0	0
III	3	13	1	4
No grading possible	4	17	2	8

of the tumor. This could have been because of lack of uptake or intracellular conversion of MB to its leuco [11], non-fluorescing form, but either way explains the lack of fluorescent signal in the tumor-positive resection margin. Tumor was a DCIS grade 3. In case 3, only images of the sliced specimen were available due to logistics, so no intraoperative fluorescent images were available. In case 4, clear fluorescent spots were identified in the wound bed intraoperatively, however, the operating surgeon believed that they were a false positive and did not resect them. Histopathology, though, confirmed positive margins at the location of the fluorescent spots. Afterwards, patient underwent a mastectomy in which the residual lobular infiltrating adenocarcinoma was found near the lumpectomy cavity.
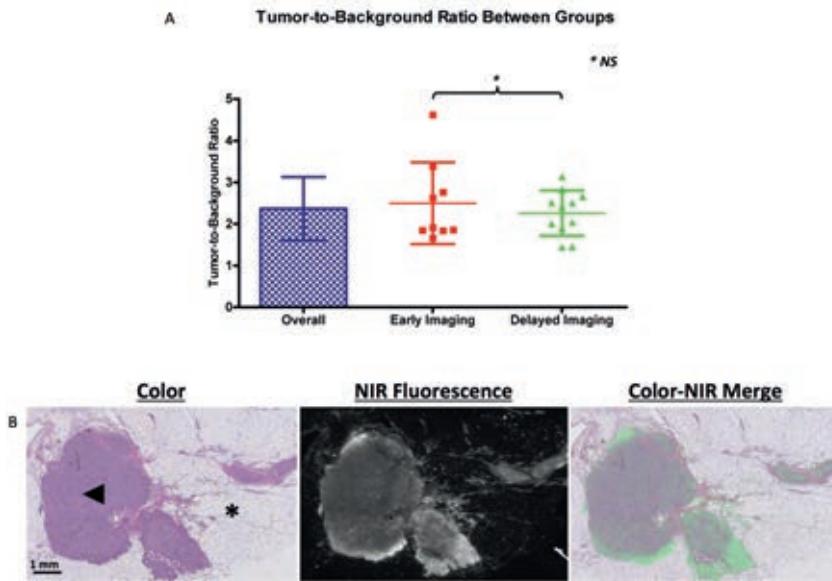
Figure 2. Tumor-to-Background Ratio and microscopic images of resected lesion

A. Overall Tumor-to-Background Ratio (TBR) and TBR per administration group are shown. No differences in TBR between administration groups were observed (P = 0.50; 95% CI -0.49 – 0.96). **B.** Microscopic images of Hematoxylin and Eosin staining of the resected lesion and fluorescent signal (Odyssey Infrared Imaging System, LI-COR). At the NIR fluorescent image, fluorescent signal is seen as white, where surrounding breast tissue remains black. A clear overlay between fluorescent signal and tumor tissue was seen. Normal breast tissue was indicated by an asterisk (*). Tumor (indicated by arrowhead) was an infiltrating ductal adenocarcinoma, grade 2, ER + PR + Her2/neu -.
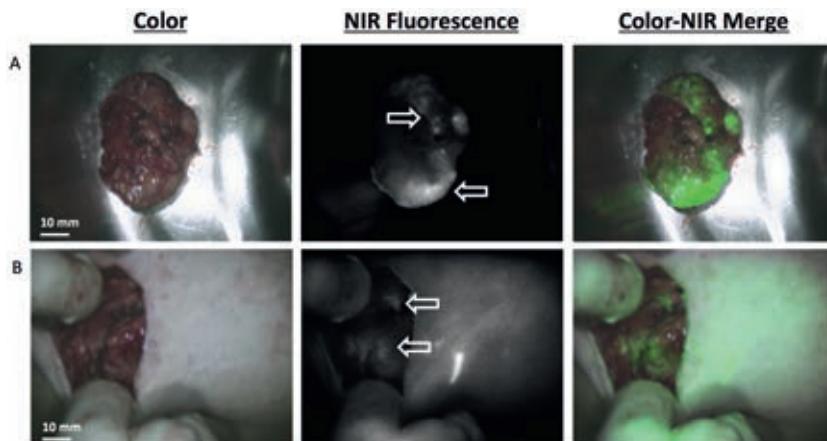
Figure 3. NIR fluorescence imaging of a tumor resection with positive margins

A. Resected specimen after wide local excision. Fluorescent signal was seen at the deep margin of the resection specimen, indicated by arrows. **B.** Inspection of wound bed after resection. Fluorescent signal was seen at resection margins indicated by arrows. Direct re-resection of the fluorescent tissue was performed, which contained malignant tumor tissue. Tumor was an infiltrating lobular adenocarcinoma, grade 2, ER+ PR- Her2/neu -.

In the patients with negative resection margins, median minimal distance of tumor tissue to resection margin was 3 (range 1-20).

Histological validation of MB positive tumors with fluorescence microscopy showed a clear overlay between fluorescent signal and tumor tissue (Figure 2B).

Three patients in the early administration group experienced transient mild pain of the lower arm during administration of MB, which disappeared after flushing the intravenous cannula with saline. No other adverse reactions associated with the use of MB or the Mini-FLARE™ image-guided surgery system were observed.

DISCUSSION

The current study demonstrated feasibility of real-time identification of breast cancer using NIR fluorescence imaging and MB. In 83% of patients, tumor demarcation as identified by NIR fluorescence imaging corresponded to histological presence of tumor. In addition, in one case surgical management was changed based on intraoperative NIR fluorescence findings, which avoided the need for re-resection.

During breast cancer surgery, the distinction between healthy and malignant tissue is often not evident, resulting in positive resection margins in up to 40% of patients undergoing breast conserving surgery[12;13]. Despite major improvements in preoperative imaging, real-time intraoperative imaging modalities are lacking[2]. Therefore, breast cancer surgeons often still have to rely on palpation and previously obtained mammography or MRI to determine the extent of resection. Optical imaging using exogenous contrast agents could usher in a new era in surgical oncology. However, to successfully use this modality both a clinical-grade intraoperative fluorescence imaging system and a tumor-specific NIR probe are obligatory. To date multiple camera systems have become clinically available, however FDA/EMA approved tumor-specific probes are still lacking. Therefore, it is important to exploit clinically available contrast agents, such as indocyanine green and MB[14] whenever possible.

Several papers have reported the intraoperative use of MB for identification of various tumors. As early as 1971, MB was used at high concentration as a visible blue dye to stain parathyroid adenomas after systemic administration[15]. Thereafter, it was shown that there was a high uptake of the tracer in various kinds of neuroendocrine tumors[16-18]. One of the disadvantages of using MB is

that the high dose (7.5 mg/kg) used in these prior studies, which was needed for visualization of the blue colored dye the human eye, brings substantial risk of serious adverse events, such as toxic metabolic encephalopathy[19].

NIR fluorescence imaging permits visualization of MB at low concentration because MB fluoresces at 700 nm. In transgenic mice, Winer et al.[20] showed intraoperative identification of insulinoma, a pancreatic neuroendocrine tumor, using NIR fluorescence imaging and MB. In a clinical setting, this technique has been used for the intraoperative identification of parathyroid adenomas and a solitary fibrous tumor of the pancreas[21;22]. In these prior studies, a dose of only 0.5 - 0.1 mg/kg MB was used, which resulted in clear fluorescent signal in the identified lesions. Although we did not explore dose in this feasibility study, our results suggest that a formal study of dose, which includes higher doses than 1.0 mg/kg, is warranted. Such a study could answer definitively if the 17% of tumors that were not identified using MB were because the dose was too low.

The exact mechanism of tracer uptake in these tumors is unclear. The physicochemical similarities of MB and ^{99m}Tc-MIBI, both lipophilic and cationic, suggest a possible common mechanism. Lipophilic captions were originally developed as myocardial perfusion agents, and subsequently used as tumor-seeking agents in a variety of tumors[23]. They emerged as suitable tools to explore specific cellular processes and functions in malignant tumors. In several studies, it was shown that lipophilic cations show passive influx into cells with large negative plasma membrane and mitochondrial membrane potentials[23;24], with influx being reversible. Cellular processes that are associated with uptake of these tracers are apoptosis, proliferation, P-glycoprotein expression, and neoangiogenesis. However, it has to be further explored whether any of these mechanisms result in MB accumulation in breast cancer tissue.

Using ^{99m}Tc-MIBI, a breast tumor identification rate of 83-90% has been reported. Although our present study was small (N = 24 subjects), our identification rate is in agreement with the sensitivity of ^{99m}Tc-MIBI described in the literature. Based on clinical experience with ^{99m}Tc-MIBI in breast cancer, early and delayed imaging is used to discriminate between malignant and benign lesions, as tracer accumulation is prolonged in malignant lesions. This is in contrary to MR imaging of breast malignancies, where malignant lesions tend to enhance but also washout quicker than benign lesions[25]. This is caused by endothelial fenestration in microvasculature, which leads to increased capillary leakage, and connections between the arteriolar and venular systems

(arteriovenous shunting), which leads to less perfusion of the capillary bed. Complicating the understanding of mechanism even further is the fact that MB can be converted to a non-fluorescent leuco form under certain intracellular redox and pH conditions[11]. Because the exact mechanism of [99mTc]-MIBI and MB uptake in breast tumors is still unclear, future studies have to be done regarding this effect. In the present study, though, no difference was seen between different administration groups in TBR and background signal, suggesting that the more convenient early imaging protocol could be used in future studies.

As NIR fluorescence imaging is a surface technology (≈ 5 mm penetration depth), it is important to understand its capabilities and limitations. To date, research and development of new imaging modalities for oncology mainly focus on the detection of small tumor deposits in the human body. In breast cancer, these small tumor deposits can change surgical decision making, but do not provide such prognostic relevance in breast conserving surgery, as postoperative radiation eliminates microscopic tumor deposits in most cases[26]. For example, the rate of small tumor deposits is 2–3 times higher than the incidence of local recurrence using preoperative MR imaging, resulting in mastectomies that may not be beneficial to patient survival[27]. On the other hand, adequate visualization of tumor margins intraoperatively would be beneficial to lower the number of R1 resections and to avoid the need for re-resections and radiotherapeutic boost therapy[28]. Using intraoperative NIR fluorescence imaging, it is not possible to image the whole breast for small tumor deposits due to the limited penetration depth. However, the optical properties of NIR fluorescence are very well suited for the visualization of possible residual tumor cells at the resection margin. Additionally, NIR fluorescence has an exceptionally high spatial resolution compared to conventional imaging techniques.

To benefit from the full potential for NIR fluorescence imaging several factors are of paramount importance and need to be optimized: 1) the concentration of the NIR fluorophore in the target tissue, 2) minimizing photon absorption and scattering in the tissue, 3) maximizing excitation power of NIR excitation without inducing photobleaching or photo damage to tissue, and 4) the sensitivity of the CCD chip on the detector. Methylene Blue becomes a moderate-strength fluorophore when used at low concentrations, with an excitation maximum of 670 nm. Contrast agents with an emission peak of ≈700 nm have several limitations compared to 800 nm fluorophores with respect to quantum yield, penetration depth, and autofluorescence. It is hoped that new

tumor-specific "800 nm" contrast agents will become widely available during the next few years, although MB could fill the gap in the meantime. Improved laser or LED light sources and cameras are under constant development to overcome the imaging system associated factors.

Another important consideration is extraneous NIR fluorescence generated from other drugs in the surgical field. During this study we found that Patent Blue, used for sentinel lymph node mapping, exhibited a weak NIR fluorescence at 700 nm that could confound the MB results (data not shown). Because we have previously demonstrated that blue dye can be omitted from sentinel lymph node mapping when indocyanine green (ICG) is used[29], and the FLARE imaging system is capable of imaging 2 independent channels of NIR fluorescence, e.g., NIR Channel 1 for MB-guided breast cancer resection and NIR Channel 2 for ICG-guided sentinel lymph node mapping, it should be possible to eliminate Patent Blue from future protocols and thus eliminate this potential confounder.

The primary endpoint of this study was the identification ratio of breast cancer using NIR fluorescence and MB and optimization of injection timing. As it was the first feasibility study with MB in breast cancer, no outcomes data were collected to correlate with intraoperative NIR fluorescence findings. Therefore, it is not possible to draw conclusions on the prognostic relevance of the technology, although one might ponder that true negative MB uptake selected for tumors of low perfusion and relatively low metastatic potential. Thereby only one patient directly benefitted from this technique with respect to direct resection of residual tumor tissue due to the reasons mentioned above. Future studies will need to address this and other remaining questions.

In conclusion, this is the first study to demonstrate the use of low dose MB for the real-time identification of breast cancer using NIR fluorescence and MB. No difference was seen between different administration groups in TBR and background signal, suggesting that the more convenient early imaging protocol could be used in future studies. Although larger studies are necessary to determine patient benefit, results with MB are promising and improved contrast agents will likely become available in the future.

ACKNOWLEDGEMENTS

REFERENCES

1. Hortobagyi GN, de la Garza SJ, Pritchard K et al. The global breast cancer burden: variations in epidemiology and survival. *Clin Breast Cancer* 2005;6:391-401.

2. Pleijhuis RG, Graafland M, de VJ, Bart J, de jong JS, van Dam GM. Obtaining adequate surgical margins in breast-conserving therapy for patients with early-stage breast cancer: current modalities and future directions. *Ann Surg Oncol* 2009;16:2717-2730.

3. Xu HB, Li L, Xu Q. Tc-99m sestamibi scintimammography for the diagnosis of breast cancer: meta-analysis and meta-regression. *Nucl Med Commun* 2011;32:980-988.

4. O'Connor M, Rhodes D, Hruska C. Molecular breast imaging. *Expert Rev Anticancer Ther* 2009;9:1073-1080.

5. Kim SJ, Kim IJ, Bae YT, Kim YK, Kim DS. Comparison of early and delayed quantified indices of double-phase (99m)Tc MIBI scintimammography in the detection of primary breast cancer. *Acta Radiol* 2005;46:148-154.

6. Nakayama A, Bianco AC, Zhang CY, Lowell BB, Frangioni JV. Quantitation of brown adipose tissue perfusion in transgenic mice using near-infrared fluorescence imaging. *Mol Imaging* 2003;2:37-49.

7. Tanaka E, Chen FY, Flaumenhaft R, Graham GJ, Laurence RG, Frangioni JV. Real-time assessment of cardiac perfusion, coronary angiography, and acute intravascular thrombi using dual-channel near-infrared fluorescence imaging. *J Thorac Cardiovasc Surg* 2009;138:133-140.

8. Vahrmeijer AL, Hutteman M, van der Vorst JR, van de Velde CJ, Frangioni JV. Image-guided cancer surgery using near-infrared fluorescence. *Nat Rev Clin Oncol* 2013.

9. Lu G, Shih WJ, Huang HY et al. 99Tcm-MIBI mammoscintigraphy of breast masses: early and delayed imaging. *Nucl Med Commun* 1995;16:150-156.

10. Mieog JS, Troyan SL, Hutteman M et al. Towards Optimization of Imaging System and Lymphatic Tracer for Near-Infrared Fluorescent Sentinel Lymph Node Mapping in Breast Cancer. *Ann Surg Oncol* 2011;18:2483-2491.

11. Matsui A, Tanaka E, Choi HS et al. Real-time, near-infrared, fluorescence-guided identification of the ureters using methylene blue. *Surgery* 2010;148:78-86.

12. Park CC, Mitsumori M, Nixon A et al. Outcome at 8 years after breast-conserving surgery and radiation therapy for invasive breast cancer: influence of margin status and systemic therapy on local recurrence. *J Clin Oncol* 2000;18:1668-1675.

13. Miller AR, Brandao G, Prihoda TJ, Hill C, Cruz AB, Jr., Yeh IT. Positive margins following surgical resection of breast carcinoma: analysis of pathologic correlates. *J Surg Oncol* 2004;86:134-140.

14. Schaafsma BE, Mieog JS, Hutteman M et al. The clinical use of indocyanine green as a near-infrared fluorescent contrast agent for image-guided oncologic surgery. *J Surg Oncol* 2011;104:323-332.

15. Dudley NE. Methylene blue for rapid identification of the parathyroids. *Br Med J* 1971;3:680-681.

16. Gordon DL, Airan MC, Thomas W, Seidman LH. Parathyroid identification by methylene blue infusion. *Br J Surg* 1975;62:747-749.

17. Keaveny TV, Fitzgerald PA, McMullin JP. Selective parathyroid and pancreatic staining. *Br J Surg* 1969;56:595-597.

18. Keaveny TV, Tawes R, Belzer FO. A new method for intra-operative identification of insulinomas. *Br J Surg* 1971;58:233-234.

19. Kartha SS, Chacko CE, Bumpous JM, Fleming M, Lentsch EJ, Flynn MB. Toxic metabolic encephalopathy after parathyroidectomy with methylene blue localization. *Otolaryngol Head Neck Surg* 2006;135:765-768.

20. Winer JH, Choi HS, Gibbs-Strauss SL, Ashitate Y, Colson YL, Frangioni JV. Intraoperative Localization of Insulinoma and Normal Pancreas Using Invisible Near-Infrared Fluorescent Light. *Ann Surg Oncol* 2009.

21. van der Vorst JR, Vahrmeijer AL, Hutteman M et al. Near-infrared fluorescence imaging of a solitary fibrous tumor of the pancreas using methylene blue. *World J Gastrointest Surg* 2012;4:180-184.

22. van der Vorst JR, Schaafsma BE, Verbeek FP et al. Intraoperative Near-Infrared Fluorescence Imaging of Parathyroid Adenomas using Low-Dose Methylene Blue. *Head Neck* 2013.

23. Del Vecchio S., Salvatore M. 99mTc-MIBI in the evaluation of breast cancer biology. *Eur J Nucl Med Mol Imaging* 2004;31 Suppl 1:S88-S96.

24. Murphy MP. Targeting lipophilic cations to mitochondria. *Biochim Biophys Acta* 2008;1777:1028-1031.

25. Millet I, Curros-Doyon F, Molinari N et al. Invasive Breast Carcinoma: Influence of Prognosis and Patient-related Factors on Kinetic MR Imaging Characteristics. *Radiology* 2014;270:57-66.

26. Clarke M, Collins R, Darby S et al. Effects of radiotherapy and of differences in the extent of surgery for early breast cancer on local recurrence and 15-year survival: an overview of the randomised trials. *Lancet* 2005;366:2087-2106.

27. Bloom S, Morrow M. A clinical oncologic perspective on breast magnetic resonance imaging. *Magn Reson Imaging Clin N Am* 2010;18:277-94.

28. Poortmans PM, Collette L, Horiot JC et al. Impact of the boost dose of 10 Gy versus 26 Gy in patients with early stage breast cancer after a microscopically incomplete lumpectomy: 10-year results of the randomised EORTC boost trial. *Radiother Oncol* 2009;90:80-85.

29. van der Vorst JR, Schaafsma BE, Verbeek FP et al. Randomized Comparison of Near-infrared Fluorescence Imaging Using Indocyanine Green and 99(m) Technetium With or Without Patent Blue for the Sentinel Lymph Node Procedure in Breast Cancer Patients. *Ann Surg Oncol* 2012;19:4104-4111.

Chapter 4

First experience on laparoscopic near-infrared fluorescence imaging of hepatic uveal melanoma metastases using indocyanine green

Quirijn R.J.G. Tummers[1], Floris P.R. Verbeek[1], Hendrica A.J.M. Prevoo[1], Andries E. Braat[1], Coen I.M. Baeten[1], John V. Frangioni[2,3], Cornelis J.H. van de Velde[1] and Alexander L. Vahrmeijer[1].

[1] Department of Surgery, Leiden University Medical Center
[2] Department of Radiology, [3] Division of Hematology/Oncology, Department of Medicine, Beth Israel Deaconess Medical Center, Boston, USA

ABSTRACT

Background: Uveal melanoma is the most common primary intraocular tumor in adults and up to 50% of patients will develop liver metastases. Complete surgical resection of these metastases can improve 5-year survival, but only a few patients are eligible for radical surgical treatment. The aim of this study was to introduce a near-infrared (NIR) fluorescence laparoscope during minimally invasive surgery for intraoperative identification of uveal melanoma hepatic metastases and to use it to provide guidance during resection.

Methods: Three patients diagnosed with one solitary liver metastasis from uveal melanoma are presented. Patients received 10 mg indocyanine green (ICG) intravenously 24 h before surgery. A NIR fluorescence laparoscope was used to detect malignant liver lesions.

Results: In all 3 patients, laparoscopic NIR fluorescence imaging using ICG successfully identified uveal melanoma metastases. In 2 patients, multiple additional lesions were identified by inspection and NIR fluorescence imaging, which were not identified by preoperative conventional imaging. In one patient, one additional lesion, not identified by computed tomography, magnetic resonance imaging, laparoscopic ultrasonography and inspection, was observed with NIR fluorescence imaging only. Importantly, NIR fluorescence imaging provided guidance during resection of these metastases.

Conclusions: We describe the successful use of laparoscopic identification and resection of uveal melanoma liver metastases using NIR fluorescence imaging and ICG. This procedure is minimally invasive, and should be used as complementary to conventional techniques for the detection and resection of liver metastases.

INTRODUCTION

Uveal melanoma is the most common primary intraocular tumor in adults and up to 50% of patients will ultimately develop distant metastases[1]. In 90-95% of these patients, the metastases will involve the liver[2;3]. Complete resection of these metastases can prolong survival, however only few patients are eligible for radical surgical treatment[4-6]. Therefore, it is of great importance to select and treat these patients carefully, to prevent unnecessary laparotomies and to fully resect sites of metastasis. Minimally invasive procedures have become important in daily clinical practice, are increasingly used for liver surgery, and might help to optimize the resection of malignant disease.

Near-infrared (NIR) fluorescence imaging using indocyanine green (ICG) is a promising technique to assist in the intraoperative identification of liver metastases in real time[7-10]. ICG is excreted exclusively into the bile after intravenous injection and it has been hypothesized that colorectal liver metastases can be visualized due to passive accumulation of ICG caused by hampered biliary excretion, which results in a fluorescent rim around metastases[7;11].

Several clinical studies describe the use of NIR fluorescence imaging to visualise primary hepatocellular carcinomas[8], as well as liver metastases from colorectal[12], and pancreatic cancers[9] after intravenous injection of ICG, 1 to 14 days prior to surgery. The dose and interval between ICG administration and surgery are key determinants of the remaining background fluorescence signal in the liver and the fluorescent rim surrounding the tumor. A dose finding study using an open intraoperative imaging system (Mini-FLARE[13]) in patients with colorectal liver metastases was recently performed in our center[12], and 10 mg ICG administered 24 h before surgery was found to be the most favorable dosage and time point of ICG administration. Moreover, in 12.5% of patients additional small and superficially located lesions were detected using NIR fluorescence, which were otherwise undetectable.

Published cases to date for intraoperative detection of liver metastases using NIR fluorescence and ICG were performed as open procedures. A laparoscopic operation is preferable for patients with liver metastases from uveal melanoma, due to the high risk of multiple small metastases. When multiple metastases are identified during surgery, patients would not benefit from liver resection, and can be saved an unnecessary laparotomy by performing this minimally

invasive technique. This technical report is the first to describe the use of ICG and laparoscopic NIR fluorescence imaging to identify and resect melanoma liver metastasis during laparoscopic liver surgery.

METHODS

Intraoperative laparoscopic near-infrared imaging system
Intraoperative NIR fluorescence imaging of the liver was performed using a newly developed laparoscopic high definition (HD) fluorescence imaging system by Karl Storz GmbH & Co. KG, Germany, which included a plasma light guide and a 30 degree angle, 10 mm laparoscope, applicable for white light (WL), autofluorescence, and ICG-imaging. The system was used for intraoperative conventional imaging (WL mode) and real-time fluorescence imaging (760 nm light, ICG mode) and allowed easy switching between WL mode and ICG mode by using a foot pedal. No overlay of conventional and fluorescent images was possible yet, but anatomical orientation could be maintained due to the easy switching between light modes, the anatomical translucence during ICG mode and the stable position of the laparoscope. Images were recorded using a charge-coupled device camera.

Preparation and administration of indocyanine green
ICG (25 mg vials) was purchased from Pulsion Medical Systems (Munich, Germany) and resuspended in 10 cc of sterile water for injection to yield a 2.5 mg/ml (3.2 mM) stock solution. Of this stock solution 4 mL, corresponding to a dose of 10 mg, was administered intravenously 24 h before surgery. This optimal timing was based on previous studies in patients with colorectal liver metastases and the Mini-FLARE open quantitative imaging system.

***Ex vivo* imaging and fluorescence microscopy of resected lesion**
After slicing of the resected lesion at the Pathology department, fluorescent imaging was performed with the FLARE imaging system, which was previously described[14]. Fluorescence microscopy images were obtained with the Odyssey Infrared Imaging System (LI-COR, USA).

Preoperative imaging modalities

Patients received standard-of-care preoperative imaging modalities including ultrasound (US), computed tomography (CT, Toshiba Aquilion 16), magnetic resonance imaging (MRI, Philips Intera 1.5T) and/or positron emission tomography (PET, Philips Gemini 64 PET/CT) scans. For PET scan imaging, the radiopharmaceutical agent 18F-FDG was used.

Clinical trial

The study was approved by the Local Medical Ethics Committee of the Leiden University Medical Center and was performed in accordance with the ethical standards of the Helsinki Declaration of 1975. The study was registered in the Netherlands Trial Register as NTR3869.

RESULTS

We present three patients; all diagnosed with a solitary liver metastasis by preoperative US or CT. One patient was referred from another hospital, diagnosed with uveal melanoma and a solitary liver metastasis. Two patients were previously treated for uveal melanoma.

The first patient was a 75-year old woman, referred from another hospital, diagnosed with uveal melanoma of the left eye. By US, CT and PET scans, a suspected 28 mm metastasis was found in the right liver lobe. She was planned for simultaneous laparoscopic metastasectomy and enucleation of the left eye. 10 mg ICG was administered intravenously 24 h before surgery. During surgery, multiple lesions of 1 to 10 mm were identified on the surface of the left and right liver lobe by inspection and by a clear fluorescent rim around the tumors (Figure 1). One of the suspected lesions proved to be malignant, and no further liver resection was performed. Enucleation of the left eye was performed, and patient was offered systemic therapy. Patient experienced progressive disease under Dacarbazine treatment and subsequent Ipilimumab treatment during 10 months of follow-up.
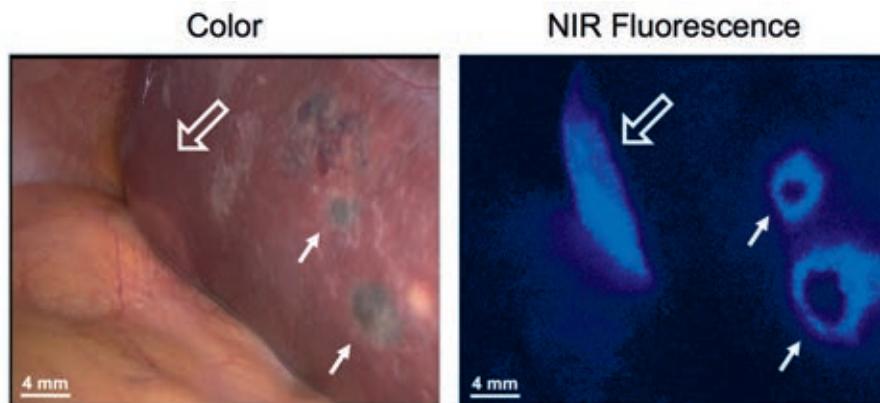
Figure 1. Identification of liver metastases

Multiple uveal liver metastases, identified by inspection and NIR fluorescence imaging as a typical fluorescent rim (arrows) around each lesion, 24 h after intravenous injection of 10 mg ICG. Open arrows indicate the preoperative known metastasis.

The second patient was a 66-year-old woman treated 22 months earlier by enucleation of the right eye because of uveal melanoma. During 20 months of follow-up using US, CT, MRI and PET scans, no liver metastases were seen. Now she was diagnosed with a 12 mm liver metastasis in liver segment III on both CT and MRI scans. There were no signs of other hepatic or extrahepatic metastatic lesions. She was planned for laparoscopic metastasectomy. Ten mg ICG was administered intravenously 24 h before surgery. The previously diagnosed lesion was detected by inspection, laparoscopic ultrasonography (LUS), and NIR fluorescence imaging, and was removed under fluorescent guidance (Figures 2a and 3; supplementary video's, online available).

Using NIR fluorescence imaging, an additional suspicious lesion in segment III was identified, which showed a typical 1.5 mm fluorescent rim (Figure 2b). This lesion was characterized as a hemangioma by inspection, and was not identified with LUS. It was resected under fluorescent guidance. Both removed lesions proved to be malignant by histological assessment and were radically removed (Figure 4). No other lesions were identified by inspection, LUS or NIR fluorescence imaging. Patient recovered well from surgery, and no recurrent disease was seen during 15 months of follow-up.
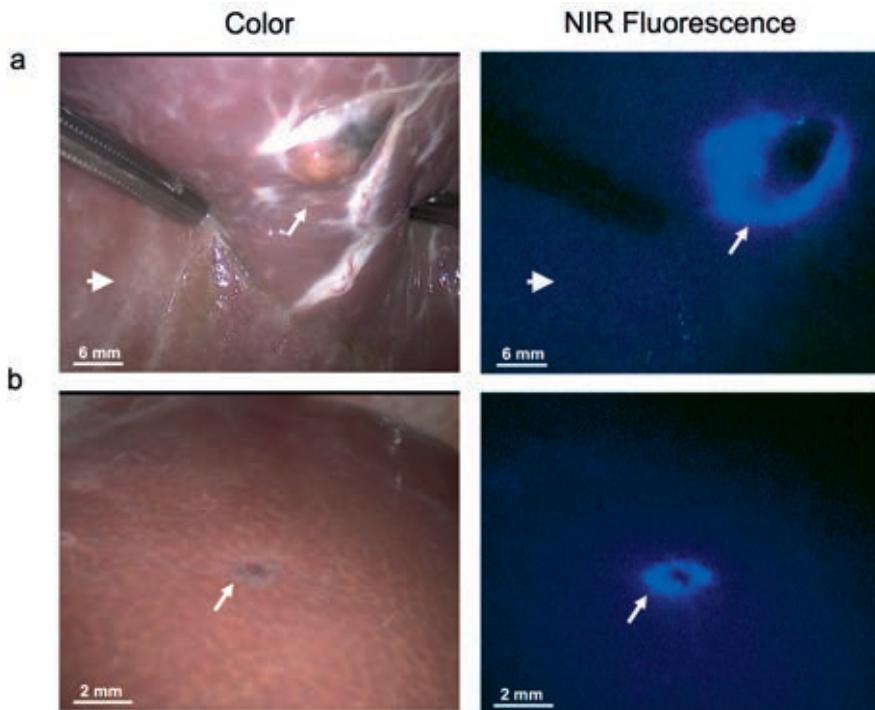
Figure 2. NIR fluorescence imaging of uveal liver metastases

A. An uveal liver metastasis (arrow) is clearly identified by a rim around the tumor *in vivo*. Normal liver tissue (arrowhead) shows minimal background fluorescence. **B.** A small superficial metastasis (arrow) was identified by NIR fluorescence imaging, but was characterized as a hemangioma by visual inspection and was not visible by LUS.

The third patient was a 65-year-old woman treated 6 months earlier with ruthenium for uveal melanoma. She was now diagnosed with a 17 mm liver metastasis in segment IV on US and CT. There were no signs of other liver lesions or extrahepatic disease and she was planned for a laparoscopic metastasectomy. Ten mg ICG was administered intravenously 24 h before surgery. During surgery, multiple lesions from 1 to 10 mm were identified on the surface of the left and right liver lobe by inspection and a clear fluorescent rim around the tumor using the ICG mode of the laparoscope. Uveal melanoma metastases were confirmed by frozen section of two lesions in segments III and IVb, respectively. No further resections were performed and the patient was offered systemic therapy. Patient experienced stable disease for 16 months under protein kinase C inhibitor treatment, whereafter new progression was seen.
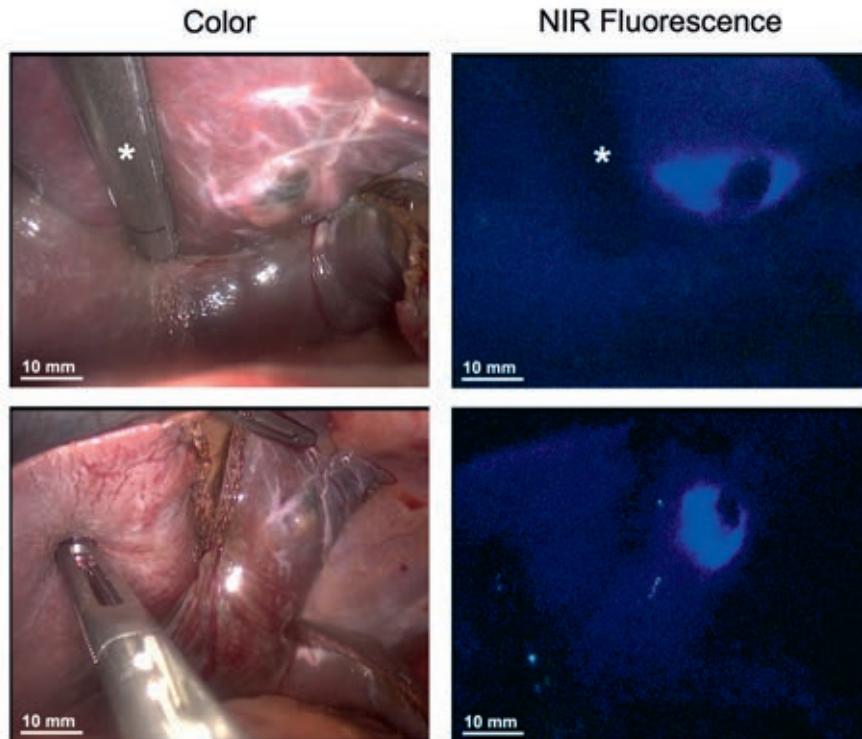
Figure 3. Fluorescent guidance during resection

NIR fluorescence imaging was used as guidance during resection of uveal liver metastases. Resection was performed using an Endo GIA™ 45 reload stapler (Covidien) (asterisk).
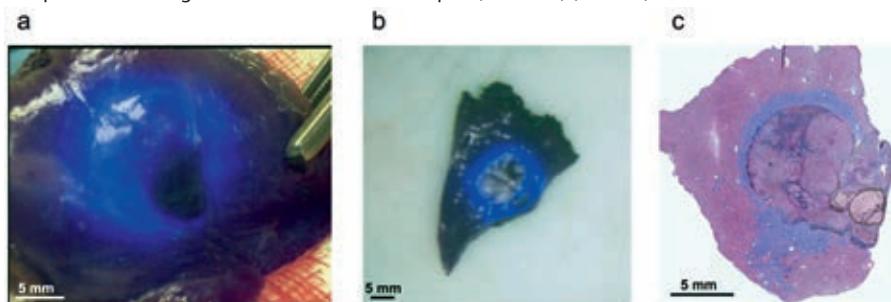
Figure 4. Ex vivo imaging and fluorescence microscopy of resected lesion

A. *Ex vivo* imaging of resected lesion using the laparoscope. **B.** *Ex vivo* imaging after slicing under FLARE imaging system guidance. **C.** Microscopic overlay of Hematoxylin and Eosin staining of the resected lesion and fluorescent signal (Odyssey Infrared Imaging System, LI-COR). A clear fluorescent rim was observed around the malignant lesion.

No adverse reactions associated with the use of ICG or NIR fluorescence imaging were observed in any patient.

DISCUSSION

Because only 3% [15;16] of patients with uveal melanoma are candidates for curative resection of hepatic metastases, a precise and minimally invasive method for selecting appropriate candidates is desperately needed. To the best of our knowledge, this is the first paper describing the use of laparoscopic NIR fluorescence imaging with ICG for the detection and removal of liver metastasis in this disease. Due to hampered visibility and the inability to palpate the liver surface during laparoscopy, NIR fluorescence imaging adds value to the procedure itself. In contrast to ultrasonography, which can only show where the resection margins can be kept before resection, NIR fluorescence imaging provides real-time guidance, helps minimize the resection of normal liver tissue, and permits inspection of the area to ensure the completeness of tumor resection.

In all 3 patients of this study, lesions were found by NIR fluorescence that were not seen on preoperative US and CT scans. Moreover, in one patient, one lesion intraoperatively characterized as hemangioma by visual inspection, and not identified by LUS, was successfully identified as metastasis with NIR fluorescence imaging and could be radically removed under real-time fluorescence guidance.

A major limitation of NIR fluorescence imaging is its limited depth penetration of ≈ 5 mm. In figure 4, a depth penetration of at least 5 mm can be inferred because the NIR fluorescence signal of the lesion was identified at the anterior surface of the liver (supplementary video part 1), while the lesion itself was located at the posterior surface of the liver. More sensitive imaging systems and fluorophores with higher quantum yield could potentially increase depth penetration even further. Preoperative CT scanning and LUS do not have this disadvantage and are consequently more appropriate for deeper lesions. However, small and superficially located occult metastases are known to be difficult to detect using LUS and inspection. Although LUS is a reliable modality to identify liver metastases[17], and still required to identify deep (≥ 5 mm) metastases in the liver, our results suggest that NIR fluorescence imaging is complementary, and helps to find small, superficially located lesions. In addition, as shown in the supplementary video, NIR fluorescence imaging becomes of value in the resection of even deep lesions once they are initially identified.

Further technical developments of laparoscopic NIR imaging systems are in progress and aim to improve the real-time intraoperative display of NIR fluorophores[18;19].

In conclusion, we describe the successful use of a novel NIR fluorescence laparoscopy procedure for the identification and resection of uveal melanoma liver metastasis using 10 mg ICG administered intravenously 24 h prior to surgery. This procedure is minimally invasive, relatively easy to perform, and is complementary to conventional techniques for the detection and complete resection of liver metastases from uveal melanoma.

ACKNOWLEDGEMENTS

REFERENCES

1. Bedikian AY. Metastatic uveal melanoma therapy: current options. *Int Ophthalmol Clin* 2006;46:151-166.

2. Spagnolo F, Caltabiano G, Queirolo P. Uveal melanoma. *Cancer Treat Rev* 2012;38:549-553.

3. Becker JC, Terheyden P, Kampgen E et al. Treatment of disseminated ocular melanoma with sequential fotemustine, interferon alpha, and interleukin 2. *Br J Cancer* 2002;87:840-845.

4. Hsueh EC, Essner R, Foshag LJ, Ye X, Wang HJ, Morton DL. Prolonged survival after complete resection of metastases from intraocular melanoma. *Cancer* 2004;100:122-129.

5. Frenkel S, Nir I, Hendler K et al. Long-term survival of uveal melanoma patients after surgery for liver metastases. *Br J Ophthalmol* 2009;93:1042-1046.

6. Vahrmeijer AL, van de Velde CJ, Hartgrink HH, Tollenaar RA. Treatment of melanoma metastases confined to the liver and future perspectives. *Dig Surg* 2008;25:467-472.

7. Ishizawa T, Fukushima N, Shibahara J et al. Real-time identification of liver cancers by using indocyanine green fluorescent imaging. *Cancer* 2009;115:2491-2504.

8. Gotoh K, Yamada T, Ishikawa O et al. A novel image-guided surgery of hepatocellular carcinoma by indocyanine green fluorescence imaging navigation. *J Surg Oncol* 2009;100:75-79.

9. Yokoyama N, Otani T, Hashidate H et al. Real-time detection of hepatic micrometastases from pancreatic cancer by intraoperative fluorescence imaging: Preliminary results of a prospective study. *Cancer* 2011;118:2813-9.

10. Tanaka T, Takatsuki M, Hidaka M et al. Is a fluorescence navigation system with indocyanine green effective enough to detect liver malignancies? *J Hepatobiliary Pancreat Sci* 2013.

11. Verbeek FP, van der Vorst JR, Schaafsma BE et al. Image-guided hepatopancreatobiliary surgery using near-infrared fluorescent light. *J Hepatobiliary Pancreat Sci* 2012;19:626-637.

12. van der Vorst JR, Schaafsma BE, Hutteman M et al. Near-infrared fluorescence-guided resection of colorectal liver metastases. *Cancer* 2013;119:3411-3418.

13. Mieog JS, Troyan SL, Hutteman M et al. Towards Optimization of Imaging System and Lymphatic Tracer for Near-Infrared Fluorescent Sentinel Lymph Node Mapping in Breast Cancer. *Ann Surg Oncol* 2011;18:2483-2491.

14. Troyan SL, Kianzad V, Gibbs-Strauss SL et al. The FLARE intraoperative near-infrared fluorescence imaging system: a first-in-human clinical trial in breast cancer sentinel lymph node mapping. *Ann Surg Oncol* 2009;16:2943-2952.

15. Herman P, Machado MA, Montagnini AL, D'Albuquerque LA, Saad WA, Machado MC. Selected patients with metastatic melanoma may benefit from liver resection. *World J Surg* 2007;31:171-174.

16. Rose DM, Essner R, Hughes TM et al. Surgical resection for metastatic melanoma to the liver: the John Wayne Cancer Institute and Sydney Melanoma Unit experience. *Arch Surg* 2001;136:950-955.

17. Vigano L, Ferrero A, Amisano M, Russolillo N, Capussotti L. Comparison of laparoscopic and open intraoperative ultrasonography for staging liver tumours. *Br J Surg* 2013;100:535-542.

18. Ashitate Y, Stockdale A, Choi HS, Laurence RG, Frangioni JV. Real-time simultaneous near-infrared fluorescence imaging of bile duct and arterial anatomy. *J Surg Res* 2011;Jul;176(1):7-13.

19. Matsui A, Tanaka E, Choi HS et al. Real-time intra-operative near-infrared fluorescence identification of the extrahepatic bile ducts using clinically available contrast agents. *Surgery* 2010;148:87-95.

-

Intraoperative identification of normal pituitary gland and adenoma using near-infrared fluorescence imaging and low-dose indocyanine green

Marco J.T. Verstegen[1*], Quirijn R.J.G. Tummers[2*], Pieter J. Schutte[1],
Alberto M. Pereira[3], Wouter R. van Furth[1], Cornelis J.H. van de Velde[2],
Martijn J.A. Malessy[1] and Alexander L. Vahrmeijer[2]

* M.J.T. Verstegen and Q.R.J.G. Tummers share first authorship.

[1] Department of Neurosurgery, Leiden University Medical Center
[2] Department of Surgery, Leiden University Medical Center
[3] Department of Medicine, Division of Endocrinology, Leiden University Medical Center

ABSTRACT

Background: The intraoperative distinction between normal and abnormal pituitary tissue is crucial during pituitary adenoma surgery to obtain a complete tumor resection, while preserving endocrine function. Near-Infrared (NIR) fluorescence imaging is a technique to intraoperatively visualize tumors by using Indocyanine Green (ICG); a contrast agent allowing visualization of differences in tissue vascularization. Although NIR fluorescence imaging has been described in pituitary surgery it has, in contrast to other surgical areas, never become widely used.

Objective: To evaluate NIR fluorescence imaging in pituitary surgery both qualitatively and quantitatively, and to assess the additional value to resect adenoma tissue under NIR fluorescence guidance.

Methods: We included ten patients planned for transnasal transsphenoidal selective adenomectomy. Patients received multiple intravenous administrations of 5 mg ICG, up to a maximum of 15 mg per patient. Endoscopic NIR fluorescence imaging was performed at multiple points in time. The NIR fluorescent signal in both the adenoma and pituitary gland was obtained and the Fluorescence Contrast Ratio (FCR) was assessed.

Results: Four patients had Cushing's disease, one had Acromegaly and one had a Prolactinoma. Four patients had a non-functioning macro-adenoma. In nine out of 10 patients with a histologically proven pituitary adenoma, the normal pituitary gland showed stronger fluorescent signal than the adenoma. A FCR of normal pituitary gland to adenoma of 1.5 ± 0.2 was obtained. In two patients, adenoma resection actually took place under NIR fluorescence guidance, instead of under white light.

Conclusion: NIR fluorescence imaging can easily and safely be implemented in pituitary surgery. Timing of ICG administration is important for optimal results and warrants further study. It appears that injection of ICG can best be postponed until some part of the normal pituitary gland is identified. Subsequent repeated low-doses ICG administration improved the distinction between adenoma and gland.

INTRODUCTION

In transsphenoidal surgery it is important to be able to distinguish between normal pituitary gland and pituitary adenoma tissue for two reasons: 1) to obtain a complete tumor resection and 2) to preserve endocrine function. The vascular pattern between the normal pituitary gland and tumor tissue differs[1;2]. This difference can be shown with preoperative magnetic resonance imaging (MRI), making use of dynamic administration of gadolinium. Normal pituitary tissue is visualized by contrast enhancement[3]. However, during surgery, the identification of normal gland and adenoma is based on differences in tissue characteristics, such as colour and consistency. This difference can be difficult to detect.

Transsphenoidal surgery is an established and relatively safe procedure. More than 95% of the pituitary tumors are operated via this approach[4]. Unfortunately, remission rates of hormone secreting tumors are not perfect, while surgery induced pituitary deficiencies still occur[5]. Moreover, in patients with initial remission, recurrences occur due to endocrine activity of postoperative tumor remnants. It is therefore likely that the success rate of surgery can be improved by increasing visual differentiation between adenoma and the normal gland.

Near-infrared (NIR) fluorescence imaging is an innovative technique to visualize tumors, vital structures, and lymph nodes during surgery[6]. It is currently clinically used for several medical indications. These are intraoperative imaging of liver metastases, breast cancer and parathyroid adenomas[7-10]. One of the clinically available NIR fluorescent contrast agents is indocyanine green (ICG). ICG is an ideal agent for real-time visualisation of differences in tissue vascularisation. The excitation and emission profiles of ICG in the NIR light spectrum make it possible to visualize blood vessels covered by a few millimetres of tissue. At present, ICG-imaging is widely used in a variety of surgical procedures[6;11], including several cerebrovascular procedures in neurosurgical practice[12;13].

Litvack et al. first reported the use of ICG in endoscopic pituitary surgery in 2012[14]. In this feasibility study, up to 75 mg ICG was administered intravenously for each procedure. An endoscopic NIR fluorescence imaging system was used to capture fluorescent signal. The authors concluded that NIR fluorescence-guided endoscopy was a promising intraoperative modality towards visually distinguishing adenoma from normal gland tissue and thus possibly facilitating

complete tumor resection. Like MRI gadolinium enhancement, NIR fluorescence imaging showed illumination of the normal gland, and delay in illumination of the adenoma. However, unlike gadolinium use for MRI of pituitary tumors, NIR fluorescence imaging has never become widely accepted in clinical practice.

The aim of the current study was to assess the feasibility and potential value of NIR fluorescence imaging in endoscopic pituitary surgery. The detection of the normal gland, with the aid of low-dose ICG was studied and the detected fluorescent signal was scored both qualitatively and quantitatively. Moreover, the possibility to resect adenoma tissue under only NIR fluorescence guidance was evaluated.

METHODS

Patients

Patients included in the study were those diagnosed with a pituitary gland adenoma and having first been scheduled for their initial endoscopic transnasal transsphenoidal surgical resection between January 2013 and March 2014. Only one endoscope and light cable suitable for NIR fluorescence imaging were available, allowing a maximum of one patient per day to be included. All patients gave informed consent. Exclusion criteria were previous transsphenoidal surgery, pregnancy, lactation, renal impairment (eGFR<55) or an allergy to iodine or ICG.

Clinical trial

This clinical trial was performed at the Leiden University Medical Center, a tertiary referral center. The study was approved by the local Medical Ethics Committee and was performed in accordance with the ethical standards of the Helsinki Declaration of 1975.

Patients underwent a standard-of-care endoscopic transnasal transsphenoidal selective adenomectomy, conducted by a team of two neurosurgeons with a vast experience in pituitary surgery. During the procedure, 5 mg ICG was administered intravenously at different time points. The first ICG gift was after exposure of the sellar dura, but prior to opening. The NIR compatible endoscopic device (Image Hub I by Karl Storz GmbH & Co. KG Germany) was used to identify the fluorescent signal. After opening the dura,

the resection of the adenoma was performed making alternating use of visual and fluorescence guidance. Additional boluses of 5 mg ICG were administered after partial resection of the adenoma, in order to obtain new NIR fluorescence images. At the surgeons' judgment of complete resection, new NIR fluorescence imaging was performed to ensure identification of any residual adenomatous tissue. For analysis of fluorescence signal, images were obtained 45 seconds after ICG administration.

Intraoperative endoscopic near-infrared fluorescence imaging system
Intraoperative NIR fluorescence imaging of the pituitary gland was performed using a newly developed endoscopic high definition (HD) fluorescence imaging system by Karl Storz GmbH & Co. KG Germany, the Image Hub I. This system consists of a plasma light guide and a 0-degree angle 5.4-mm endoscope, applicable for white light (WL), autofluorescence and ICG-imaging. The system was used for intraoperative conventional imaging (WL mode) and real-time fluorescence imaging (760-nm light, ICG mode). It allows for easy switching between WL mode and ICG mode using a foot pedal. The overlay of conventional and fluorescent images is not yet possible but anatomical orientation could be maintained due to the easy switching between light modes. Images were recorded using a charge-coupled device camera.

Statistical and image analysis
SPSS statistical software package (Version 20.0, Chicago, IL) was used for statistical analysis. Fluorescent signal of pituitary adenoma and normal gland were reported both qualitatively and quantitatively. Snapshots were taken from the recorded operating videos, for further analysis. For qualitative analysis, fluorescent signal was classified as ++, +, +/- and -. Two observers – M.V. (one of the operating neurosurgeons) and Q.T. – scored the fluorescent signal independently. Where scoring discrepancies occurred, agreement was reached by reassessing the images. Quantitative fluorescent signal was measured using ImageJ version 1.49b (a public domain Java-based image processing program developed at the National Institute of Health). With ImageJ, regions of interest (RoI) were drawn circumventing the fluorescent signal of the adenoma and normal pituitary tissue. Fluorescence Contrast Ratios (FCRs) were calculated by dividing the fluorescent signal of both RoIs. FCRs were reported as mean. Patient age was reported as median and range.

RESULTS

In the inclusion period 58 patients underwent a transnasal transsphenoid operation. Fourteen patients had a different pathology than adenoma. Six patients had been operated before. One patient was allergic to iodine. Ten patients refused participation in the study for a variety of reasons.

The light cable was temporarily broken leading to an inclusions stop for 4 weeks and subsequently exclusion of 7 patients. From the remaining 20 patients always the first patient of the two cases scheduled for surgery that day was included, leading to 10 included patients.

Median age was 50 years, ranging between 28 and 74. Six patients were female. Patients had either clinical features and imaging consistent with Non-Functioning macro-Adenoma (NFMA) (N=4), or were biochemically diagnosed with a functional adenoma (Cushing's disease (N=4), Acromegaly (N=1) and Prolactinoma (N=1)). Patient and tumor characteristics are shown in Table 1. All resected lesions were histologically proven to be a pituitary adenoma.

The first NIR fluorescence images were obtained before opening of the dura. Figure 1 shows an example of fluorescent images of the dura. A clear fluorescent signal in the blood vessels was visible, however no discrimination between normal gland and the adenoma was possible at this point. Enhanced vascularity due to dural invasion of the tumor was not present in our series.
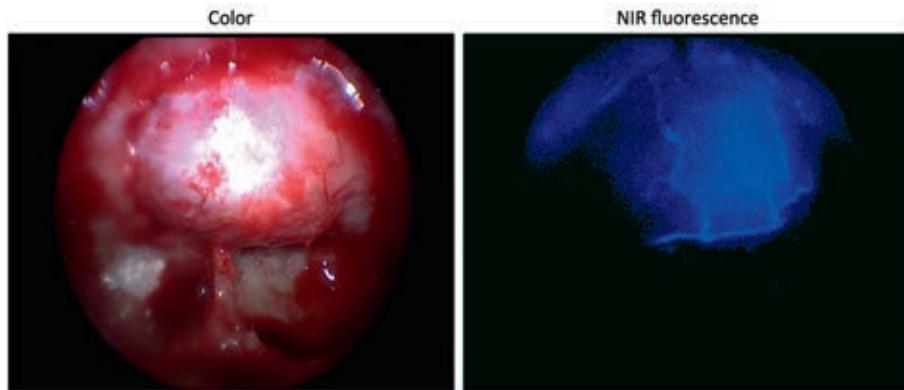

Figure 1. NIR fluorescence imaging of the dura

NIR fluorescence imaging of the unopened dura mater after administration of 5 mg ICG. Fluorescent vessels are visible on the dura. No identification of adenoma or normal pituitary gland is observed.

Table 1. Patient and tumor characteristics

Characteristic	Median	Range	
Age	50	28 - 74	
	N (n = 10)	**%**	
Gender			
M	4	40	
F	6	60	
	Preoperative		**Postoperative**
	N		**N**
Visual deficits			
No deficits	7		10
Minor deficits	2		0
Mild bitemporal deficits	1		0
Cranial nerve deficits			
None	8		8
Total N.III OS	1		0
Mild N.III OD	0		1*
Moderate N.III, slight N.VI OD	1		0
Minor N.VI OD	0		1*
Pituitary Function			
No deficits	6		8
Hypogonadism	3		1
Hypothyriodism	1		1
Hypersecretion			
None	4		10
ACTH	4		0
PRL	1		0
GH and PRL	1		0
Pathology			
Biochemical			
NFMA	4		4
Cushing's disease	4		4
Acromegaly	1		1
Prolactinoma	1		1
IHC			
GH+; PRL +	N/A		2
ACTH+	N/A		5
LH+	N/A		1
Null-cell	N/A		2

Abbreviations: ACTH, adrenocorticotropic hormone; DI, Diabetes Insipidus; GH, Growth hormone; IHC, immunohistochemistry; LH, Luteinizing hormone; N/A, not applicable; OD, oculus dextra; OS, oculus sinistra; PRL, prolactin.
* Recovered completely after 6 months

After opening of the dura, the normal pituitary gland showed a more intense fluorescent signal than the adenoma in nine of the ten patients. In one patient intercavernous sinus venous bleeding prevented assessment of the fluorescent signal. Figure 2 shows images of the fluorescent signal in adenoma and normal gland during resection. In general, during resection, a bright fluorescent normal gland became visible after ICG administration.
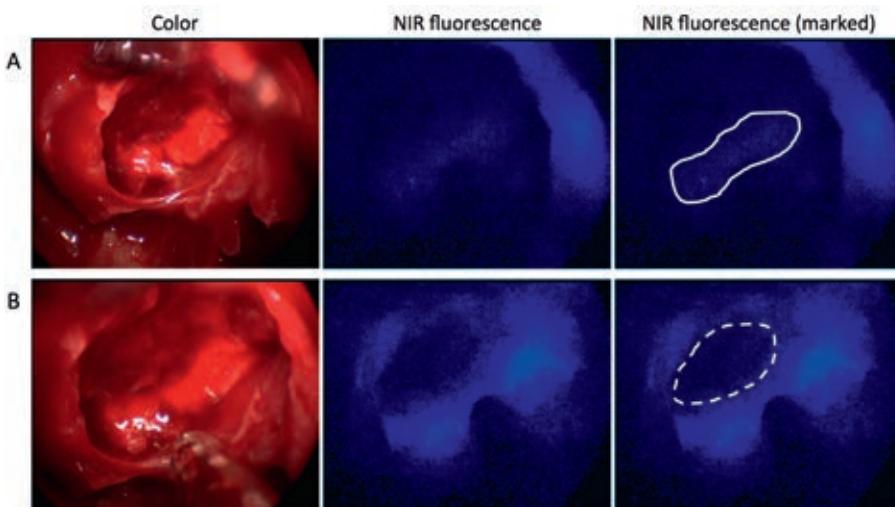
Figure 2. NIR fluorescence imaging of a pituitary adenoma

A. NIR fluorescence imaging of adenoma and normal gland after partial resection of the adenoma. ICG was administered just before opening of the dura, a second bolus of ICG was planned just after making this image. In the color image, a dark red colored remnant of the adenoma is visible. In the NIR fluorescence image, a slightly fluorescent normal gland is visible (circle). The adenoma remnant does not stain fluorescent. **B.** NIR fluorescence imaging of the same patient 60 seconds after the second ICG administration. A bright fluorescent normal pituitary gland is visible. The adenoma remnant remains still non-fluorescent (dashed circle).

Fluorescence intensities were measured 45 seconds after administration. Fluorescent signal with optimal contrast ratios were present for 1-2 minutes, where after the signal slowly decreased over time. The adenomas showed no, or only a weak fluorescent signal. After complete resection of the adenoma, a bright, consistent fluorescent pituitary gland was visible, and no non-fluorescent remnants of adenoma tissue were present anymore (Figure 3).
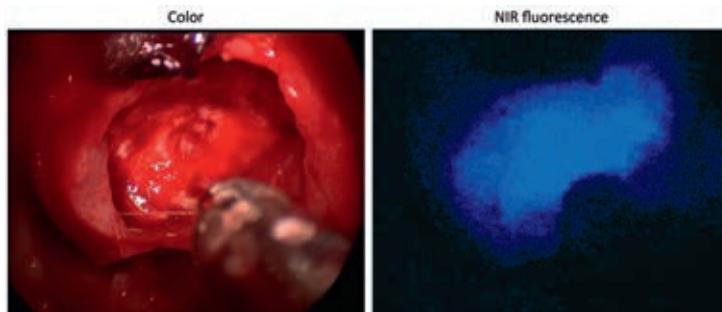

Figure 3. NIR fluorescence imaging after pituitary adenoma resection

NIR fluorescence imaging after resection of the adenoma. A complete fluorescent normal pituitary gland is visible. No non-fluorescent adenoma remnants can be identified.

Table 2 shows the imaging characteristics of the detected lesions. In five patients, no fluorescent signal was observed in the adenoma. In three patients, only weak fluorescence (qualitatively rated as +/-) was observed and in the case of one patient, fluorescent signal was rated as + (#9). The observed FCRs were confirmed by quantitative analysis, wherein a mean FCR of normal pituitary gland to adenoma of 1.5 ± 0.2 was obtained. In addition, two patients suffering from a microadenoma (#6 and #7) exhibited an FCR of 1.3 and 1.4 respectively. In one patient (#2), no discrimination in NIR fluorescent signal between normal gland and adenoma could be observed due to suboptimal timing of the imaging. In this patient, NIR fluorescence imaging was performed according to protocol just before opening of the dura. During resection of the adenoma, venous bleeding occurred that stopped after resection of the adenoma. After the second ICG administration and imaging, no remnant tissue was observed. Therefore, no NIR fluorescent images of the adenoma could be obtained.

Table 2. Imaging characteristics

| Patient ID | Identification of normal gland and stalk on MRI | | | NIR Fluorescence Imaging | | | | |
	Preoperative	Post-operative	WH-class. grade	Dose ICG received (mg)	Location of adenoma	Fluorescent signal pituitary gland	Fluorescent signal adenoma	FCR
1	Cranial on top of adenoma	NP	IV	10	R	++	-	1.4
2	Stalk R; clear normal gland R	Normal	IIBE left	10	L	No distinction possible		
3	Stalk L; suggestion of normal gland	Remnant left side	IIIa	10	R	++	+/-	1.7
4	Stalk R; no normal gland	Normal	IIC	10	Mid - L	+	-	1.8
5	Stalk R; clear normal gland R	Normal	IIAE left	10	L	+	-	1.3
6	Stalk mid; clear normal gland	Normal	I	10	R	+	+/-	1.3
7	Stalk mid; clear normal gland	Normal	I	10	R	+	+/-	1.4
8	Stalk R; clear normal gland R	Normal	IIAE left	10	L	+	-	1.4
9	Stalk L; suggestion of normal gland	Remnant left side	IIB	5	R	++	+	1.5
10	Stalk L; suggestion of normal gland	Remnant left side	IIBE right	15	R	++	-	1.8

Abbreviations: FCR, Fluorescence Contrast Ratio; L, left; mid; midline; N/A, not applicable; NP, not performed; R, right; WH-class, Wilson-Hardy classification

The total individual dose of ICG varied, depending on the ease of surgical resection of the adenoma. The initial ICG gift was prior to tumor removal, the second gift at the end of the procedure, to control for completeness of resection. Most patients thus received a total dose of 10 mg ICG. In one patient, NIR fluorescence imaging showed tumor remnants, which were subsequently removed. A third ICG dose was administered to again check for remnants. The longest time-interval between ICG administration and obtaining images in fluorescence mode was 62 minutes (#12). At this point, weak fluorescence signal was still present, but did not show any contrast ratio. According to study protocol, this led to additional administration of ICG.

Tumor resection was typically done with conventional white light. In two patients (#1 and #3) we performed the tumor resection using predominantly the blue light of NIR fluorescence imaging (up to 9:15 minutes after ICG administration). Although visibility under these lighting conditions is clearly much poorer than with conventional white light, tumor resection seemed facilitated. It was possible to remove the pituitary adenoma in a standard way with curretes and suction. Tumor resection was deemed complete when the gland showed an even bright enhancement under NIR fluorescence imaging. In one of these two patients, a Cerebro Spinal Fluid (CSF) leakage occurred at the opening of the dura and was not related to the resection of the tumour under NIR fluorescence imaging.

In this limited number of patients, we did not find a relation between tumour type and ICG signal. No adverse reactions associated with the use of ICG or the NIR fluorescence imaging system, were observed. Complications associated with the surgical procedure included: 1) leakage of intraoperative CSF in one case (#3); and 2) intraoperative venous bleeding in another case (#9).

DISCUSSION

In this study, successful identification of the normal pituitary gland and pituitary adenomas was possible using endoscopic NIR fluorescence imaging using low dose ICG. In all assessable patients with a histologically proven adenoma, a contrast ratio between adenoma and normal gland was observed. In the only one study on NIR fluorescence imaging in pituitary surgery of Litvack et al.[14] the administered dose of ICG (up to 75 mg) was relative high for NIR fluorescence

imaging. In comparison, in other studies an ICG dose between 2.5 mg, or 0.2 – 0.5 mg/kg was demonstrated successful for the assessment of tissue perfusion after intravenous administration[15-17]. For tumor imaging of colorectal or uveal melanoma liver metastases, intravenous administration of 10 mg ICG proved to be sufficient[7;18]. Furthermore it allows for repeated injections, so that NIR fluorescence imaging can be used during various phases of the tumor resection. The lower dose used in this study compared to the dose used by Litvack et al. appears sufficient and leads to satisfactory results within the timing windows of imaging we used.

The observed FCR between normal gland and tumor tissue was 1.5 ± 0.2. The dynamic character of the imaging facilitated detection of a clear gradient between the normal pituitary gland and the adenoma. Our obtained quantitative ratios cannot be compared to results obtained by others, because only semi-qualitative results are reported yet[14]. To the best of our knowledge, to-date, no quantitative analysis of NIR fluorescence imaging in pituitary surgery had been reported. In future studies, quantitative analysis of NIR fluorescence imaging in pituitary surgery should become a standard in order to further objectively assess the additional value of this technique. A contrast ratio above 2 is generally considered optimal for intraoperative differentiation between tissues. For example, in colorectal liver metastases[18], breast cancer[10] and parathyroid adenomas[9] imaging, FCRs of respectively 7.0, 2.4 and 6.1 are reported. The FCR in pituitary surgery is thus relatively low, although sufficient. In the future hopefully improved contrast agents and imaging systems could potentially further enhance the FCR in pituitary surgery as well.

Optimal timing of ICG administration is crucial to obtain optimal distinction between normal and abnormal tissue. In the current research protocol, the first ICG administration was performed before opening of the dura. The vascularisation of the dura was thereby visualised, but no additional value for identification of the gland or the adenoma was obtained. In our experience, this first gift of ICG was too early. It may help to assess changes in the vascularisation of the dura, suggesting invasive growth of the adenoma. However, we believe that the optimal timing of ICG administration is when the surgeon detects differences in tissue colour and consistency, suggesting that the normal pituitary gland may be identified. The FCR was sufficient to reliably differentiate adenoma from normal gland. Interestingly, adenoma resection only under NIR fluorescence guidance, e.g. without alternating between white and blue

light, was technically possible. Possibly tumor resection under continuous NIR fluorescence guidance, instead of only checking for tumor remnants at the end of surgery may be the best way to use NIR fluorescence guidance in pituitary surgery. From the current study, no optimal interval between ICG administration and peak fluorescence signal can be recommended. For all measurements, an interval of 45 seconds was taken to obtain and analyse fluorescent signal. In our experience, the fluorescent signal and contrast ratio stayed optimal for 1-2 minutes in all patients, and than slowly decreased over time. Timing of ICG administration warrants further systematic study.

For NIR fluorescence imaging during pituitary surgery a special endoscope is needed equipped with an excitation light source to excite fluorophores, and a detection device to capture emitted fluorescence from the exited fluorophores. The dimensions and functionality of this scope are otherwise identical with the regular HD Storz endoscope. ICG was readily available at the pharmacy. The technique of imaging was not complicated and was not associated with any sided effects. In one patient cavernous sinus bleeding prevented assessment of the fluorescence. As long as venous bleeding is well controlled, NIR fluorescence imaging can be used to remove adenoma tissue from the cavernous sinus. NIR fluorescence imaging during endoscopic pituitary surgery is easily implemented in current daily practice. As ICG can be visualized under specially equipped surgical microscopes, which are already clinically available, NIR fluorescence imaging is also possible in microscopic transsphenoidal procedures.

Although transsphenoidal surgery is an established, relatively safe procedure, iatrogenic pituitary dysfunction is still a considerable drawback. A postoperative rate of hypopituitarism of 22% is reported[4]. Diabetes insipidus (DI) and pituitary insufficiency are commonly reported following transsphenoidal surgery. DI can be divided in temporary DI (incidence if 10 - 60%) and the uncommon permanent DI (0.5 – 15%)[4]. The cause of DI has been ascribed to stalk manipulation during surgery, and is more common after resection of microadenomas. Postoperative pituitary insufficiency is reported in 1-10% of patients; however outliers of 27% are documented[4]. In a recent structured review and meta-analysis of the available literature, Roelfsema et al. reported the onset of new, surgery-related pituitary insufficiency in 6.9 ± 1.8% of patients treated for prolactinoma, 6.7 +/- 1.6 for acromegaly, 12.5 +/- 4.6 % for NFA and 25.4 +/- 3.6 % for Cushing's disease[5].

Furthermore, surgical remission is not always achieved after resection of a functional adenoma and recurrence of a pituitary adenoma after apparent cure is also frequently reported[5]. Mean remission values and ranges of 68.8% (27-100) in prolactinoma, 47.3% (3-92) in NFA, 61.2% (37-88) in acromegaly, and 71.3% (41-98) in Cushing's disease, are reported. Overall remission rates of 53–64% for macroadenomas and 84-88% for microadenomas are reported[4].

Patients can suffer from recurrent disease, with the incidence peaking between 1 and 5 years after surgery. It is suggested that recurrence originates from small postoperative tumor remnants[5]. Consequently, there is a clear unmet need for improved peri-operative identification of pituitary adenomas, normal gland and surrounding structures, so as to improve surgical outcomes. A more aggressive attempt to attain complete adenoma resection will increase the number of patients achieving biochemical remission but will also increase the likelihood of postoperative complications such as DI and hypopituitarism. Thus, it is plausible to postulate that improved optical guidance during surgery could assist in resecting the adenoma in total while minimizing iatrogenic injury.

Only a limited number of imaging techniques during surgery, are described to improve completeness of tumor resection; for example intraoperative MRI[19] and intraoperative transcranial-transdural real-time ultrasonography[20]. Both techniques are reported as complementary imaging techniques and require the use of different, additional imaging devices that until now, interfere with the normal surgical procedure. Moreover, both techniques do not allow real-time merging of the surgical field and additional tumor imaging. NIR fluorescence imaging, as we describe here, has shown the ability to overcome these constraints.

We noticed several limitations to the described technique. Firstly, NIR fluorescence imaging identification was based on the principle that the normal gland stained after ICG administration, whereas tumor tissue stains to a lesser degree and with a time delay. For high-sensitive identification of adenomas and especially microadenomas, fluorescence signal in tumor tissue instead of healthy tissue would be of greater value. Should tumor tissue be stained, only fluorescent tissue has to be resected. The development of tumor-specific contrast agents targeting specific ligands could potentially facilitate this. Secondly, the imaging system used in the current study did not allow real-time overlay of color (white light) and NIR (blue light) images. Therefore, anatomical

orientation was difficult in some procedures and surgery under fluorescence guidance could only be performed when sufficient fluorescent signal was present. This would also allow a more detailed analysis of the optimal window between administration of ICG and peak fluorescence measurements, and gives a better insight in the decrease of fluorescent signal over time, as fluorescent signal can be measured all procedure long. In addition, to improve visual contrast, the fluorescence images displayed by the endoscopy system as blue on black could be converted to white on black. Further technical developments of endoscopic NIR fluorescence imaging systems are in progress and aim to improve the real-time intraoperative display of NIR fluorophores[17;21;22].

One limitation in the study was that only one endoscope and light cable suitable for NIR fluorescence imaging was available. Therefore only one patient could be included daily, potentially leading to selection bias. An aselect procedure was used to prevent this bias: always the first patient of the day was included, the order of cases was determined by chance.

CONCLUSION

NIR fluorescence imaging using intraoperative intravenous administration of low-dose ICG, can safely and easily be implemented in daily clinical practice. A useful differentiation between adenoma and pituitary gland was possible with NIR fluorescence.

Timing of the ICG administration warrants future study to optimize this technique. Better discrimination of tumor versus normal pituitary tissue, will likely facilitate improved surgical remission rates and reduced surgical morbidity after endoscopic transnasal transsphenoidal selective adenomectomy. With improved techniques and imaging protocols, we advocate that the potential additional value has to be evaluated prospectively in a randomized study design.

REFERENCES

1. Yamada S, Takada K. Angiogenesis in pituitary adenomas. *Microsc Res Tech* 2003;60:236-243.

2. Jugenburg M, Kovacs K, Stefaneanu L, Scheithauer BW. Vasculature in Nontumorous Hypophyses, Pituitary Adenomas, and Carcinomas: A Quantitative Morphologic Study. *Endocr Pathol* 1995;6:115-124.

3. Bonneville JF, Bonneville F, Cattin F. Magnetic resonance imaging of pituitary adenomas. *Eur Radiol* 2005;15:543-548.

4. Sudhakar N, Ray A, Vafidis JA. Complications after trans-sphenoidal surgery: our experience and a review of the literature. *Br J Neurosurg* 2004;18:507-512.

5. Roelfsema F, Biermasz NR, Pereira AM. Clinical factors involved in the recurrence of pituitary adenomas after surgical remission: a structured review and meta-analysis. *Pituitary* 2012;15:71-83.

6. Vahrmeijer AL, Hutteman M, van der Vorst JR, van de Velde CJ, Frangioni JV. Image-guided cancer surgery using near-infrared fluorescence. *Nat Rev Clin Oncol* 2013.

7. Tummers QR, Verbeek FP, Prevoo HA et al. First Experience on Laparoscopic Near-Infrared Fluorescence Imaging of Hepatic Uveal Melanoma Metastases Using Indocyanine Green. *Surg Innov* 2014.

8. van der Vorst JR, Schaafsma BE, Hutteman M et al. Near-Infrared Fluorescence-Guided Resection of Colorectal Liver Metastases. *Cancer*. In press.

9. van der Vorst JR, Schaafsma BE, Verbeek FP et al. Intraoperative near-infrared fluorescence imaging of parathyroid adenomas with use of low-dose methylene blue. *Head Neck* 2013.

10. Tummers QR, Verbeek FP, Schaafsma BE et al. Real-time intraoperative detection of breast cancer using near-infrared fluorescence imaging and Methylene Blue. *Eur J Surg Oncol* 2014;40:850-858.

11. Schaafsma BE, Mieog JS, Hutteman M et al. The clinical use of indocyanine green as a near-infrared fluorescent contrast agent for image-guided oncologic surgery. *J Surg Oncol* 2011;104:323-332.

12. Simal-Julian JA, Miranda-Lloret P, Evangelista-Zamora R et al. Indocyanine green videoangiography methodological variations: review. *Neurosurg Rev* 2014.

13. Zehri AH, Ramey W, Georges JF et al. Neurosurgical confocal endomicroscopy: A review of contrast agents, confocal systems, and future imaging modalities. *Surg Neurol Int* 2014;5:60.

14. Litvack ZN, Zada G, Laws ER, Jr. Indocyanine green fluorescence endoscopy for visual differentiation of pituitary tumor from surrounding structures. *J Neurosurg* 2012;116:935-941.

15. Jafari MD, Lee KH, Halabi WJ et al. The use of indocyanine green fluorescence to assess anastomotic perfusion during robotic assisted laparoscopic rectal surgery. *Surg Endosc* 2013;27:3003-3008.

16. Kudszus S, Roesel C, Schachtrupp A, Hoer JJ. Intraoperative laser fluorescence angiography in colorectal surgery: a noninvasive analysis to reduce the rate of anastomotic leakage. *Langenbecks Arch Surg* 2010;395:1025-1030.

17. Ris F, Hompes R, Cunningham C et al. Near-infrared (NIR) perfusion angiography in minimally invasive colorectal surgery. *Surg Endosc* 2014;28:2221-2226.

18. van der Vorst JR, Schaafsma BE, Hutteman M et al. Near-infrared fluorescence-guided resection of colorectal liver metastases. *Cancer* 2013;119:3411-3418.

19. Schwartz TH, Stieg PE, Anand VK. Endoscopic transsphenoidal pituitary surgery with intraoperative magnetic resonance imaging. *Neurosurgery* 2006;58:ONS44-ONS51.

20. Atkinson JL, Kasperbauer JL, James EM, Lane JI, Nippoldt TB. Transcranial-transdural real-time ultrasonography during transsphenoidal resection of a large pituitary tumor. Case report. *J Neurosurg* 2000;93:129-131.

21. Ashitate Y, Stockdale A, Choi HS, Laurence RG, Frangioni JV. Real-time simultaneous near-infrared fluorescence imaging of bile duct and arterial anatomy. *J Surg Res* 2011;Jul;176(1):7-13.

22. Matsui A, Tanaka E, Choi HS et al. Real-time intra-operative near-infrared fluorescence identification of the extrahepatic bile ducts using clinically available contrast agents. *Surgery* 2010;148:87-95.

Chapter 6

Intraoperative near-infrared fluorescence imaging of a paraganglioma using methylene blue: a case report

Quirijn R.J.G. Tummers[1], Martin C. Boonstra[1], John V. Frangioni[2,3],
Cornelis J.H. van de Velde[1], Alexander L. Vahrmeijer[1] and Bert A. Bonsing[1].

[1] Department of Surgery, Leiden University Medical Center
[2] Department of Radiology, [3] Division of Hematology/Oncology, Department of Medicine,
Beth Israel Deaconess Medical Center, Boston, USA

ABSTRACT

Introduction: Intraoperative identification of tumors can be challenging. Near-infrared (NIR) fluorescence imaging is an innovative technique that can assist in intraoperative identification of tumors, which may otherwise be undetectable.

Presentation of case: A 19-year-old patient with symptoms, normetanephrine levels and radiological findings suspicious for a paraganglioma, a rare tumor arising from extra-adrenal chromaffin cells within the sympathetic nervous system, is presented. Intraoperative NIR fluorescence imaging using intravenous administration of Methylene Blue (MB) assisted in intraoperative detection of the tumor, and even identified a smaller second lesion, which was not identified during surgery by visual inspection.

Discussion: Although the exact mechanism of MB accumulation in neuroendocrine tumors is unclear, it is described in both preclinical and clinical studies.

Conclusion: In this report, we describe the first case of intraoperative NIR fluorescence imaging of a paraganglioma using MB, which identified an otherwise undetectable lesion.

INTRODUCTION

Paragangliomas are rare tumors arising from extra-adrenal chromaffin cells within the sympathetic nervous system[1-3]. They can be found anywhere from the neck to the pelvis in the vicinity of sympathetic ganglions, and belong to the family of neuroendocrine tumors. An incidence rate of 2-8 cases per million is reported, and tumors can be either functional or non-functional. When functional there can be production of catecholamine, epinephrine, or norepinephrine.

The only curative treatment of paraganglioma is complete surgical resection. To help localize all sites of disease, preoperative identification can be performed using different anatomical and functional imaging modalities[4]. However, no specific imaging modalities are available for the intraoperative identification of these tumors.

Near-infrared (NIR) fluorescence imaging is a promising technique to assist in the intraoperative identification of sentinel lymph nodes, tumors, and vital structures[5]. Advantages of this optical imaging technique include real-time imaging, high sensitivity, and high resolution, with penetration depths several millimeters into tissue.

Methylene Blue (MB) is a clinically available tracer, which can be used at low dosage as a fluorescent tracer during NIR fluorescence imaging. Winer et al.[6] described the successful identification of insulinomas, a pancreatic neuroendocrine tumor in transgenic mice, and clinically, the intraoperative identification of parathyroid adenomas was described[7].

Based on these results, we explored the possibility to identify paragangliomas during surgery, using NIR fluorescence imaging and MB.

PRESENTATION OF CASE

A 19-year-old female patient presented with complaints of fainting, nausea, vomiting, headaches, excessive sweating, flushing attacks, hand tremors, and heart palpitations. She had a negative family history for endocrine diseases or paragangliomas. While volunteering to donate blood, her systolic blood pressure was found to be 180 mm Hg. After referral, physical examination revealed a blood pressure of 180/110 mm Hg on the left arm, 190/115 mm Hg

on the right arm, but no other abnormalities. Laboratory evaluation showed a normetanephrine level of 3227 umol/mol creatinine (norm. value 64 - 260) in the urine.

CT scan showed a 46 x 38 mm retroperitoneal mass, just caudal to the aortic bifurcation (Figure 1). Cranial to this, a smaller lesion of 6 mm was seen, which was characterized as a para-aortic lymph node. MRI scan confirmed the retroperitoneal mass just caudal to the aortic bifurcation, with features suspicious for a paraganglioma. A slight encasement of the common iliac vein was seen. The cranially located smaller lesion was not clearly identified by MRI.
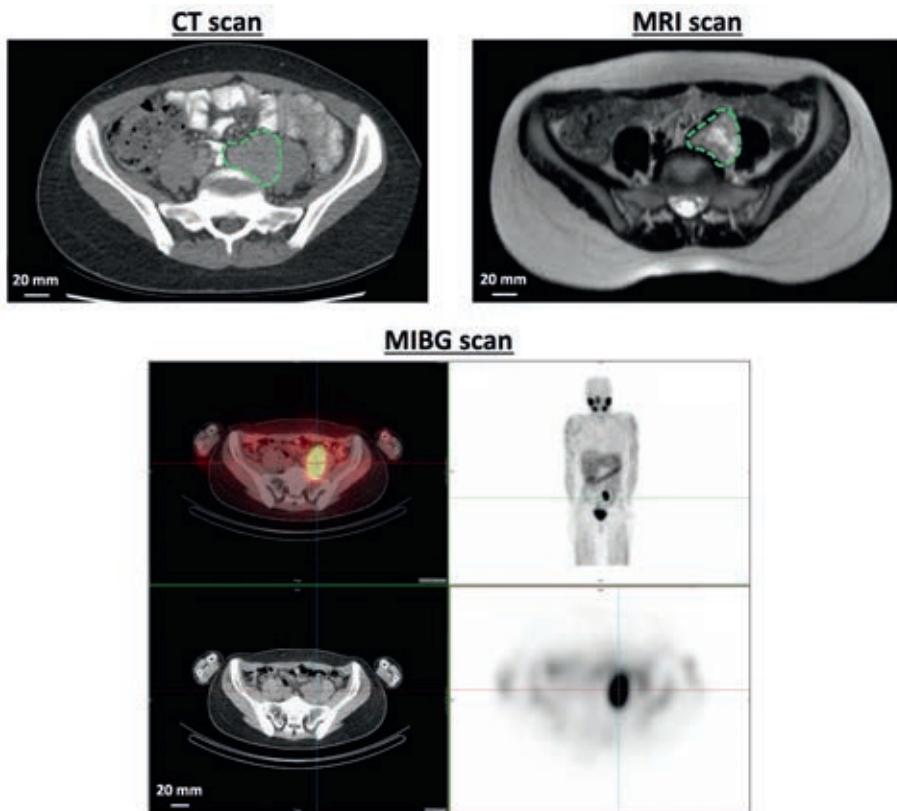

Figure 1. Preoperative imaging of paraganglioma

Preoperative CT, T2 weighed MRI and MIBG scan of the paraganglioma (dashed circle), retroperitoneal located, just caudal to the aortic bifurcation.

A ^{123}I-metaiodobenzylguanidine (MIBG) scan was performed to search for lesions located elsewhere in the body. Strong accumulation of the tracer was seen in the lesion just caudal to the aortic bifurcation, but no other uptake was seen (Figure 1).

The patient was scheduled for resection. She was successfully pretreated with doxazosine, a selective alpha1-receptor blocking sympatholytic drug, metoprolol, a beta-receptor blocking sympatholytic drug, and nifedipine, a dihydropyridine, in order to prevent a hypertensive crisis during surgery.

Intraoperative NIR fluorescence imaging
The current study was approved by the Medical Ethics Committee of the Leiden University Medical Center and was performed in accordance with the clinical standards of the Helsinki Declaration of 1975. Written informed consent was obtained.

During surgery, and directly after exposure of the lesion distal to the aortic bifurcation, MB was administered intravenously (0.5 mg/kg; 33 mg in 3.3 mL of water; 10 mg/ mL final stock solution concentration) over 5 min and NIR fluorescence imaging was performed using the Mini-FLARE image-guided surgery system as described previously[8]. Directly after infusion, imaging was performed at fixed time points (0, 1, 2, 3, 4, 5, 15, 30 and 45 min).

NIR fluorescence imaging showed a strong, but patchy, fluorescent signal corresponding to the suspected lesion (Figure 2A, lesion indicated by dashed circle). Moreover, the additional small lesion that was only identified by CT but not by MRI or by visual inspection during surgery, was clearly identified using NIR fluorescence imaging, located approximately 5 cm cranial to the main lesion (indicated by arrow). This lesion was otherwise undetectable. Already two minutes after administration, a Tumor-to-background batio (TBR) of approximately 3.5 was reached for both lesions, which slowly decreased over the next 30 min (Figure 3).

After en bloc resection of the 2 lesions, the specimen was sent to Pathology for further evaluation. After surgical treatment, symptoms disappeared and normetanephrine levels normalized.

No surgical complication or adverse reactions associated with the use of MB or fluorescence imaging were observed.
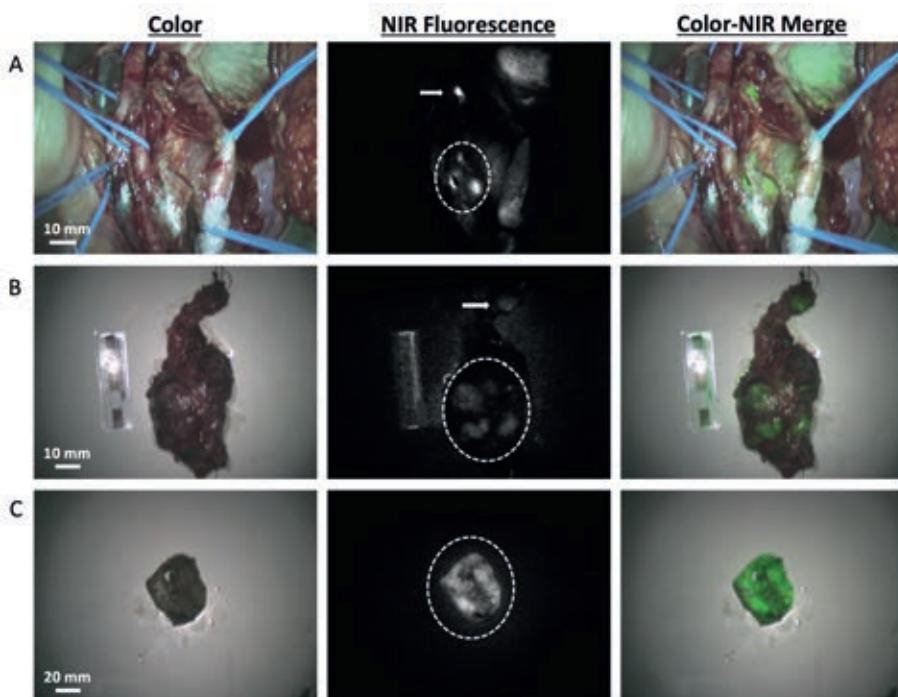
Figure 2. Intraoperative and ex vivo NIR fluorescence imaging of primary and metastatic paragangliomas

A. Intraoperative NIR fluorescence imaging of the surgical field. A bright, patchy fluorescent signal was identified at the location of the tumor (dashed circle). A second, small, lesion located approximately 5 cm cranial to the main lesion, was also identified using NIR fluorescence imaging (arrow). **B.** *Ex vivo* (T = 45 min) imaging of the resection specimens. Fluorescent signal was seen in the large (dashed circle) and small lesion (arrow). A weaker fluorescent intensity was seen than *in vivo*, because fluorescent signal decreased over time during surgery. **C.** *Ex vivo* imaging of the bisected main lesion. Bright fluorescent signal was seen throughout the paraganglioma (dashed circle).
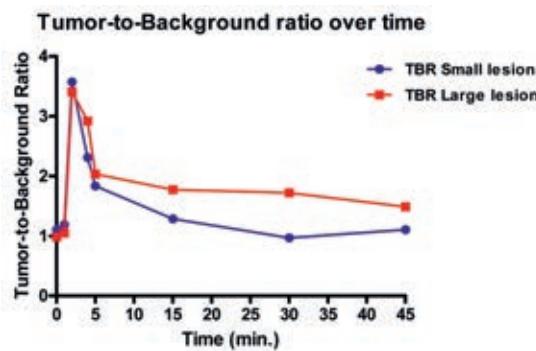
Figure 3. Tumor-to-background ratio of resected lesions

Tumor-to-background ratio of the large main lesion and small second lesion over time after intravenous administration of MB.

Ex vivo **imaging of resected lesion and sliced specimen**
*Ex vivo* imaging of the resected specimens was performed at the Pathology department using the FLARE imaging system, which was previously described[9]. Images showed a fluorescent signal in both lesions (Figure 2B). Of special note, the intensity of the fluorescent signal decreased significantly over time, so a much weaker fluorescence signal was measured during *ex vivo* imaging (i.e., T = 45 min after MB injection). The patchy fluorescent signal of the main tumor was seen both *in vivo* and *ex vivo*. This was due to fibrous connective tissue lying over the paraganglioma. After bisection of the resected main lesion, a clear fluorescent signal was seen throughout the tumor (Figure 2C).

Histopathology
Macroscopically, a nodular lesion was seen, yellow to black on cross section and surrounded by a thin capsule. The maximum diameter was 65 mm. Cranial from this lesion, a smaller lesion of 12 mm was seen, suspicious for a tumor-positive lymph node (figure 2B). The excised tissue was fixed in formalin, embedded in paraffin and tissue slides were stained with hematoxylin and eosin (HE). Immunohistochemical staining was also performed (Figure 4). Based on histopathological findings, both lesions were diagnosed as paraganglioma with diameters of 65 and 12 mm, respectively.
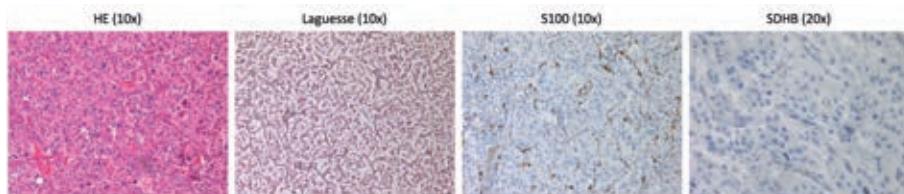
Figure 4. Histopathological staining of resected lesions
Hematoxylin and Eosin, Laguesse, S100 and SDHB staining of the resected specimen. Microscopy showed a characteristic pattern of cell nests. This pattern was accentuated by a reticulin stain. The cells had a moderate amount of eosinophilic cytoplasm and nuclei with finely clumped chromatin. Dispersed throughout the lesion, hemorrhagic foci were seen. The second, small, cranially located lesion showed the same characteristics as the larger lesion, without the presences of surrounding lymphoid tissue. Additional immunohistochemical staining for S100 showed the presence of sustentacular cells around the nests. SDHB staining was not conclusive.

DISCUSSION

Despite many preoperative imaging modalities, intraoperative identification and demarcation of paragangliomas can be challenging. Because complete surgical removal of the tumor is the only curative treatment option, real-time intraoperative imaging modalities which can assist in tumor identification are desperately needed. To the best of our knowledge, this is the first report showing the intraoperative identification of paragangliomas using NIR fluorescence imaging and MB in a clinical setting.

In the presented patient, the main lesion just caudal to the aortic bifurcation was clearly identified by CT, MRI, and MIBG-scan. CT also showed a cranially located smaller lesion, which was not identified by MRI or MIBG, and not recognized as a paraganglioma, probably due to its small size and/or lack of adequate tracer photon flux from small tumors[3;10]. Importantly, intraoperative identification of all tumors is of paramount importance for the complete surgical resection and thereby curative treatment. Although not identified by MRI or MIBG, the second, smaller, lesion was intensely fluorescent and was confirmed histologically to be paraganglioma. In daily practice, there still is a discrepancy between identification of lesions during preoperative imaging and intraoperative recognition of these lesions, especially when they are smaller sized. Intraoperative NIRF imaging could potentially overcome this gap.

The pharmacokinetics of MB in the observed lesions are consistent with a perfusion effect, but not for a retention effect, because TBR decreases rapidly over time after initially high values. This makes the administration of MB for intraoperative identification of paragangliomas very useful for the direct identification of lesions, and apparently local metastases or second primary tumors.

Although the exact mechanism of MB accumulation in tumors and especially neuroendocrine tumors is mainly unclear, it has been described in several studies. Previous clinical studies show staining of neuroendocrine tumors and parathyroid adenomas using MB as a visible dye using high concentrations[11-14] and with NIR fluorescence imaging using low-dose MB[7]. Also in breast cancer, identification of tumors by NIR fluorescence imaging using MB is described[15]. The mechanism behind this accumulation is based on physicochemical similarities between MB and sestamibi, a nuclear tracer used for MIBI-scans. Reports which describe the identification of paragangliomas using MIBI-scan

are rare[16;17], but strengthens the hypothesis that MB and sestamibi have a comparable biodistribution. A better understanding of the exact mechanism would be of obvious clinical importance, since this technique could potentially enhance patient cure rates.

CONCLUSION

In conclusion, we describe the successful use of NIR fluorescence imaging for the intraoperative identification of a paraganglioma using MB. This procedure is easy to perform and could result in an increased number of complete resections in paraganglioma surgery. In general, this technique could usher in a new era of optical assistance in the detection of tumors during surgery.

ACKNOWLEDGEMENTS

REFERENCES

1.   Erickson D, Kudva YC, Ebersold MJ et al. Benign paragangliomas: clinical presentation and treatment outcomes in 236 patients. *J Clin Endocrinol Metab* 2001;86:5210-5216.

2.   Lenders JW, Eisenhofer G, Mannelli M, Pacak K. Phaeochromocytoma. *Lancet* 2005;366:665-675.

3.   Brink I, Hoegerle S, Klisch J, Bley TA. Imaging of pheochromocytoma and paraganglioma. *Fam Cancer* 2005;4:61-68.

4.   Timmers HJ, Brouwers FM, Hermus AR et al. Metastases but not cardiovascular mortality reduces life expectancy following surgical resection of apparently benign pheochromocytoma. *Endocr Relat Cancer* 2008;15:1127-1133.

5.   Vahrmeijer AL, Hutteman M, van der Vorst JR, van de Velde CJ, Frangioni JV. Image-guided cancer surgery using near-infrared fluorescence. *Nat Rev Clin Oncol* 2013.

6.   Winer JH, Choi HS, Gibbs-Strauss SL, Ashitate Y, Colson YL, Frangioni JV. Intraoperative Localization of Insulinoma and Normal Pancreas Using Invisible Near-Infrared Fluorescent Light. *Ann Surg Oncol* 2009.

7.   van der Vorst JR, Schaafsma BE, Verbeek FP et al. Intraoperative near-infrared fluorescence imaging of parathyroid adenomas with use of low-dose methylene blue. *Head Neck* 2013.

8.   Mieog JS, Troyan SL, Hutteman M et al. Towards Optimization of Imaging System and Lymphatic Tracer for Near-Infrared Fluorescent Sentinel Lymph Node Mapping in Breast Cancer. *Ann Surg Oncol* 2011;18:2483-2491.

9.   Troyan SL, Kianzad V, Gibbs-Strauss SL et al. The FLARE intraoperative near-infrared fluorescence imaging system: a first-in-human clinical trial in breast cancer sentinel lymph node mapping. *Ann Surg Oncol* 2009;16:2943-2952.

10.   Campeau RJ, Garcia OM, Correa OA, Rege AB. Pheochromocytoma: diagnosis by scintigraphy using iodine 131 metaiodobenzylguanidine. *South Med J* 1991;84:1221-1230.

11.   Dudley NE. Methylene blue for rapid identification of the parathyroids. *Br Med J* 1971;3:680-681.

12.   Fedorak IJ, Ko TC, Gordon D, Flisak M, Prinz RA. Localization of islet cell tumors of the pancreas: a review of current techniques. *Surgery* 1993;113:242-249.

13.   Gordon DL, Airan MC, Thomas W, Seidman LH. Parathyroid identification by methylene blue infusion. *Br J Surg* 1975;62:747-749.

14.   Ko TC, Flisak M, Prinz RA. Selective intra-arterial methylene blue injection: a novel method of localizing gastrinoma. *Gastroenterology* 1992;102:1062-1064.

15.   Tummers QR, Verbeek FP, Schaafsma BE et al. Real-time intraoperative detection of breast cancer using near-infrared fluorescence imaging and Methylene Blue. *Eur J Surg Oncol* 2014;40:850-858.

16.   Bhattacharya A, Mittal BR, Bhansali A, Radotra BD, Behera A. Cervical paraganglioma mimicking a parathyroid adenoma on Tc-99m sestamibi scintigraphy. *Clin Nucl Med* 2006;31:234-236.

17.   Piga M, Farina GP, Loi GL et al. Visualisation of a paraganglioma by technetium-99m-sestamibi scintigraphy. *J Endocrinol Invest* 1999;22:296-300.

-

Chapter 7

Intraoperative guidance in parathyroid surgery using near-infrared fluorescence imaging and low-dose methylene blue

Quirijn R.J.G. Tummers[1], Abbey Schepers[1], Jaap F. Hamming[1] Job Kievit[1], John V. Frangioni[2,3,4], Cornelis J.H. van de Velde[1] and Alexander L. Vahrmeijer[1]

[1] Department of Surgery, Leiden University Medical Center
[2] Department of Radiology, [3] Division of Hematology/Oncology, Department of Medicine, Beth Israel Deaconess Medical Center, Boston, USA
[4] Curadel, LLC, 377 Plantation Street, Worcester, USA

ABSTRACT

Background: Identification of diseased and normal parathyroid glands during parathyroid surgery can be challenging. The aim of this study was to assess whether near-infrared (NIR) fluorescence imaging using administration of a low-dose Methylene Blue (MB) at the start of surgery could provide optical guidance during parathyroid surgery and assist in the detection of parathyroid adenomas.

Methods: Patients diagnosed with primary hyperparathyroidism planned for parathyroid resection were included. Patients received 0.5 mg/kg MB intravenously directly after start of anesthesia. During surgery, NIR fluorescence imaging was performed to identify parathyroid adenomas. Imaging results were compared to a previous published feasibility study in which 12 patients received MB after surgical identification of the adenoma.

Results: 13 patients were included in the current study. In 10/12 patients with a histologically proven adenoma, the adenoma was fluorescent. Mean Signal to Background Ratio (SBR) was 3.1 ± 2.8. Mean diameter of the resected lesions was 17 ± 9 mm (range 5 - 28 mm). Adenomas could be identified up to 145 minutes after administration, which was the longest timespan until resection. Interestingly, in 3 patients, a total of 6 normal parathyroid glands (median diameter 2.5 mm) with a SBR of 1.8 ± 0.4 were identified using NIR fluorescence imaging.

Conclusion: Early administration of low dose MB provided guidance during parathyroid surgery by identifying both parathyroid adenomas and normal parathyroid glands. In patients where difficult identification of the parathyroid adenoma is expected, or when normal glands have to be identified, administration of MB could improve surgical outcome.

INTRODUCTION

Primary hyperparathyroidism is a common endocrine disorder caused by parathyroid adenomas or hypertrophic parathyroid glands[1]. Complete surgical resection of these lesions is the only curative treatment. For diagnosis and surgical planning, preoperative imaging can be performed with several imaging modalities. Available imaging modalities currently consist of ultrasound (US), radionuclide scanning, magnetic resonance imaging, and both conventional and "4 D" computed tomography[2]. In daily practice, various combinations of these imaging options are used.

During surgery, adequate identification of parathyroid adenomas and parathyroid glands is of utmost importance for a curative treatment and to minimize the need for surgical exploration of the neck. However, few intraoperative imaging modalities are available. In 1971 Dudley et al. reported the use of intravenous administration of high dose Methylene Blue (MB) for the intraoperative identification of parathyroid adenomas[3]. Since then, this technique has been repeated by many groups[4-6]. However, administration of high dose MB (7.5 mg/kg) is associated with serious adverse events such as toxic metabolic encephalopathy[7] and can lead to blue staining of the complete surgical field due to leakage when surgical procedures takes longer.

Besides the use of high dose MB, several intraoperative imaging modalities are described, all with their own disadvantages. Radio-guided identification using ^{99m}Tc-sestamibi and hand-held gamma probes lacks real-time visual guidance[5;8;9]. Moreover, nuclear isotopes are scarce in large areas of the world. Aminolevulinic acid (ALA) was successfully tested in clinical studies, but can cause phototoxic reactions for which patients have to be protected from direct light exposure for 48 hours[10-12]. Moreover, ALA is mainly fluorescent in the visual light spectrum, which leads to high absorption and scatter of visible light in living tissue.

One of the techniques that could overcome these issues is near-infrared (NIR) fluorescence imaging. NIR fluorescence imaging is an innovative technique to visualize tumors, vital structures and lymphatic channels and lymph nodes[13]. Recently, our research group showed feasibility of intraoperative identification of parathyroid adenomas using NIR fluorescence imaging and low dose MB as fluorescent tracer[14]. In this previous study, parathyroid adenomas were identified by surgical identification; whereafter 0.5 mg/kg MB (low-dose) was

administered intravenously to assess feasibility. In 9 out of 12 patients, the exposed adenoma became fluorescent after MB administration within 5 - 10 minutes. For intraoperative guidance in parathyroid surgery, it would be of great added value if MB could be administered before surgical exploration, resulting in faster identification of parathyroid adenomas.

Therefore, the aim of this study was to assess whether early MB administration provides guidance in parathyroid adenoma identification during surgery. Subsequently, the obtained results were compared with previous published data to compare early and late MB administration protocols.

MATERIALS AND METHODS

Clinical study

This study was approved by the Medical Ethics Committee of the Leiden University Medical Center and was performed in accordance with the ethical standards of the Helsinki Declaration of 1975. All patients planning to undergo a resection of a parathyroid adenoma for primary hyperparathyroidism were eligible for participation in the study. Exclusion criteria were pregnancy or lactation, the use of serotonin reuptake inhibitors, serotonin, and noradrenalin reuptake inhibitors and/or tricyclic antidepressants, severe renal failure, G6PD-deficiency, or an allergy to MB. All patients gave informed consent and were anonymized. Patients received standard of care diagnostic work-up, which for our center included a preoperative cervical US and a preoperative ^{99m}Tc-sestamibi-SPECT, combined with a low-dose computed tomography (CT) scan for preoperative surgical planning.

Directly before or after start of anesthesia, 0.5 mg/kg MB was administered intravenously over 5 minutes. During surgery, after subplatysmal dissection, retraction and initial exploration, visual inspection combined with NIR fluorescence imaging was used for identification of parathyroid adenomas and normal parathyroid glands. After identification and resection of the adenoma, an intraoperative parathyroid hormone (PTH) assay was performed. Postoperative histopathological assessment of the resected specimen served as gold standard for parathyroid adenoma identification. No standard intraoperative frozen section analysis was performed.

Intraoperative NIR fluorescence imaging
For NIR fluorescence imaging, the Mini-FLARE imaging system was used[15]. Briefly, the system consists of 2 wavelength isolated light sources: a "white" light source, generating 26,600 lx of 400 to 650 nm light, and a "near-infrared" light source, generating 1.08 mW/ca^{me} of $\approx$ 670 nm light. Color video and NIR fluorescence images are simultaneously acquired and displayed in real time using custom optics and software that separate the color video and NIR fluorescence images. A pseudo-colored (lime green) merged image of the color video and NIR fluorescence images is also displayed. The imaging head is attached to a flexible gooseneck arm, which permits positioning of the imaging head at extreme angles virtually anywhere over the surgical field. For intraoperative use, the imaging head and imaging system pole stand are wrapped in a sterile shield and drape (Medical Technique Inc., Tucson, AZ).

Comparison between early and late MB administration protocol
The obtained results were compared to the previous performed and published feasibility trial (NTR3403)[14]. This trial was performed using the same imaging system and identical surgical workup. In both studies, patients received 0.5 mg/kg MB. The only difference was that in the previous published study, MB was administered directly after surgical exposure of the suspected parathyroid adenoma. In the current study, MB was administered directly after start of anesthesia, before the surgical incision and assisted with parathyroid adenoma identification.

Statistical analysis
For statistical analysis, SPSS statistical software package (Version 20.0, Chicago, IL) was used. Signal-to-background ratios (SBR) were calculated by dividing the fluorescent signal in the parathyroid adenoma by fluorescent signal of surrounding healthy tissue. Patient age and body mass index (BMI) were reported in mean and range and SBR was reported in mean and standard deviation. To compare characteristics between different administration protocols, the independent-sample t test and chi-square test were used was used. $P < 0.05$ was considered significant.

RESULTS

Patient characteristics
Thirteen consecutive patients with primary hyperparathyroidism planned for surgical resection of a parathyroid adenoma were included in this study. Patient and surgical characteristics are shown in Table 1. Mean age was 53 years (range, 21 – 75) and 5 patients were male. Mean BMI was 26.6 ± 3.6, mean preoperative calcium level was 2.8 ± 0.1 mmol/L and mean preoperative PTH level was 11.9 ± 7.2 pmol/L. All patients were diagnosed with primary hyperparathyroidism and in one patient this was associated with multiple endocrine neoplasia (MEN) 1 syndrome. One patient was treated for recurrent disease, after earlier resection of a parathyroid adenoma. The mean diameter of the resected lesions was 17 ± 9 mm (range 5 - 28 mm).

Preoperative imaging
Table 2 shows the preoperative imaging characteristics. In 12 out of 13 patients, a ^{99m}Tc-sestamibi single-photon emission computed tomography (SPECT)/CT was performed. In 8 of 13 patients, a suspected parathyroid adenoma could be localized, whereas in 4 patients no evidence for localization of the adenoma was found. In 12 of 13 patients preoperative US was performed. In 5 patients a lesion suspect for parathyroid adenoma was identified. In 1 patient no preoperative US was performed because she was referred from a foreign clinical for surgery and ^{99m}Tc-sestamibi SPECT/CT showed clear localization of a parathyroid adenoma.

Intraoperative NIR fluorescence imaging
In 9 out of 13 patients, intraoperative NIR fluorescence imaging clearly identified a parathyroid adenoma or hyperplastic parathyroid gland. Figure 1 shows a representative example of the intraoperative fluorescent signal in a parathyroid adenoma. The mean SBR of the identified NIR fluorescent adenomas or hyperplastic parathyroid glands was 3.1 ± 2.8.

Table 1. Patient and surgical characteristics

Patient no.	Sex	Age	BMI	Disease	Previous treatment	Preoperative calcium, mmol/L	Preoperative PTH, pmol/L	Surgical procedure	Histology	Maximum diameter, mm
1	F	40	24.0	PH	No	2.70	7.60	PAR right	Parathyroid adenoma	20
2	M	34	31.8	PH	No	3.03	28.30	PAR left	Parathyroid adenoma	25
3	M	60	26.8	PH	No	2.80	13.30	PAR left, thymectomy right, hemithyroidectomy left	Parathyroid hyperplasia	6; 7
4	M	59	24.0	PH	PAR right	2.85	6.90	PAR right, thymectomy right	Parathyroid adenoma	14
5	M	21	27.8	PH by MEN1	No	2.89	11.80	PAR right, parathyroidectomy left and right, thymectomy	Parathyroid adenoma and normal PTG	23
6	F	67	25.1	PH	No	2.72	24.00	PAR left	Parathyroid adenoma	19
7	F	60	24.8	PH	No	2.89	9.30	PAR right	Parathyroid adenoma	20
8	F	75	21.5	PH	No	2.72	6.60	PAR left	Parathyroid adenoma	14
9	F	44	28.1	PH	No	2.88	15.70	Identification normal PTGs, LN resection, thymectomy left	Reactive lymph nodes	N/A
10	F	47	32.9	PH	No	2.62	12.60	PAR left	Parathyroid hyperplasia	6
11	M	62	30.7	PH	No	2.66	4.20	PAR left	Parathyroid adenoma	5
12	F	70	26.8	PH	No	2.78	9.80	PAR left and right, thymectomy	Parathyroid hyperplasia and normal PTGs	28; 20
13	F	52	22.8	PH	No	2.67	8.30	PAR left	Parathyroid hyperplasia	22

Abbreviations: BMI, body-mass index; LN, lymph nodes; MEN1, multiple endocrine neoplasia 1 syndrome; N/A, not applicable; PAR, parathyroid adenoma resection; PH, primary hyperparathyroidism; PTG, parathyroid gland; PTH, parathyroid hormone.

Table 2. Identification characteristics of parathyroid adenomas

Patient no.	Sestamibi-SPECT-CT	Preoperative ultrasound	NIRF detection	PTH decrease post-resection	Time between administration and NIRF detection (minutes)	SBR
1	+	+	+	+	106	1.5
2	-	-	-	+	N/A	N/A
3	+	-	+	+	102 and 132	5.7 and 2.3
4	+	-	+	+	113	2.3
5	+	+	+	+	115; 109 and 134	2.4 (adenoma); 1.4 and 2.0 (normal PTGs)
6	+	+	+	+	34	10.7
7	NP	+	-*	+	60	1.8 (ex vivo)
8	+	+	+	+	87	1.8
9	-	-	+**	+	78 and 78	2.4 and 1.6 (normal PTGs)
10	-	-	-	+	N/A	N/A
11	-	-	+	+	54	1.7
12	+	NP	+	+	61 and 145; 135 and 136	3.8 and 1.7 (hyperplasia); 1.4 and 1.7 (normal PTGs)
13	+	-	+	+	41	2.2

Abbreviations: N/A, not applicable; NIRF, Near-infrared fluorescence; NP, not performed, PTG, parathyroid gland; PTH parathyroid hormone; SBR, Signal-to-Background ratio; SPECT, single photon emission computed tomography.

* No in vivo NIRF detection of parathyroid adenoma. Ex vivo, the deepest located part of adenoma appeared to be fluorescent. ** Identification of normal PTGs only using NIRF imaging.
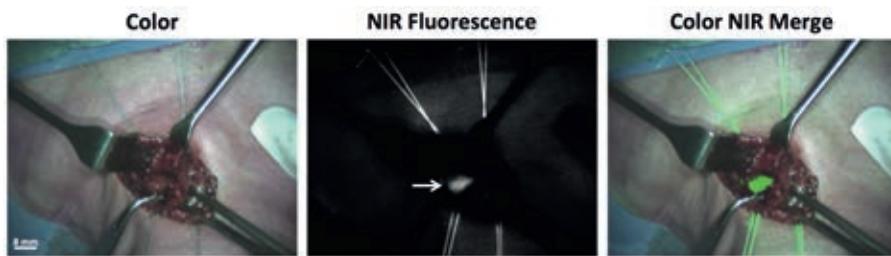
Figure 1. Intraoperative NIR fluorescence-guided resection of a parathyroid adenoma located in the neck

During minimally-invasive parathyroid surgery, a 19 mm parathyroid adenoma is identified using NIR fluorescence imaging (arrow).

In 1 patient, the intraoperatively identified parathyroid adenoma appeared non-fluorescent *in vivo*, but this was caused by a hemorrhage on the ventral side of the adenoma. *Ex vivo*, the deepest located part of this adenoma also showed clear fluorescence. In 12 patients, histological evaluation confirmed

that the resected tissue was parathyroid adenoma (N = 8) or hyperplastic parathyroid gland (N = 4). In 2 patients, the resected parathyroid adenoma did not fluoresce. In summary, in 10 out of 12 patients with a proven parathyroid adenoma or hyperplastic parathyroid gland, the lesion was fluorescent.

In 1 patient (#9), no adenoma was found during exploration of the neck. A thymectomy was performed and 6 non-fluorescent lymph nodes were removed. During histological assessment of the resected tissue, no parathyroid adenomas were identified as well, although her intraoperative PTH assay showed a decrease from 25.0 to 1.4 pmol/L.

Interestingly, in 3 patients, a total of 6 normal parathyroid glands were identified using NIR fluorescence imaging (median size 2.5 mm, range 1-4). Figure 2A and 2B show an example of 2 small (1 and 2 mm) normal parathyroid glands located in the left and right thymus. These were not identified without NIR fluorescence imaging. Both glands were biopsied for frozen section analysis and were found histologically to be normal parathyroid glands. Subsequently, the non-biopsied part of both glands were re-transplanted in the sternocleidomastoid muscle. Mean SBR of the normal parathyroid glands was 1.8 ± 0.4. The smallest normal parathyroid gland identified by NIR fluorescence imaging was 1 mm.
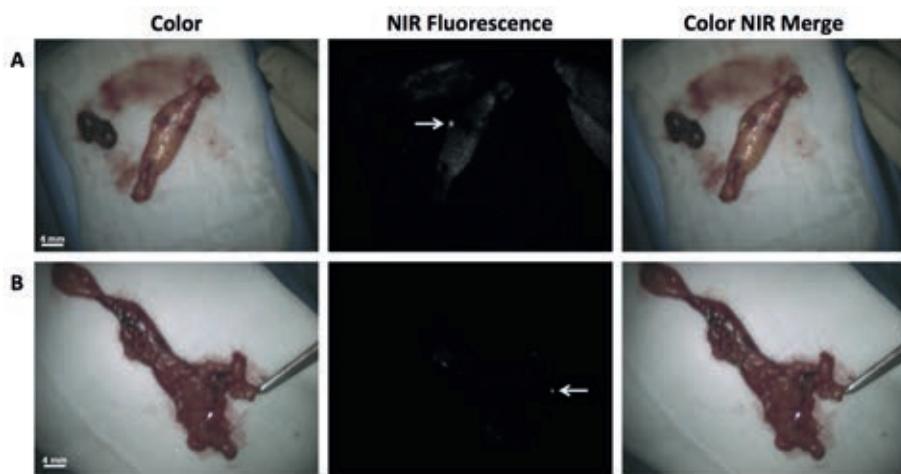
**Figure 2.** Intraoperative NIR fluorescence imaging of normal parathyroid glands

A. A 2 mm normal parathyroid gland (arrow) was identified in the right thymus using NIR fluorescence imaging after thymectomy. **B.** A 1 mm normal parathyroid gland (arrow) was identified in the left thymus using NIR fluorescence imaging after thymectomy. Both glands in A and B could not be identified using visual inspection.

Mean time interval between administration of MB and detection of the adenoma was 77 ± 34 minutes. Parathyroid adenomas could be identified up to 145 minutes after administration, which was the longest timespan until resection. No adverse effects regarding the use of MB or NIRF fluorescence imaging were seen.

Correlation ^{99m}Tc-sestamibi-SPECT/CT scan and NIR fluorescence imaging
In all patients where a suspected adenoma was identified on ^{99m}Tc-sestamibi-SPECT/CT, the resected parathyroid tissue was fluorescent (8 out of 8). Moreover, when analyzing all patients with an adenoma (N=12) that received a ^{99m}Tc-sestamibi-SPECT/CT (N=11), concordance between ^{99m}Tc-sestamibi-SPECT/CT status and NIR fluorescence status of the resected lesion was observed in 10 out of 11 patients. In 1 patient where the ^{99m}Tc-sestamibi-SPECT/CT was negative, the adenoma appeared to be fluorescent, and in 1 patient where the ^{99m}Tc-sestamibi-SPECT/CT was negative, 2 normal glands were identified using NIR fluorescence imaging.

Comparison between early and late MB administration protocol
There were no significant differences in patient characteristics between of the current study and the previous reported study regarding age, gender, BMI, preoperative calcium, preoperative PTH and diameter (Table 3). The most important difference, although not significant, was found in SBR between different administration protocols. Mean SBR was 3.1 in the early administration group versus 6.1 in the group that received MB after surgical exposure of the adenoma (P=0.08; mean difference 2.95; -0.40 - 6.29 95% CI).

Table 3. Comparison between early and late Methylene blue administration

Characteristic	Early MB administration (N=13)	Late MB administration (N=12)	P-value
Sex			0.67
Female	8	9	
Male	5	3	
	Mean	**Mean**	
Age	53	56	0.65
BMI	26.7	27.1	0.82
Preoperative calcium	2.79	2.68	0.42
Preoperative PTH	12.2	119.4	0.22
Diameter	17	16	0.80
SBR	3.11	6.10	0.08

Abbreviations: BMI, Body mass index; MB, Methylene Blue; PTH, parathyroid hormone; SBR, signal-to-Background ratio.

Combining the two groups showed that in 16/25 patients the preoperative ^{99m}Tc-sestamibi-SPECT/CT scan indicated an adenoma. In 15 out of these 16 patients, the detected adenoma was NIR fluorescent, leading to a positive predictive value of 94%. The only patient who had a ^{99m}Tc-sestamibi-SPECT/CT positive lesion, that appeared non-fluorescent, was a patient who suffered from parathyroid carcinoma.

DISCUSSION

Despite the fact that surgical resection of parathyroid adenomas is a commonly performed and overall successful surgical procedure, intraoperative detection of an adenoma can be challenging. Moreover, the anatomical site where parathyroid adenomas are located contains many vital structures like arteries, veins, and nerves. When preoperative localization fails, and extended surgical neck exploration is needed, the risk of iatrogenic damage to these structures and associated complications increase[16]. Therefore, intraoperative optical guidance in parathyroid surgery using exogenous contrast agents could assist in a faster and more accurate identification of parathyroid adenomas, without causing iatrogenic injury to surrounding vital structures.

Previously our research group showed feasibility of intraoperative identification of parathyroid adenomas using NIR fluorescence imaging and low-dose MB in humans[14]. In that clinical trial, MB was administered after surgical exposure of the adenoma. The current study confirmed the results of the previous described study, showing the possibility to intraoperatively identify parathyroid adenomas using MB and its correlation with preoperative a ^{99m}Tc-sestamibi-SPECT/CT scan. Combining the two groups showed that 16 out of these 25 patients had a ^{99m}Tc-sestamibi-SPECT/CT scan indicating an adenoma. In 15 out of these 16 patients, the detected adenoma was NIR fluorescent, leading to a positive predictive value of 94% for a NIR fluorescent adenoma after a positive ^{99m}Tc-sestamibi-SPECT/CT scan. These findings suggest that all patients with a positive ^{99m}Tc-sestamibi-SPECT/CT scan should receive MB for the improved identification of parathyroid adenomas.

In the current study, 2 parathyroid adenomas did not fluoresce. The histopathological analysis of these 2 adenomas were comparable with the NIR fluorescent positive adenomas, so the reason for non-fluorescence remains unclear.

Interestingly, we identified normal parathyroid glands, as small as 1 mm, during surgical exploration of the neck. These glands were not detected by the surgeon by visual inspection or palpation. Normal parathyroid glands can be difficult to distinguish during surgery because of their small size, their variability in location, and similar appearance to lymph nodes. Detection of these normal glands can be of great added value during subtotal parathyroid glands resection in the case of MEN1 syndrome, where 3.5 glands are removed and a portion of the most normal appearing gland is left in site or is auto-transplanted[17]. Also when normal glands are suppressed by hyperfunctional parathyroid glands, as in patient #9 of the current study, imaging can be useful. These glands were very small, and located in the thymus on both sides, and would not have been auto-transplanted if not detected in the thymectomy specimens by NIR fluorescence imaging. Improved identification of both parathyroid adenoma and normal glands can limit the extent of neck exploration. Especially small normal glands are at risk of iatrogenic injury when not identified in time during neck exploration. The identification of normal glands using NIR fluorescence imaging and MB was described by Antika et al.[18] in rabbits. They used escalating dosages from 0.025 mg/kg to 3 mg/kg (human equivalent dose 0.008 mg/kg to 0.97 mg/kg calculated by using allometric dose translation based on body surface area[19]) for identification of thyroid and parathyroid glands. However, to the best of our knowledge, this is the first clinical trial to demonstrate the intraoperative identification of normal glands using NIR fluorescence imaging and MB.

When early administration of MB is compared to late administration (after visual identification of the adenoma), a mean SBR of the adenoma of 3.1 in the early administration group versus 6.1 in the late administration group is seen. Although this difference was not significant (P = 0.08), it shows that MB follows the kinetics of a perfusion tracer, and don't show clear (active) accumulation in parathyroid adenomas. Nevertheless, a mean SBR of 3.1 is suitable for intraoperative identification of parathyroid adenoma's and normal glands as clearly shown in the current study.

Developing probes that specifically accumulate in parathyroid glands could enhance SBR and the time window of which optimal SBRs are achieved. A recent published study of our research group showed the high-sensitivity identification of parathyroid and thyroid glands in several animal models using novel tissue-specific NIR fluorophores[20]. However, probes such as these are not

clinically available yet, and development of these probes is expensive and time consuming. Therefore, it is important to exploit clinically available contrast agents, such as MB[21].

Recently, several studies reported the use of autofluorescence characteristics of parathyroid tissue for discrimination between different tissue types using spectroscopy[22;23]. They found autofluorescent properties in parathyroid and thyroid glands with a peak fluorescence at 822 nm when excited with 785 nm light. Using autofluorescence would make the development of exogenous contrast agents superfluous. However, no 2-D optical guidance from spectroscopy is yet possible. And, although the spectroscopy results were validated in a larger patient cohort using a customized endoscopic imaging system[24], this autofluorescent signal has not been seen in previous studies by our research group using our imaging system in humans or different animal species[14;20].

NIR fluorescence imaging is a growing field of interest worldwide, more imaging systems have been introduced for both open and endoscopic imaging[25;26]. Prices of NIR fluorescence imaging systems are starting from $40.000. NIR fluorescence imaging in parathyroid surgery has the potential to speed up the surgical procedure by assisting in the identification of parathyroid adenomas and normal parathyroid gland. In the current study, time interval between administration and detection of adenomas are reported, however they could not be compared to patients not undergoing NIR fluorescence-assisted surgery. Therefore, randomized controlled trials in which patients are receiving NIR fluorescence imaging or not are needed.

To conclude, NIR fluorescence imaging using MB can provide guidance during parathyroid surgery by identifying both parathyroid adenomas and normal parathyroid glands, for at least 145 minutes after MB administration. In patients where difficult identification of the parathyroid adenoma is expected, or when normal glands have to be identified, administration of MB could potentially improve surgical outcome.

REFERENCES

1. Fraser WD. Hyperparathyroidism. *Lancet* 2009;374:145-158.

2. Phillips CD, Shatzkes DR. Imaging of the parathyroid glands. *Semin Ultrasound CT MR* 2012;33:123-129.

3. Dudley NE. Methylene blue for rapid identification of the parathyroids. *Br Med J* 1971;3:680-681.

4. Han N, Bumpous JM, Goldstein RE, Fleming MM, Flynn MB. Intra-operative parathyroid identification using methylene blue in parathyroid surgery. *Am Surg* 2007;73:820-823.

5. Harrison BJ, Triponez F. Intraoperative adjuncts in surgery for primary hyperparathyroidism. *Langenbecks Arch Surg* 2009;394:799-809.

6. Orloff LA. Methylene blue and sestamibi: complementary tools for localizing parathyroids. *Laryngoscope* 2001;111:1901-1904.

7. Kartha SS, Chacko CE, Bumpous JM, Fleming M, Lentsch EJ, Flynn MB. Toxic metabolic encephalopathy after parathyroidectomy with methylene blue localization. *Otolaryngol Head Neck Surg* 2006;135:765-768.

8. Flynn MB, Bumpous JM, Schill K, McMasters KM. Minimally invasive radioguided parathyroidectomy. *J Am Coll Surg* 2000;191:24-31.

9. Fujii T, Yamaguchi S, Yajima R et al. Use of a handheld, semiconductor (cadmium zinc telluride)-based gamma camera in navigation surgery for primary hyperparathyroidism. *Am Surg* 2011;77:690-693.

10. Prosst RL, Gahlen J, Schnuelle P, Post S, Willeke F. Fluorescence-guided minimally invasive parathyroidectomy: a novel surgical therapy for secondary hyperparathyroidism. *Am J Kidney Dis* 2006;48:327-331.

11. Prosst RL, Willeke F, Schroeter L, Post S, Gahlen J. Fluorescence-guided minimally invasive parathyroidectomy: a novel detection technique for parathyroid glands. *Surg Endosc* 2006;20:1488-1492.

12. Prosst RL, Weiss J, Hupp L, Willeke F, Post S. Fluorescence-guided minimally invasive parathyroidectomy: clinical experience with a novel intraoperative detection technique for parathyroid glands. *World J Surg* 2010;34:2217-2222.

13. Vahrmeijer AL, Hutteman M, van der Vorst JR, van de Velde CJ, Frangioni JV. Image-guided cancer surgery using near-infrared fluorescence. *Nat Rev Clin Oncol* 2013.

14. van der Vorst JR, Schaafsma BE, Verbeek FP et al. Intraoperative near-infrared fluorescence imaging of parathyroid adenomas with use of low-dose methylene blue. *Head Neck* 2013.

15. Mieog JS, Troyan SL, Hutteman M et al. Toward optimization of imaging system and lymphatic tracer for near-infrared fluorescent sentinel lymph node mapping in breast cancer. *Ann Surg Oncol* 2011;18:2483-2491.

16. Udelsman R. Six hundred fifty-six consecutive explorations for primary hyperparathyroidism. *Ann Surg* 2002;235:665-670.

17. Pieterman CR, Vriens MR, Dreijerink KM, van der Luijt RB, Valk GD. Care for patients with multiple endocrine neoplasia type 1: the current evidence base. *Fam Cancer* 2011;10:157-171.

18. Antakia R, Gayet P, Guillermet S et al. Near infrared fluorescence imaging of rabbit thyroid and parathyroid glands. *J Surg Res* 2014.

19. Reagan-Shaw S, Nihal M, Ahmad N. Dose translation from animal to human studies revisited. *FASEB J* 2008;22:659-661.

20. Hyun H, Park MH, Owens EA et al. Structure-Inherent Targeting of NIR Fluorophores for Parathyroid and Thyroid Gland Imaging. *Nat Med* 2014.

21. Schaafsma BE, Mieog JS, Hutteman M et al. The clinical use of indocyanine green as a near-infrared fluorescent contrast agent for image-guided oncologic surgery. *J Surg Oncol* 2011;104:323-332.

22. McWade MA, Paras C, White LM, Phay JE, Mahadevan-Jansen A, Broome JT. A novel optical approach to intraoperative detection of parathyroid glands. *Surgery* 2013;154:1371-1377.

23. Paras C, Keller M, White L, Phay J, Mahadevan-Jansen A. Near-infrared autofluorescence for the detection of parathyroid glands. *J Biomed Opt* 2011;16:067012.

24. McWade MA, Paras C, White LM et al. Label-free Intraoperative Parathyroid Localization with Near-Infrared Autofluorescence Imaging. *J Clin Endocrinol Metab* 2014;jc20142503.

25. Handgraaf HJ, Verbeek FP, Tummers QR et al. Real-time near-infrared fluorescence guided surgery in gynecologic oncology: a review of the current state of the art. *Gynecol Oncol* 2014;135:606-613.

26. Zhu B, Sevick-Muraca EM. A review of performance of near-infrared fluorescence imaging devices used in clinical studies. *Br J Radiol* 2015;88:20140547.

Chapter 8

The value of intraoperative near-infrared fluorescence imaging based on enhanced permeability and retention of indocyanine green: feasibility and false-positives in ovarian cancer

Quirijn R.J.G. Tummers[1*], Charlotte E.S. Hoogstins[1*], Alexander A.W. Peters[2], Cor D. de Kroon[2], J. Baptist M.Z. Trimbos[2], Cornelis J.H. van de Velde[1], John V. Frangioni[3,4,5], Alexander L. Vahrmeijer[1] and Katja N. Gaarenstroom[2]

* Q.R.J.G. Tummers and C.E.S. Hoogstins share first authorship.

[1] Department of Surgery, Leiden University Medical Center
[2] Department of Gynecology, Leiden University Medical Center
[3] Department of Radiology, [4] Department of Medicine, Division of Hematology/Oncology, Beth Israel Deaconess Medical Center, Boston, USA
[5] Curadel, LLC, Worcester, USA

ABSTRACT

Objective: In ovarian cancer, two of the most important prognostic factors for survival are completeness of staging and completeness of cytoreductive surgery. Therefore, intra-operative visualization of tumor lesions is of great importance. Preclinical data already demonstrated tumor visualization in a mouse-model using near-infrared (NIR) fluorescence imaging and indocyanine green (ICG) as a result of enhanced permeability and retention (EPR). The aim of this study was to determine feasibility of intraoperative ovarian cancer metastases imaging using NIR fluorescence imaging and ICG in a clinical setting.

Methods: Ten patients suspected of ovarian cancer scheduled for staging or cytoreductive surgery were included. Patients received 20 mg ICG intravenously after opening the abdominal cavity. The mini-FLARE NIR fluorescence imaging system was used to detect NIR fluorescent lesions.

Results: 6 out of 10 patients had malignant disease of the ovary or fallopian tube, of which 2 had metastatic disease outside the pelvis. Eight metastatic lesions were detected in these 2 patients, which were all NIR fluorescent. However, 13 non-malignant lesions were also NIR fluorescent, resulting in a false-positive rate of 62%. There was no significant difference in tumor-to-background ratio between malignant and benign lesions (2.0 vs 2.0; P=0.99).

Conclusions: This is the first clinical trial demonstrating intraoperative detection of ovarian cancer metastases using NIR fluorescence imaging and ICG. Despite detection of all malignant lesions, a high false-positive rate was observed. Therefore, NIR fluorescence imaging using ICG based on the EPR effect is not satisfactory for the detection of ovarian cancer metastases. The need for tumor-specific intraoperative agents remains.

INTRODUCTION

Ovarian cancer has a worldwide incidence of 225,500 making it the 6th most common cancer in women. With 140,200 deaths worldwide per year, it has the highest mortality rates amongst all gynaecological cancers[1-3]. In general, ovarian cancer can be classified as early stage (FIGO I to IIa) or advanced stage (FIGO IIb to IV). Prognosis and treatment are mainly dependent on this classification.

Early stage ovarian cancer has a 5 year survival of 75-100%, with the most important factors influencing survival being differentiation grade of the tumor and the completeness of staging[1]. During surgical staging, blind biopsy samples of predefined areas and biopsy samples of suspected lesions are obtained. The primary aim of the staging procedure is to determine whether there is occult metastatic disease not primarily visible by the naked eye. When no metastases are present, resection of the primary tumor is the treatment of choice and chemotherapy can be avoided[4]. When metastases are present, surgical resection is supplemented with chemotherapy. Optimal staging has been shown to improve survival in low stage ovarian cancer because it discriminates true early stage ovarian cancer from occult tumor spread, which results in more advanced disease[4].

However, most patients (around 75%) present with advanced disease[5]. The most important prognostic factor for overall survival in advanced stage disease is the amount of residual tumor after cytoreductive surgery[6-8]. Therefore complete cytoreduction, defined as no visible residual tumor left after surgery, or optimal cytoreduction, not consistently defined as a maximal diameter of residual tumor of 0-2 cm[5;9-11], is the goal for advanced stage ovarian cancer surgery.

In order to achieve either optimal staging or complete or optimal cytoreduction, visualization of tumor lesions is of great importance. With imaging modalities such as CT and MRI, pre-operative identification and localization of tumor lesions is reasonably achievable, however intraoperative visualization of tumor tissue can be challenging.

Near-infrared (NIR) fluorescence imaging is a promising technique to assist in the real time intraoperative identification of malignant lesions[12]. This technique makes use of NIR fluorescent light (700-900 nm) emitted by contrast agents after excitation by an imaging system able to detect this NIR fluorescent

signal. NIR fluorescence is relatively easy and provides sufficient contrast due to high tissue penetration and low auto-fluorescence[13].

For tumor identification, it is essential that contrast agents accumulate in tumor tissue either actively or passively. Active accumulation can be achieved by targeting ligands that are over-expressed on tumor tissue. Van Dam et al. were the first to show tumor identification using a folate receptor alpha (FR-a) targeting agent[14]. In their series they were able to identify tumor tissue in 3 patients with FR-a positive ovarian cancer intraoperatively. However, these results have not yet been reproduced in other studies using a FR-a or different targeting agents. A possible cause for this may be the expensive and time-consuming nature of the development of these tumor-specific agents. Therefore, it is of great importance to exploit clinically available contrast agents, such as indocyanine green (ICG)[15].

In vivo ICG binds to serum proteins and therefore behaves as a macromolecule in the circulation. It is known that macromolecules accumulate in tumor tissue due to increased vascular permeability and reduced drainage. This phenomenon is called the "enhanced permeability and retention" (EPR) effect and has been observed in most solid tumors[16;17].

Clinical feasibility trials using this effect with ICG in breast cancer patients in a pre-operative diagnostic setting and in gastric cancer patients during endoscopic surgery showed that it was possible to distinguish tumor from surrounding tissue[18-23]. In addition, Kosaka et al.[24] detected small ovarian (1-2 mm in size) cancer implants using NIR fluorescent imaging after intravenous (IV) administration of ICG in a mouse model. Pathophysiological heterogeneity of solid tumors, for examples in size, presence of necrosis, or presence of vascular mediators may influence accumulation of macromolecules in tumor tissue[25;26]. It is therefore not clear if all preclinical results can be translated to the clinic.

The primairy aim of the current study was to determine the feasibility of ovarian cancer metastases detection using ICG and NIR fluorescence imaging in a clinical setting. Secondary aim was to assess concordance between fluorescence signal and tumor status on histopathology. In addition, we sought to determine if a sufficient tumor-to-background ratio (TBR), based on the EPR effect, could be obtained to discriminate between malignant and non-malignant tissue.

MATERIAL AND METHODS

Tracer preparation

ICG was prepared in the operating room following preparation instructions of the institutional pharmacist. ICG (25 mg vials, purchased from Pulsion Medical Systems Munich, Germany) was diluted in 10 cc of sterile water for injection to yield a 2.5mg/ml (3.2 mM) stock solution.

Clinical trial

The study protocol (S1 and S2 files, online available) was approved by the Local Medical Ethics Committee of the Leiden University Medical Center (LUMC) on 27-06-2012 and was performed in accordance with the ethical standards of the Helsinki Declaration of 1975. Due to administrational error, trail registration was performed after the start of the study (date trial registration 11-09-2014; ISRCTN16945066). This non-randomised study adheres to the Transparent Reporting of Evaluations with Non-Randomised designs (TREND) guidelines (S3 file). The authors confirm that all ongoing and related trials for this intervention are registered. Because this study was set up as feasibility study, no formal sample size could be calculated. Determination of feasibility was expected after inclusion of 15 patients. In case apparent non-feasibility was observed, earlier termination of the study could be performed.

Eventually, ten patients presenting at the department of Gynaecological Oncology of LUMC between 14 October 2012 and 11 December 2013 suspected of either early stage ovarian cancer scheduled to undergo staging surgery or of advanced ovarian cancer scheduled to undergo cytoreductive surgery, were included. All surgical procedures were performed by laparotomy through a midline abdominal incision. All patients gave written informed consent. Exclusion criteria were pregnancy, severe renal insufficiency (GFR < 55 mL/min/1.73 m^2), or an allergy to iodine or ICG.

In the operating theatre, after opening of the abdominal cavity, 20 mg of ICG was administered intravenously as single bolus by the anaesthesiologist. The average time between administration of ICG and imaging of the first lesion was 37 minutes. The last lesion was imaged on average 141 minutes post-administration of ICG. First the surgical field was searched for metastases visible by the naked eye. After resection of the primary tumor, uterus and ovaries, the Mini-FLARE was used to identify NIR fluorescent signals. When a fluorescent

signal was observed, the operating surgeon performed a biopsy or resection of the fluorescent tissue, unless this would jeopardize patient health or success of surgery. In case of non-fluorescence, only macroscopically suspected lesions were resected. Resected specimens were marked as fluorescent or non-fluorescent and were routinely examined by a pathologist for the presence of malignant cells.

Intraoperative near-infrared fluorescence imaging
Intraoperative imaging procedures were performed using the Mini-Fluorescence-Assisted Resection and Exploration (Mini-FLARE) image-guided surgery system, as described earlier[27]. Briefly, the system consists of 2 wavelength isolated light sources: a "white" light source, generating 26,600 lx of 400 to 650 nm light, and a "near-infrared" light source, generating 1.08 mW/came of ≈ 760 nm light. Color video and NIR fluorescence images are simultaneously acquired and displayed in real time using custom optics and software that separate the color video and NIR fluorescence images. A pseudo-colored (lime green) merged image of the color video and NIR fluorescence images is also displayed. The imaging head is attached to a flexible gooseneck arm, which permits positioning of the imaging head at extreme angles virtually anywhere over the surgical field. For intraoperative use, the imaging head and imaging system pole stand are wrapped in a sterile shield and drape (Medical Technique Inc., Tucson, AZ).

Statistical analysis
For statistical analysis, SPSS statistical software package (Version 20.0, Chicago, IL) was used. TBRs were calculated by dividing the fluorescent signal of the tumor by fluorescent signal of surrounding tissue. Patient age was reported in median, standard deviation (SD), and range, and TBR was reported in mean, SD, and range. To compare patient characteristics, independent samples t-test and chi-square tests were used. To compare TBR and background signal between malignant and benign lesions, independent samples t-test was used. $P < 0.05$ was considered significant.

RESULTS

Patient characteristics

Ten patients were included in this study. Figure 1 shows the CONSORT flow diagram for enrollment of patients. Median age was 58 years (range 42-74). Table 1 shows the patient characteristics. Seven patients underwent a staging procedure (70%), and 3 patients underwent a debulking procedure (30%). All staging and debulking procedures were open procedures.
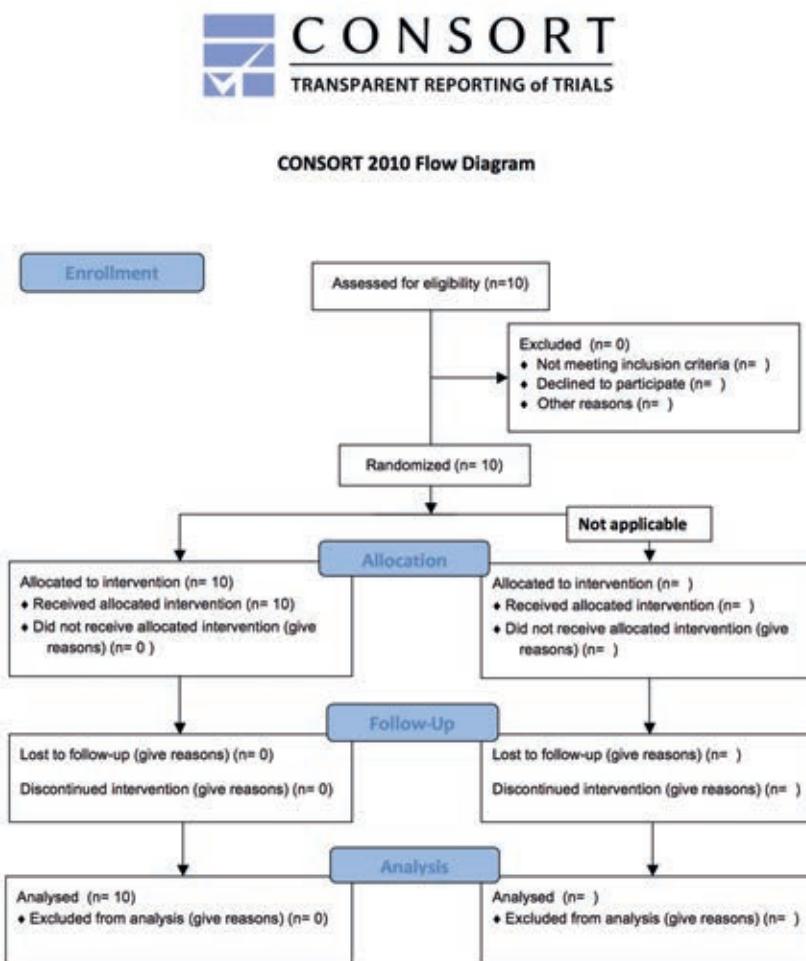

Figure 1. CONSORT flow diagram for patient enrollment

Histological assessment by the pathologist of the resected lesions confirmed the following diagnosis: 6 patients were diagnosed with either ovarian cancer (5) or cancer of the fallopian tube (1), of which the following subtypes were diagnosed: serous (3), clear-cell (1), endometrioid (1), mixed (1); one patient was diagnosed with endometrial cancer (endometriod type); and 3 patients had benign ovarian tumors. An overview of the final histological diagnoses and FIGO stage is given in Table 1.

Table 1. Patient and tumor characteristics

Study number	Age	Origin	Histologic type	FIGO stage	Surgical procedure	Metastases found during procedure
1	58	Ovary	Clearcell	1a	Staging	No
2	69	*Benign disease*	n.a.	n.a.	Staging	No
3	74	*Benign disease*	n.a.	n.a.	Staging	No
4	73	Ovary	Serous	3c	Cytoreduction	Yes
5	42	Ovary	Serous	2c	Cytoreduction	Yes
6	50	Endometrium	Endometrioid	3a	Staging	No*
7	73	*Benign disease*	n.a.	n.a.	Staging	No
8	58	Ovary	Endometrioid	1a	Staging	No
9	54	Fallopian Tube	Serous	1a	Staging	No
10	50	Ovary	Serous, Mucinous	2c	Cytoreduction	No†

* Staging was performed because an ovarian metastasis was detected at pathology after an earlier polipectomy procedure
† No biopsies were taken due to the presence of adhesions and tumor spill during the procedure, therefore defining the tumor stage as IIc with a concomitant indication for postoperative chemotherapy

Metastatic lesions

Two out of the 6 patients with malignant disease of the ovary or fallopian tube, suffered from histologically proven metastatic disease (patients #4 and #5). A total of 8 metastatic lesions, confirmed by the pathologist, were found in these 2 patients (4 lesions in both #4 and #5). Lesions were localized at the pouch of Douglas (N=3), bladder peritoneum (N=2), para iliacal lymphnodes (N=2) and omentum (N=1).

NIR fluorescence imaging

A total of 21 fluorescent lesions were identified. Figure 2A shows an example of a clinically suspected lesion, which was NIR fluorescent. This lesion was anatomically located next to the right iliac vein. Figure 2B shows the *ex vivo* images of the same NIR fluorescent lesion. This lesion was found histologically to be a metastasis of serous adenocarcinoma of the ovary. Figure 3A and 3B

show 2 NIR fluorescent lesions located in the greater omentum of the same patient as presented in Figure 2, both containing serous adenocarcinoma.
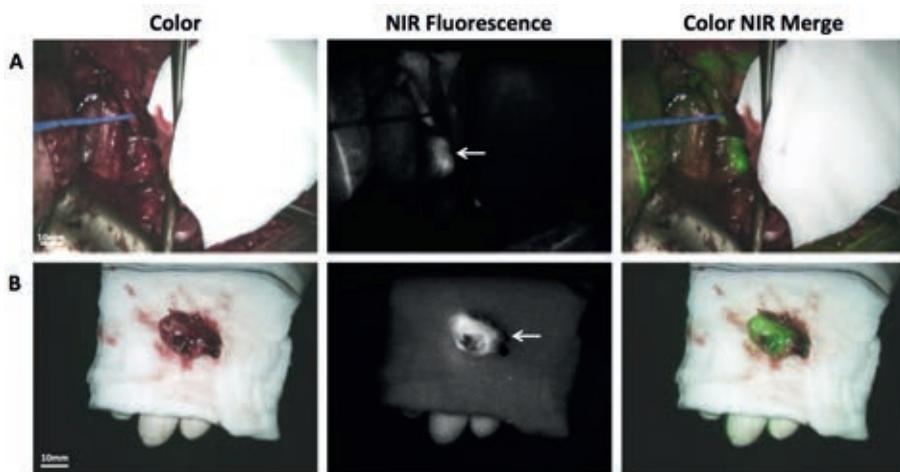

Figure 2. Identification of ovarian cancer metastases using NIR fluorescence imaging

A. Identification of ovarian cancer metastases located in a lymph node next to the right iliac vein (arrow) using NIR fluorescence imaging. The lesion was found histologically to be a metastasis of serous adenocarcinoma. **B.** *Ex vivo* imaging of the same ovarian cancer metastases located in a lymph node next to the right iliac vein (arrow).
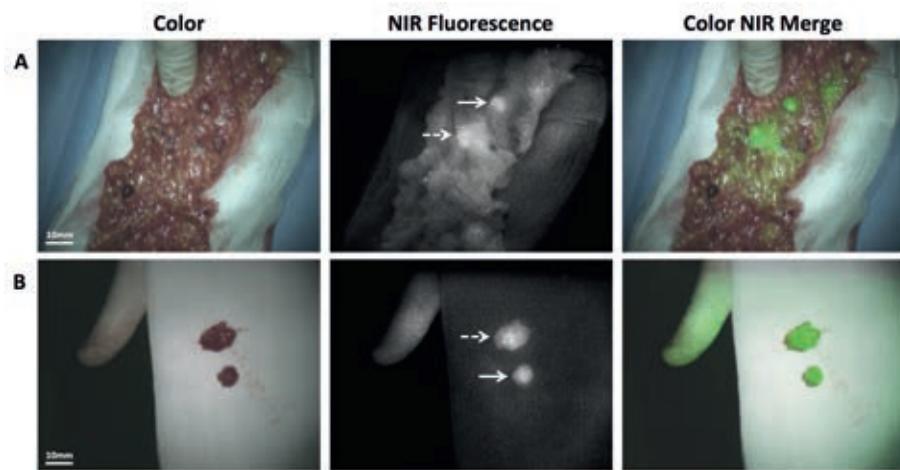
**Figure 3.** Identification of ovarian cancer omental metastases using NIR fluorescence imaging

A. Identification of 2 ovarian cancer metastases located in the greater omentum (arrow and dashed arrow) using NIR fluorescence imaging. **B.** Imaging of the same two NIR fluorescent lesions removed from the omentum (arrow and dashed arrow). Both lesions were found histologically to be metastases of serous adenocarcinoma.

All 8 histologically proven malignant metastatic lesions were NIR fluorescent, so detection of metastatic lesions of ovarian cancer with ICG had a sensitivity of 100% in this study (Table 2). The specificity of NIR fluorescence imaging could not be calculated, since lesions that were neither clinically suspect nor fluorescent were not resected.

Table 2. Characteristics lesions found with ICG NIR fluorescence imaging

	Ovarian / tubal carcinomas with metastatic disease N=2	Ovarian / tubal carcinomas with non-metastatic disease N=4	Endometrium carcinoma N=1	Benign N=3	Total N=10
NIR fluorescent lesions	8	9	2	2	21
Concordance histopathology	N (%)	N (%)	N (%)	N (%)	N (%)
True-positive	8 (100)	0 (0)	0 (0)	0 (0)	8 (38)
False-positive	0 (0)	9 (100)	2 (100)	2 (100)	13 (62)

Clinically none of these 8 malignant and fluorescent lesions had a benign appearance; therefore the use of NIR fluorescence did not lead to the detection of otherwise undetected malignant lesions. In addition 13, on histological assessment, non-malignant lesions were also NIR fluorescent, resulting in a false-positives rate of 62% (Table 2). Of these lesions, 2 were clinically characterized as malignant, 6 as suspicious for malignancy, and 5 as not suspicious for malignancy. Figure 4 shows an example of a NIR fluorescent lesion that was found to be histologically benign, thus a false-positive lesion. This particular lesion was a calcified lymph node. The localization, clinical appearance, pathology, and TBR for each false-positive lesion are listed in Table 3. Globally these false-positive lesions can be divided into two groups: normal tissue (N=10) and tissue with reactive changes (N=3).

Figure 4. Identification of ovarian cancer omental metastases using NIR fluorescence imaging

Identification of a NIR fluorescent lesion located in the mesentery of the intestine. The lesion was classified clinically as a metastasis but was found histologically to be a calcified lymph node.

Table 3. Overview of false-positive lesions detected using ICG

	Patient	Localisation	Clinically suspect for malignancy	Pathology	TBR
Tissue with reactive changes	2	Mesenterium small bowel	Uncertain	Fibrosis and hemorrhages	2.7
	3	Mesenterium ileum	Yes	Calcified lymph node	2.9*
	6	Ligamentum infundibulum pelvicum left	No	Mature fat and connective tissue, vascular structures, inflammatory infiltrate with giant cell clean-up reaction	2.4
Healthy tissue	1	Omentum	Yes	Fat and connective tissue	2.1
	6	Omentum	Uncertain	Muscle	1.3
	8	Peritoneum right	Uncertain	Connective tissue and some tubulair structures	1.6
	8	Iliaca interna right	Uncertain	Lymph node	1.7
	8	Omentum	Uncertain	Muscle	1.6 1.3
	9	Bladder peritoneum	No	Fat and connective tissue	
	9	Rectosigmoid	Uncertain	Fat and connective tissue	1.3
	9	Superficial pelvic right	No	Lymph node	1.8
	9	Superficial pelvic left	No	Lymph node	2.6
	9	High paracolic right	No	Fat and connective tissue	†

* Image shown in Fig. 4
† TBR could not be calculated

Mean TBR of the fluorescent lesions was 2.0 ± 0.6. There was no significant difference in TBR between histologically confirmed malignant and benign lesions (2.0 vs 2.0; P=0.99). Although the numbers are small, within the group of false-positive lesions a significant difference in TBR (P = 0.003) did exist between the histologically normal (1.7 ± 0.4) and reactive tissue (2.7 ± 0.2).

No adverse reactions regarding the use of ICG or NIR fluorescence imaging were seen.

DISCUSSION

In this feasibility study we investigated the use of NIR fluorescence imaging with the clinically available, non-targeted fluorescent tracer ICG in ovarian cancer patients who underwent a surgical staging procedure or cytoreductive surgery. Malignant metastatic lesions were present in 2 out of 10 patients only, but we found that 100% of these histologically proven malignant lesions were fluorescent using this technique. However, there was also a high false-positive rate of 62%.

In cytoreductive surgery, the goal is to remove as much tumor as possible, aiming for complete (no tumor visible after surgery) or leastwise optimal cytoreduction (residual tumor maximized to 10 mm), because the amount of residual tumor is one of the most important prognostic factors for survival in advanced stage patients. Van Dam et al.[14] already showed that with the use of fluorescence imaging using a folate receptor alpha targeting probe (that is over-expressed in 90-95% of ovarian cancer patients), it was possible to identify more tumor deposits than by the naked eye. In our study we could not demonstrate such an added value of NIR fluorescence using the non-specific agent ICG, because all of the fluorescent, histologically malignant lesions were identified with the naked eye.

Treatment decisions in early stage ovarian cancer patients, for instance regarding adjuvant chemotherapy, are based on the presence of occult metastases and the extent of disease found during surgical staging procedures. If staging is not done properly, this could lead to under treatment of the patient. It has been shown that completeness of surgical staging is an independent prognostic factor for overall survival in early stage patients[4]. If the use of NIR fluorescence imaging leads to more accurate detection of (occult) ovarian cancer metastases, more patients could be optimally staged, possibly leading to better treatment decision making and overall survival. In none of the 3 patients with early stage ovarian or fallopian tube cancer who underwent a staging procedure in this study, metastatic disease was found. Therefore, no added value of NIR fluorescence imaging could be demonstrated in this study using ICG. A total of 13 fluorescent lesions were observed in the 7 patients undergoing surgical staging. On pathologic testing, all 13 lesions were benign and thus false-positive. To conclude, NIR fluorescence imaging could not demonstrate added value in staging procedures because no otherwise

undetected metastatic disease could be found, but did result in the resection of non-malignant lesions.

The intended effect of NIR fluorescence imaging with ICG was based on the EPR effect. Due to tumor-induced angiogenesis, solid tumors exhibit leaky and immature vessels. Because of this macromolecules are able to permeate through the vessels and into tumor tissue where they are retained due to impaired lymph drainage[16]. ICG is not a macromolecule, but behaves like one after binding to serum proteins. This, combined with the rapid clearance from the circulation, makes ICG a potentially good probe for NIR fluorescence imaging of solid tumors. This theory has proven to be true for gastric and breast cancer[18-23]. But it should be noted that all the trials in breast cancer patients were conducted in a pre-operative diagnostic setting and results may differ from intraoperative usage of ICG.

The large number of false-positives found in this study may be due to the lack of specificity of the EPR effect. It is known that the EPR effect is influenced by multiple factors, such as size, presence of necrosis, tumor type, presence of vascular mediators such as bradykinin or prostaglandins, and location (including primary tumor vs metastatic lesion) of the lesion. Moreover, reactive processes and cancer have parallels in pathophysiological pathways and in vascular mediators. It has been shown that the EPR effect also occurs in inflammatory lesions[25;28;29]. This is in agreement with part of the false-positive lesions identified in the current study. Especially since the EPR effect in reactive tissue is more prominently present hours after injection (coinciding with our imaging window) versus days to weeks after injection in tumor tissue[26].

Several studies describe the intraoperative identification of solid tumors using clinically available, non-targeted fluorescent probes as ICG and methylene blue (MB). These studies report higher TBRs than found in the current study. For example, imaging of colorectal liver metastases using ICG (TBR 7.0)[30], parathyroid adenomas using MB (6.1)[31] and breast cancer using MB (2.4)[32] all showed higher TBRs than the observed 2.0. A possible explanation for this is that in these studies other mechanisms causing accumulation of the fluorescent probe in or around tumor tissue played a role in addition to the possible EPR effect. The EPR effect on its own may not be sufficient in providing high enough TBRs for tumor imaging. Finally, the average TBR of false-positive, benign lesions was just as high as the average TBR of true positive malignant lesions, while the average TBR of reactive benign lesions was even higher

than that of malignant lesions. This lack of discriminative power makes NIR fluorescence imaging based on the EPR effect unsuitable for further clinical implementation in ovarian cancer.

CONCLUSIONS

This is the first clinical trial demonstrating the feasibility of intraoperative detection of ovarian cancer metastases using NIR fluorescence imaging and ICG. However, a high number of false-positive lesions that could be explained by the lack of specificity of the EPR effect was found. Moreover, no distinction between malignant, reactive, or benign tissue based on TBR of the different lesions could be made. Therefore, the use of ICG, even when optimized, is not satisfactory for intraoperative NIR fluorescence imaging of ovarian cancer metastases and the need for more tumor-specific targeting agents remains. These results should be confirmed in other solid tumors where intraoperative NIR fluorescence imaging based on the EPR effect is being contemplated.

ACKNOWLEDGEMENTS

REFERENCES

1. Oncoline, www.oncoline.nl/epitheliaal-ovariumcarcinoom, Accessed 28th August 2014.

2. Ferlay J, Shin HR, Bray F, Forman D, Mathers C, Parkin DM. Estimates of worldwide burden of cancer in 2008: GLOBOCAN 2008. *Int J Cancer* 2010;127:2893-2917.

3. Jemal A, Bray F, Center MM, Ferlay J, Ward E, Forman D. Global cancer statistics. *CA Cancer J Clin* 2011;61:69-90.

4. Trimbos B, Timmers P, Pecorelli S et al. Surgical staging and treatment of early ovarian cancer: long-term analysis from a randomized trial. *J Natl Cancer Inst* 2010;102:982-987.

5. Fader AN, Rose PG. Role of surgery in ovarian carcinoma. *J Clin Oncol* 2007;25:2873-2883.

6. Bristow RE, Tomacruz RS, Armstrong DK, Trimble EL, Montz FJ. Survival effect of maximal cytoreductive surgery for advanced ovarian carcinoma during the platinum era: a meta-analysis. *J Clin Oncol* 2002;20:1248-1259.

7. Hoskins WJ, McGuire WP, Brady MF et al. The effect of diameter of largest residual disease on survival after primary cytoreductive surgery in patients with suboptimal residual epithelial ovarian carcinoma. *Am J Obstet Gynecol* 1994;170:974-979.

8. Griffiths CT. Surgical resection of tumor bulk in the primary treatment of ovarian carcinoma. *Natl Cancer Inst Monogr* 1975;42:101-104.

9. Colombo N, Van GT, Parma G et al. Ovarian cancer. *Crit Rev Oncol Hematol* 2006;60:159-179.

10. Vergote I, De W, I, Tjalma W, Van GM, Decloedt J, van DP. Neoadjuvant chemotherapy or primary debulking surgery in advanced ovarian carcinoma: a retrospective analysis of 285 patients. *Gynecol Oncol* 1998;71:431-436.

11. Vergote I, Trimbos BJ. Treatment of patients with early epithelial ovarian cancer. *Curr Opin Oncol* 2003;15:452-455.

12. Vahrmeijer AL, Hutteman M, van der Vorst JR, van de Velde CJ, Frangioni JV. Image-guided cancer surgery using near-infrared fluorescence. *Nat Rev Clin Oncol* 2013.

13. Frangioni JV. In vivo near-infrared fluorescence imaging. *Curr Opin Chem Biol* 2003;7:626-634.

14. van Dam GM, Crane LM, Themelis G et al. Intraoperative tumor-specific fluorescence imaging in ovarian cancer by folate receptor-alpha targeting: first in-human results. *Nat Med* 2011;Sep 18;17(10):1315-9.

15. Schaafsma BE, Mieog JS, Hutteman M et al. The clinical use of indocyanine green as a near-infrared fluorescent contrast agent for image-guided oncologic surgery. *J Surg Oncol* 2011;104:323-332.

16. Maeda H, Wu J, Sawa T, Matsumura Y, Hori K. Tumor vascular permeability and the EPR effect in macromolecular therapeutics: a review. *J Control Release* 2000;65:271-284.

17. Matsumura Y, Maeda H. A new concept for macromolecular therapeutics in cancer chemotherapy: mechanism of tumoritropic accumulation of proteins and the antitumor agent smancs. *Cancer Res* 1986;46:6387-6392.

18. Alacam B, Yazici B, Intes X, Nioka S, Chance B. Pharmacokinetic-rate images of indocyanine green for breast tumors using near-infrared optical methods. *Phys Med Biol* 2008;53:837-859.

19. Hagen A, Grosenick D, Macdonald R et al. Late-fluorescence mammography assesses tumor capillary permeability and differentiates malignant from benign lesions. *Opt Express* 2009;17:17016-17033.

20. Kimura T, Muguruma N, Ito S et al. Infrared fluorescence endoscopy for the diagnosis of superficial gastric tumors. *Gastrointest Endosc* 2007;66:37-43.

21. Mataki N, Nagao S, Kawaguchi A et al. Clinical usefulness of a new infrared videoendoscope system for diagnosis of early stage gastric cancer. *Gastrointest Endosc* 2003;57:336-342.

22. Ntziachristos V, Yodh AG, Schnall M, Chance B. Concurrent MRI and diffuse optical tomography of breast after indocyanine green enhancement. *Proc Natl Acad Sci U S A* 2000;97:2767-2772.

23. Poellinger A, Burock S, Grosenick D et al. Breast cancer: early- and late-fluorescence near-infrared imaging with indocyanine green--a preliminary study. *Radiology* 2011;258:409-416.

24. Kosaka N, Mitsunaga M, Longmire MR, Choyke PL, Kobayashi H. Near infrared fluorescence-guided real-time endoscopic detection of peritoneal ovarian cancer nodules using intravenously injected indocyanine green. *Int J Cancer* 2011;129:1671-1677.

25. Fang J, Nakamura H, Maeda H. The EPR effect: Unique features of tumor blood vessels for drug delivery, factors involved, and limitations and augmentation of the effect. *Adv Drug Deliv Rev* 2011;63:136-151.

26. Maeda H. Vascular permeability in cancer and infection as related to macromolecular drug delivery, with emphasis on the EPR effect for tumor-selective drug targeting. *Proc Jpn Acad Ser B Phys Biol Sci* 2012;88:53-71.

27. Mieog JS, Troyan SL, Hutteman M et al. Towards Optimization of Imaging System and Lymphatic Tracer for Near-Infrared Fluorescent Sentinel Lymph Node Mapping in Breast Cancer. *Ann Surg Oncol* 2011;18:2483-2491.

28. Maeda H, Fang J, Inutsuka T, Kitamoto Y. Vascular permeability enhancement in solid tumor: various factors, mechanisms involved and its implications. *Int Immunopharmacol* 2003;3:319-328.

29. Maeda H. The link between infection and cancer: tumor vasculature, free radicals, and drug delivery to tumors via the EPR effect. *Cancer Sci* 2013;104:779-789.

30. van der Vorst JR, Schaafsma BE, Hutteman M et al. Near-infrared fluorescence-guided resection of colorectal liver metastases. *Cancer* 2013;119:3411-3418.

31. van der Vorst JR, Schaafsma BE, Verbeek FP et al. Intraoperative near-infrared fluorescence imaging of parathyroid adenomas with use of low-dose methylene blue. *Head Neck* 2013.

32. Tummers QR, Verbeek FP, Schaafsma BE et al. Real-time intraoperative detection of breast cancer using near-infrared fluorescence imaging and Methylene Blue. *Eur J Surg Oncol* 2014;40:850-858.

Part II

Clinical translation of innovative tumor-specific fluorescent contrast agents

Chapter 9

Intraoperative imaging of folate receptor alpha positive ovarian and breast cancer using the tumor specific agent EC17

Quirijn R.J.G. Tummers[1,5*], Charlotte E.S. Hoogstins[1,5*], Katja N. Gaarenstroom[2], Cor D. de Kroon [2], Mariette I.E. van Poelgeest[2], Jaap Vuyk[3], Tjalling Bosse[4], Vincent T.H.B.M Smit[4], Cornelis J.H. van de Velde[1], Adam F. Cohen[5], Philip S. Low[6], Jacobus Burggraaf[5] and Alexander L. Vahrmeijer[1]

* Q.R.J.G. Tummers and C.E.S. Hoogstins share first authorship.

[1] Department of Surgery, Leiden University Medical Center
[2] Department of Gynecology, Leiden University Medical Center
[3] Department of Anesthesiology, Leiden University Medical Center
[4] Department of Pathology, Leiden University Medical Center
[5] Centre for Human Drug Research, Leiden, the Netherlands.
[6] Department of Chemistry, Purdue University, West Lafayette, USA

ABSTRACT

Introduction: Intraoperative fluorescence imaging of the folate-receptor alpha (FRα) could support completeness of resection in cancer surgery. Feasibility of EC17, a FRα-targeting agent that fluoresces at 500nm, was demonstrated in a limited series of ovarian cancer patients. Our objective was to evaluate EC17 in a larger group of ovarian cancer patients. In addition, we assessed the feasibility of EC17 in patients with breast cancer.

Methods: Two-to-three hours before surgery 0.1mg/kg EC17 was intravenously administered to 12 patients undergoing surgery for ovarian cancer and to 3 patients undergoing surgery for biopsy-proven FRα-positive breast cancer. The number of lesions/positive margins detected with fluorescence and concordance between fluorescence and tumor- and FRα-status was assessed in addition to safety and pharmacokinetics.

Results: Fluorescence imaging in ovarian cancer patients allowed detection of 57 lesions of which 44 (77%) appeared malignant on histopathology. Seven out of these 44 (16%) were not detected with inspection/palpation. Histopathology demonstrated concordance between fluorescence and FRα- and tumor status. Fluorescence imaging in breast cancer patients, allowed detection of tumor-specific fluorescence signal. At the 500nm wavelength, autofluorescence of normal breast tissue was present to such extent that it interfered with tumor identification.

Conclusions: FRα is a favorable target for fluorescence-guided surgery as EC17 produced a clear fluorescent signal in ovarian and breast cancer tissue. This resulted in resection of ovarian cancer lesions that were otherwise not detected. Notwithstanding, autofluorescence caused false-positive lesions in ovarian cancer and difficulty in discriminating breast cancer-specific fluorescence from background signal. Optimization of the 500nm fluorophore, will minimize autofluorescence and further improve intraoperative tumor detection.

INTRODUCTION

Over the past decades multiple imaging modalities have become available for preoperative detection of tumors, staging disease and identifying sentinel lymph nodes[1;2]. However, translation of preoperative obtained images to the surgical theatre can be challenging. Consequently, surgeons largely have to rely on visual inspection and palpation to discriminate between healthy and malignant tissue. As a result, incomplete resection of malignant tissue may occur. In breast cancer surgery, for example, positive resection margins are reported in up to 20% of patients after resection of the primary tumor[3]. In metastasized disease, intraoperative imaging of tumor tissue can be of great advantage. In ovarian cancer for example, clear intraoperative detection of metastatic lesions can improve staging procedures in early stage ovarian cancer (FIGO I and IIa), and facilitate complete or optimal cytoreductive surgery in advanced stage disease (FIGO IIb to IV). Both the prevention of positive margins in solid tumors and the performance of adequate staging and complete/optimal cytoreduction will improve individual patient outcome[4-9]. Hence there is a clear unmet need for intraoperative modalities that can identify tumor tissue with high sensitivity and specificity.

An innovative intraoperative optical imaging technique is fluorescence imaging. Over the past years multiple studies have been performed on tumor imaging, sentinel lymph node (SLN) mapping and identification of vital structures, using fluorescence imaging[10;11].

Optical properties of fluorescent contrast agents are of importance for successful tumor imaging. The wavelength of the fluorescent light largely determines the degree of penetration of photons into the tissue. Photons in the visible light range have a depth penetration limited to a few millimeters and are suitable for detection of superficial targets. Conversely photons in the NIR range (650-900 nm) can travel more than a centimeter through tissue, which also enables detection of targets below the tissue surface[12]. Moreover, the wavelength of the fluorescent light also plays a role in autofluorescence. Autofluorescence is fluorescence arising from intrinsic tissue components after excitation with UV, visible, or NIR radiation of suitable wavelength. To detect cancer cells targeted with an optical contrast agent, the signal of the target-specific fluorescence must be significantly higher than the autofluorescence. The occurrence of autofluorescence is determined by the tissue type and excitation wavelength[13;14].

Biological characteristics of fluorescent contrast agents are essential to achieve target-specific fluorescence imaging. Ideally, a contrast agent binds exclusively to a cancer specific ligand, while being excreted rapidly from the rest of the body. Over the past years, extensive preclinical validation of tumor-specific contrast agents targeting a variety of ligands was reported, however only very few were clinically introduced[15;16]. For this reason, several clinical studies have been performed to explore feasibility of clinically available fluorescent contrast agents like methylene blue (MB) and indocyanine green (ICG) for intraoperative tumor imaging of breast cancer tissue and ovarian cancer tissue[17;18]. These agents do not specifically bind to the tumor, but make use of other mechanisms such as the Enhanced Permeability and Retention (EPR)[19;20] effect and disturbed excretion profiles causing accumulation in or around tumor tissue. Although promising results were described, resection of non-malignant lesions due to false positive fluorescence proved an insurmountable problem in the road to clinical application. Consequently, the need for newly developed contrast agents with highly specific binding to tumor-specific targets remains.

A promising target for image-guided surgery is the folate receptor alpha (FRα). Normally the FRα is expressed only at low levels and due to its location on the apical membrane of epithelial cells it is not accessible for molecules transported by blood[21;22]. In contrast, in many types of epithelial cancers, the FRα is highly expressed. As a result of the loss of cell polarity in cancer, the FRα is easily accessible by blood making it an ideal tumor target. Over 90% of all epithelial ovarian cancers over-express FRα, and in ovarian cancers of serous morphology this percentage is even higher (90-100%)[23-25]. Moreover, expression is not altered by chemotherapy[26;27], allowing use of this target in both primary and interval cytoreductive surgical procedures. In breast cancer, FRα overexpression is reported in 30% of tumors, this percentage is even higher (67%) in tumors with a "triple-negative" receptor profile[28]. In almost all breast cancer patients, preoperative biopsies are available, allowing characterization of FRα status before surgery to select patients who will benefit from FRα targeted imaging agents.

While multiple preclinical studies have been performed on the imaging of FRα positive tumors[29-31], clinical experience is very limited. Van Dam et al. showed feasibility of intraoperative imaging of ovarian cancer metastases using EC17, a FRα targeting contrast agent with fluorescent properties in

the visible light spectrum (500nm). In a limited series of patients undergoing surgery for suspected ovarian cancer, fluorescent tumor tissue was observed intraoperatively after intravenous administration of EC17 in 3 out of 4 patients with proven ovarian cancer. However, the intra-operative detection of additional tumor lesions due to the use of EC17 and fluorescence imaging was not reported. Moreover, administration of the contrast agents had to be interrupted, although the study could be completed, in several (4 out of 10) patients due to mild adverse events. As a result the initial dose of 0.3 mg/kg was decreased to 0.1 mg/kg, which reduced adverse events while maintaining fluorescent signal. To demonstrate the tolerability and additional value of fluorescence imaging using EC17 in ovarian cancer, evaluation in a larger patient cohort is required. Although the overexpression of the FRα on selected breast cancer cells has been shown, feasibility of fluorescence imaging using EC17 in patients with FRα positive breast cancer has not yet been demonstrated.

Our objective was to evaluate a relatively low dose of EC17 (0.1 mg/kg) in a larger group of ovarian cancer patients and to assess feasibility of intraoperative fluorescence imaging in patients with FRα positive breast cancer.

RESULTS

Patient characteristics
A total of 13 ovarian cancer patients were included. Surgery was cancelled in 1 patient due to deterioration of the medical condition of the patient prior to surgery. Thus 12 ovarian cancer patients received EC17 and underwent open surgery; a tabular overview of the patient characteristics, FIGO status and histology of the tumor type is given in Table 1. Six patients underwent a primary cytoreductive procedure, 4 patients an interval cytoreductive procedure and 2 patients a staging procedure.

Table 1. Demographic and baseline characteristics of ovarian cancer patients

Patient ID	Age	Surgical procedure	Diagnosis	FIGO stage	Metastases identified	Tumor FRα+	Fluorescence imaging successful
1	71	Primary debulking	Serous adenocarcinoma	3c	Yes	Yes	Yes
2	51	Primary debulking	Endometroid type adenocarcinoma	3b	Yes	Yes	Yes
3	59	Staging	Endometroid type adenocarcinoma	2c	No	Yes	Yes
4	61	Interval debulking	Serous adenocarcinoma of endometrium	4	Yes	Yes	Yes
5	64	Primary debulking	Borderline serous adenocarcinoma	3b	Non-invasive implants	Yes	Yes
6	71	Primary debulking	Serous adenocarcinoma	3c	Yes	Yes	Yes
7	71	Primary debulking	Serous adenocarcinoma	3b	Yes	Yes	Yes
8	78	Interval debulking	Serous adenocarcinoma	3c	Yes	Yes	Yes
9	57	Interval debulking	Serous adenocarcinoma	3c	Yes	Yes	Yes
10	52	Interval debulking	Serous adenocarcinoma	4	Yes	Yes	Yes
11	42	Primary debulking	Mucinous adenocarcinoma	3c	Yes	No	No
12	73	Staging	Endometroid type adenocarcinoma	2b	No	Yes	Yes

For breast cancer, a total of 53 potentially eligible breast cancer patients were selected for characterization of FRα status on preoperatively obtained biopsies. Samples of six patients stained positive for FRα (11%). Of the 6 patients, 2 patients eventually did not meet the inclusion criteria and 1 patient declined participation. Three patients were included in the study and their characteristics are provided in Table 2.

Table 2. Demographic and baseline characteristics of breast cancer patients

Patient ID	Age	Surgical procedure	Diagnosis	Tumor size in mm	ER status	PR Status	HER2 Status	SLN metastasis	Tumor FRα+	Fluorescence imaging successful
1	54	BCS	IBC NST	19	Neg	Neg	Neg	Yes, 9mm	Yes	Yes*
2	61	BCS	Metaplastic carcinoma	42	Neg	Neg	Neg	No	Yes	Yes
3	53	Mastectomy	IBC NST	23	Pos	Pos	Neg	No	Yes	Yes

Abbreviations: BCS, Breast Conserving Surgery; IBC, infiltrative breast cancer; NST, No Special Type
* Tumor successfully identified in resection specimen. SLN metastasis not identified due to lack of tissue penetration.

Safety

All patients received 0.1 mg/kg EC17 over 10 minutes, and no infusion was intermitted or stopped. Infusion of EC17 was associated with mild, self-limiting hypersensitivity reactions in 7 out of 15 patients. The symptoms consisted of abdominal discomfort, itching throat and sneezing (for a summary list of treatment related adverse events, see Table S1, online available). One patient vomited after EC17 administration and received ondansetron 8 mg intravenously, followed by the planned surgical procedure. There were no clinical relevant changes in blood pressure or pulse rate compared to baseline.

Intraoperative fluorescence imaging

Intraoperative fluorescence imaging in ovarian cancer patients allowed clear detection of ovarian cancer lesions. Figure 1 shows an example of fluorescent ovarian cancer metastases.
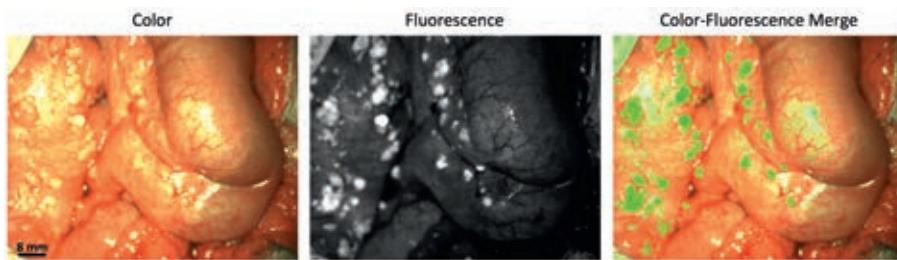

Figure 1. Identification of ovarian cancer metastases using fluorescence imaging

Identification of ovarian cancer metastases located on the intestine and mesentery using fluorescence imaging. Biopsies of lesions were found histologically to be metastases of serous adenocarcinoma.

In total, 57 fluorescent lesions that were identified during surgery were resected. Of these resected lesions 44 (77%) appeared to be malignant on histopathology. Seven (16%) of these 44 lesions were not detected by visual inspection with the naked eye or palpation either because they appeared benign or because they were missed during inspection due to small size (<10mm) and flat nature. These lesions were only removed because these could be identified using fluorescence imaging. Mean TBR was 7.0 ± 1.2. Fluorescence imaging was successful up to about 5.5 hours after EC17 administration, which was the longest time interval measured between administration and the end of a surgical procedure.

Histopathology demonstrated clear concordance between fluorescence and FRα- and tumor status. Fluorescence microscopy showed clear membranous and cytoplasmic accumulation of EC17 in tumor cells (Figure 2).
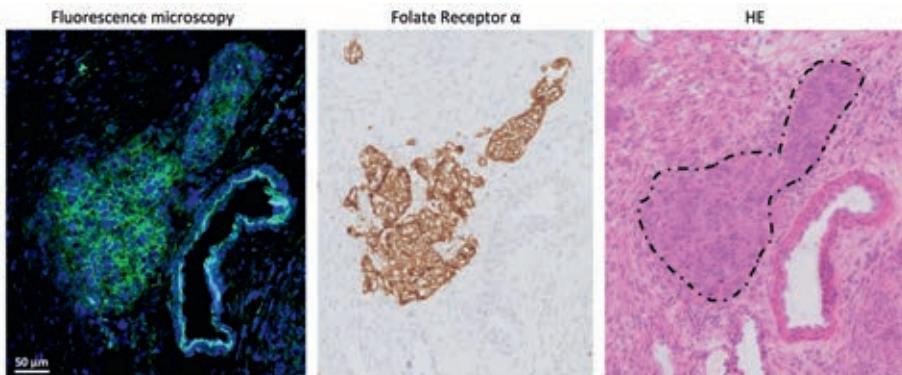

Figure 2. Histopathological evaluation of fluorescence signal in ovarian cancer

Fluorescence signal is indicated with green, blue color represents cell nuclei stained with DAPI. Fluorescence microscopy showed clear membranous and cytoplasmic accumulation of EC17 in tumor cells .The fluorescent signal is located on all sites that stain positive for FRα expression, which is the anatomical site that appears to be a metastasis of serous ovarian adenocarcinoma on hematoxylin and eosin staining (dashed circle).

The (ex-vivo) assessment of the stills obtained from the videos made during the surgical procedure showed that on average (SD) 23.3 (± 11.9) lesions per still were identified with the naked eye. When the stills were supplemented with the fluorescence image, 39.6 (± 22.7) lesions per still were identified, a 70% increase.

In total, 3 false-negative lesions were identified. These lesions were all metastases in the greater omentum. The lesions were considered suspicious for malignancy by the surgeons, but showed no intraoperative fluorescence signal from the outside (Figure 3A). However, upon dissection of the omentum on the backtable, strong fluorescent signal was identified (Figure 3B), suggesting that the intraoperative non-fluorescence was caused by the lack of tissue penetration at 500nm wavelength.
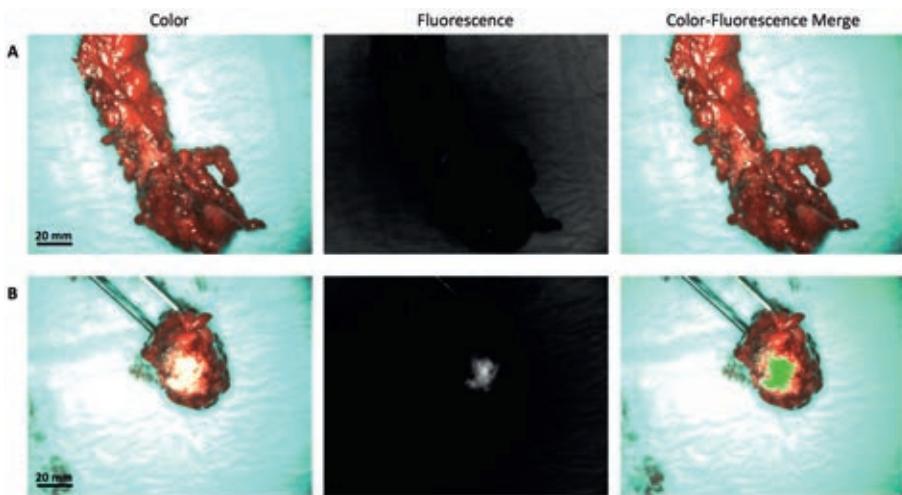
**Figure 3.** False-negative fluorescent signal caused by a lack of depth penetration

A. Example of a metastasized greater omentum, which was clinical suspicious, but showed no fluorescence signal from the outside. **B.** After dissecting the omentum, strong fluorescent signal was identified. This observation shows the lack of tissue penetration at 500nm.

Thirteen out of the 57 (23%) fluorescent lesions appeared benign. Five of these false positive lesions were identified as normal fallopian tube tissue on histopathological evaluation, showing FRα expression. These lesions were thus expected to bind EC17, and were resected anyway as part of the standard surgical procedure. Six lesions were structures mainly containing collagen, which is known to cause autofluorescence at 500nm. Mean TBR of the false-positives was 5.4 ± 1.0. There was no significant difference in TBR between true-positives and false-positives (7.0 vs. 5.4; $P = 0.47$). Characteristics of false positive and false negative lesions are provided in Table 3.

Also in breast cancer, tumor-specific fluorescence signal was observed. Median TBR was 2.3 (range 2.1 – 6.2). However, autofluorescence of normal breast tissue was present to such extent that it interfered with tumor identification. Figure 4 shows fluorescent signal in breast cancer tissue and in normal, autofluorescent breast tissue. Fluorescence microscopy showed clear membranous and cytoplasmic accumulation of EC17 in tumor cells (Figure 5). In addition, high background fluorescent signal was observed, which is in concordance with images obtained with the intraoperative Artemis imaging system.

Table 3. Characteristics of false positive and false negative fluorescent lesions in ovarian cancer

Patient ID	Location lesion	False positive or negative	Probable cause
1	Fallopian tube	False positive	FRα expression
2	Iliacal lymph node	False positive	FRβ expression activated macrophages
2	Ligamentum rotundum	False positive	Autofluorescence collagen containing structure
4	Omentum	False negative	Inadequate penetration depth
5	Leiomyoma Uterus	False positive	Autofluorescence collagen containing structure
5	Leiomyoma Uterus	False positive	Autofluorescence collagen containing structure
5	Omentum biopsy	False positive	Unknown
7	Omentum	False negative	Inadequate penetration depth
8	Omentum	False negative	Inadequate penetration depth
8	Fallopian tube	False positive	FRα expression
10	Fallopian tube	False positive	FRα expression
12	Cervix	False positive	Autofluorescence collagen containing structure
12	Myometrium uterus	False positive	Autofluorescence collagen containing structure
12	Fallopian tube	False positive	FRα expression
12	Infundibulopelvic ligament	False positive	Autofluorescence collagen containing structure
12	Ovary (contralateral)	False positive	FRα expression
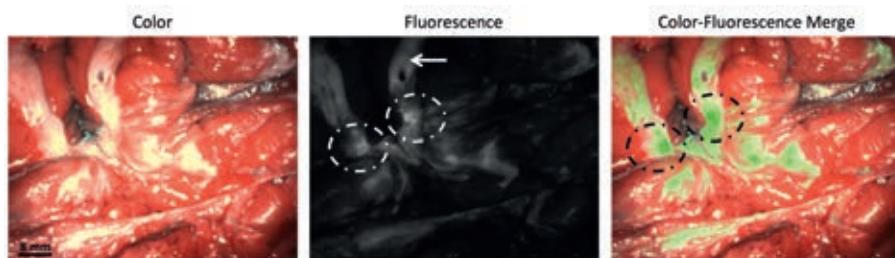
Figure 4. Identification of breast cancer metastases using fluorescence imaging

Identification of a bisected primary breast cancer lesion using fluorescence imaging (dashed circles). The arrow indicated autofluorescence signal from normal breast tissue. The tumor was found histologically to be an infiltrating breast cancer of no special type.

In one patient with breast cancer, a tumor-positive SLN was found on histopathological evaluation. This SLN however was not detected with fluorescence imaging. After HE and FRα staining, the metastasis appeared to be in the center of the SLN, and was therefore not detected due to lack of tissue penetration.

Pharmacokinetics

The maximal concentration for each dose was obtained directly after the end of the infusion and declined thereafter with a half-life of 86.8 minutes.
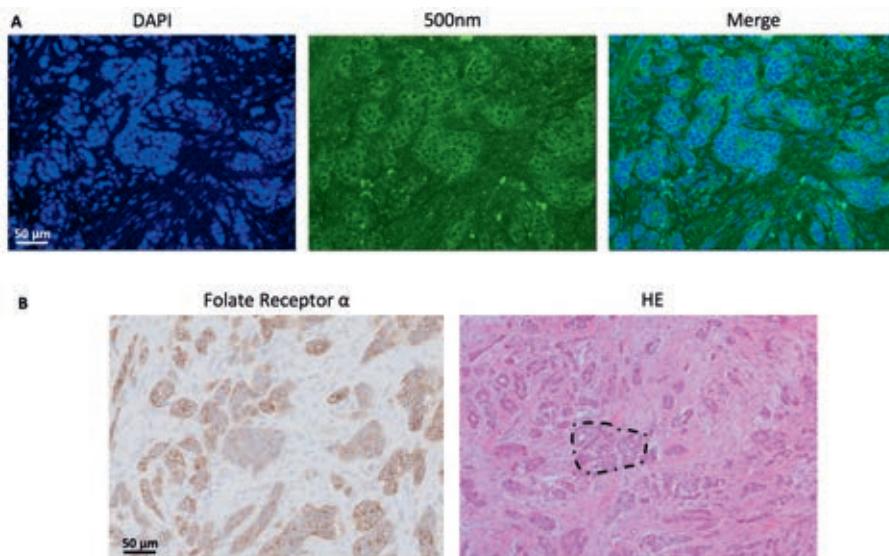
Figure 5. Histopathological evaluation of fluorescence signal in breast cancer
A. Fluorescence microscopy showed clear membranous and cytoplasmic accumulation of EC17 in tumor cells. Blue color represents cell nuclei stained with DAPI, fluorescence signal is indicated with green. Also a relatively high diffusely fluorescent background signal is seen, which is in concordance with the fluorescence images obtained with the intraoperative imaging system. **B.** Immunohistological staining for FRα expression shows a FRα positive infiltrating breast cancer of no special type (example in dashed circle). Clear concordance is observed between fluorescent signal and FRα positive malignant lesions.

DISCUSSION

Intraoperative imaging of tumor tissue may improve patient outcome by enhanced identification and subsequent resection of tumor tissue. Fluorescence guided surgery using the FRα specific contrast agents EC17 allowed real time identification of both ovarian- and breast cancer cells. In ovarian cancer, the intraoperative use of fluorescence imaging resulted in the resection of 16% more malignant lesions compared to inspection with the naked eye and/or palpation only. Visual identification was improved on stills made from intraoperative videos, supporting the notion that fluorescent imaging improves detection even when other techniques like palpation are not available.

The biophysical properties of imaging agents are of paramount importance for successful tumor identification. Ideally, high fluorescence signal is observed in malignant lesions, while normal or healthy tissue shows minimal fluorescence

because of a low binding constant and fast excretion of the imaging agent after initial biodistribution. The size of the compound greatly influences this profile. Currently monoclonal antibodies, antibody fragments, such as single-chain (scFv) of fab fragments, small peptides or structure-inherent targeting fluorophores are used for tumor-specific imaging[32-36]. The biodistribution, excretion and binding profile of EC17 shows several great advantages in imaging. The maximum concentration (Cmax) of EC17 is observed directly after the end of administration and is followed by a rapid excretion from the blood. While fluorescence signal of the tumor is observed up to more than 5 hours after administration of the compound. This short terminal half-life in blood, strong tumor specific signal and low background signal allows tumor imaging from 2 hours post dosing and during a relative long time.

Around 75% of patients with ovarian cancer present with advanced stage of the disease[37]. Multiple studies have shown that the amount of residual disease is the most important prognostic factor for survival in ovarian cancer patients. As a result of these studies, consensus exists that all attempts should be made to achieve complete cytoreduction i.e. complete removal of all macroscopically visible tumor tissue[4;6;8;38;39]. In this study, real-time visualization of malignant lesions using fluorescence imaging during surgery led to the detection of 16% additional malignant lesions. This may improve cytoreduction and hereby patient outcome. The effect of the addition of intraoperative fluorescence imaging on survival was already shown by Stummer et al. in patients with brain glioma. They demonstrated that fluorescence imaging with 5-ala not only leads to more complete resections but also to improved progression free survival[5]. For ovarian cancer more prospective research is necessary to establish the effect on overall survival.

When patients present with clinically early stage ovarian cancer, a staging procedure is recommended. During this procedure, biopsies of suspicious lesions are taken, supplemented with "blind" biopsies from predefined locations. Ultimate goal is to identify metastatic lesions whenever present in order to give adequate treatment i.e. systemic chemotherapy. Visualizing metastatic lesions by fluorescence imaging may optimize staging procedures, as less "blind" biopsies have to be taken. This could facilitate discrimination between true early stage ovarian cancer and more advanced stage with occult tumor spread. Especially in minimal-invasive surgery, when tactile information (palpation) of lesions cannot be obtained, fluorescence imaging could be of additional value.

In breast cancer, up to 20% of patients have positive resection margins after resection of the primary tumor[3]. Visualizing tumor cells during surgery could lower the risk of an incomplete resection as identification of a positive margin can result in direct resection of residual tumor tissue. Although this will probably not influence overall survival, as patient with positive resection margins are currently treated with a re-resection or more intensive radiotherapy, significantly lower healthcare costs and burden to the patient could result. To investigate this concept, both FRα positive breast cancer patients treated with BCS and breast ablation were included in the current feasibility study. However, for future applicability of fluorescence imaging in breast cancer surgery, the most added value is to be expected in BCS. Moreover, a significant number of patients with breast carcinoma is pre-treated with neoadjuvant systemic chemotherapy to reduce the primary tumor to facilitate BCS instead of radical mastectomy[40]. Although pre-treatment with systemic therapy does not result in an increased number of positive resection margins[41], recognition of vital tumor tissue can be challenging. As FRα status is not changed by chemotherapy[27;42], fluorescence imaging could be of added value in these challenging cases.

In literature, FRα positive breast cancer lesions are described in up to 30% of patient[43-45]. In our series however, only 11% of the obtained biopsies stained positive for FRα. No explanation was found for this lower expression level. A high number of normal breast tissue stained weak positive for FRα, mainly located at the apical surface of epithelial cells and at myoepithelial cells. This finding has been described previously[43;45], and does not necessarily cause a pitfall for FRα as target for fluorescence guided surgery, because the myoepithelium is not accessible for blood carried contrast agents.

Several limitations of the described technique and contrast agent were caused by the optical properties of the contrast agent. EC17 fluoresces at 488nm, which does not allow identification of lesions located beneath the surface. In 3 patients with ovarian cancer, the greater omentum was suspected for malignancy, but only showed fluorescence after dissection of the tissue and this clearly showed the low tissue penetration of the photons emitted by EC17. We identified 23% false-positive lesions in the patients with ovarian cancer. The non-malignant lesions that fluoresced in this study were in particular collagen-containing structures, from which it is known that they can show autofluorescence in the visible light spectrum[14;46].

All the above-mentioned limitations could be overcome by conjugating the folate analog to a fluorophore that fluoresces in the NIR spectrum. This allows identification of structures located deeper beneath the surface due to a lower absorption coefficient, and causes less autofluorescence of normal tissue[47]. For surface detection of malignant cells, as in breast cancer, depth penetrating is less important, but currently the autofluorescent signal prevented clinical decision-making. Figure S1 (online available) shows fluorescence imaging at 500nm and 800nm of breast tissue containing a tumor. These tissue specimens, from patients that were not treated with an exogenous contrast agent as EC17, are thus suitable to demonstrate background autofluorescence. At 500nm high background autofluorescence is observed, while at 800nm no background autofluorescence signal is seen (Supplementary Methods, online available). This illustrates the need for tumor-specific contrast agents in the NIR spectrum. Currently, our research group is performing a first-in-human clinical trial in ovarian cancer patients using the FRα specific near-infrared contrast agent OTL38. Preclinical tests comparing OTL38 with EC17 have demonstrated superiority of OTL38 in sensitivity and brightness[48].

In conclusion, administration of EC17 was reasonably well-tolerated and produced clear fluorescent signals in ovarian and breast cancer tissue. This allowed resection of 16% more ovarian cancer lesions. Notwithstanding, autofluorescence of benign, predominantly collagen-containing tissues led to detection of a significant proportion of false positive lesions in ovarian cancer. Further, autofluorescence resulted in difficulty in discriminating breast cancer tissue specific fluorescence from background fluorescence. We conclude that FRα is a favorable tumor-specific target, but EC17 lacks the full set of requirements for fluorescence-guided surgery in FRα-positive ovarian and breast cancer, especially because of autofluorescence and insufficient penetration depth. Replacing the 500nm fluorophore by a fluorophore in the NIR spectrum could likely further improve optical properties and thereby clinical relevance of fluorescence-guided surgery.

METHODS

Investigational agent
EC17 (molecular formula: $C_{42}H_{36}N_{10}Na_2O_{10}S$; On Target Laboratories LLC, West Lafayette, USA) consists of a folate analogue conjugated to 5-fluorescein isothiocyanate (FITC), which is exited between the wavelengths of 465 and 490nm and fluoresces at wavelengths of 520-530 nm. Before administration, the frozen vials containing 5 mg/mL EC17 in 3 mL water for injection were thawed and diluted in 10 mL sterile saline. Patients received 0.1 mg/kg EC17 intravenously over 10 minutes, 2-3 hours before surgery.

Patients
Patients suspected of early stage epithelial ovarian cancer presenting at the department of Gynecology of the Leiden University Medical Center (LUMC) between February 2014 and September 2014 scheduled to undergo staging surgery or of advanced epithelial ovarian cancer scheduled to undergo cytoreductive surgery, were included in this study. All patients gave written informed consent.

For breast cancer, patients presenting at the department of Surgery of the LUMC between May 2014 and February 2015 planned for, either breast conserving surgery (BCS) or breast ablation, were eligible for participation. After selection, preoperatively obtained biopsies of potentially eligible patients were stained for FRα expression using immunohistochemistry (IHC). FRα expression was assessed by using a membranous scoring method with a scale ranging from 0 to 3+, as described by O'Shannessy et al.[49] A score of 0 corresponded to absence of staining; 1+ equaled faint staining on luminal borders; 2+ equaled moderate staining on apical and sometimes lateral borders and 3+ indicated strong circumferential staining. The tumor was considered positive when more than 10% of malignant cells were positively stained (>0). Assessment of the stained biopsies was performed by a pathologist (VTHBMS or TB), and after presence of FRα positive tumor cells was confirmed, patients were eligible for EC17 administration. All patients gave written informed consent.

Exclusion criteria were age<18, pregnancy (excluded by pregnancy test in woman of childbearing potential), renal impairment (defined as eGFR<50 mL/min/1.73m^2), impaired liver function (defined as evidenced by greater than 3x the upper limit of normal (ULN) for ALT, AST, or total bilirubin), or a history of anaphylactic reaction to EC17, insect bites or fluorescein.

Clinical Trial

The study was approved by the Medical Ethics Committee of the LUMC and was performed in accordance with the laws and regulations of the Netherlands. Suitability of selected patients was further assessed by a medical screening consisting of a medical history, physical examination including vital signs, weight, 12-lead ECG, and routine laboratory assessments.

Before administration of EC17, two iv cannulas were inserted. One iv cannula was used for study drug administration and the cannula in the contralateral arm for PK sampling (Supplementary Methods, online available). After administration, safety assessments (blood pressure, pulse, peripheral oxygen saturation and temperature) and blood collection for pharmacokinetics were performed regularly from just prior to administration up to the end of surgery. A stopping rule was defined in the protocol. In case of treatment-related serious adverse events or results suggesting futility to continue, the trial would be halted or stopped.

Surgical procedure in ovarian cancer patients

All surgical procedures were performed by laparotomy through a midline abdominal incision. After opening of the abdominal cavity, the surgical field was searched for the primary tumor and metastases visible by the naked eye or palpation. Thereafter, the Artemis imaging system (see below for details) was used to identify fluorescent signals. When a fluorescent signal was observed, the operating surgeon performed a biopsy or resection of the fluorescent tissue. In case of non-fluorescence, only lesions macroscopically suspect for malignancy were resected. Resected specimens were marked as clinically suspect or not clinically suspect and as fluorescent or non-fluorescent. All resected lesions were examined by a pathologist for tumor status. In addition, an immunohistochemical (IHC) staining for FRα expression and fluorescence microscopy (Leica DM5500B fluorescence microscope) were performed to assess concordance of fluorescence with tumor and FRα presence and to evaluate binding sites of EC17 (Supplementary Methods, online available).

To assess the number of malignant lesions that were identified by the naked eye and/or fluorescence imaging, stills from intraoperative obtained videos were analyzed by three dedicated gynecologic oncologists, experienced in ovarian cancer surgery. A total of 5 different images were analyzed. Each image was analyzed 3 times (normal, horizontally and vertically flipped), leading to a

total of 15 images to be analyzed. First, only colour images were used to score the number of observed metastatic lesions. When this was completed, colour images supplemented with fluorescence images were scored.

Surgical procedure in breast cancer

Patients underwent standard of care breast ablation or BCS both combined with SLN biopsy. The Artemis fluorescence imaging system was used to identify fluorescent signal during surgery and on resected specimens transferred to the pathology department. Intra-operative images of SLNs, the surgical field, resected specimen, and wound bed after resection were obtained. Following standard procedure, the resected specimen was dissected at the pathology department, where images from the dissected tumor were obtained as well. The resected specimens were routinely examined by a pathologist for tumor status. In addition, IHC staining for FRα expression and fluorescence microscopy (Leica DM5500B fluorescence microscope) were performed to evaluate binding site of EC17 (Supplementary Methods, online available).

Artemis fluorescence imaging system

Imaging procedures were performed using the Artemis fluorescence imaging system (Quest Medical Imaging, The Netherlands). The system consists of 3 wavelength isolated light sources: a "white" light source, and a two different "near-infrared" light sources. For this study, the camera and light engine were optimized for EC17 to generate 7.5 mW/cm^2 at 490 nm light. Color video and fluorescence images are simultaneously acquired on separate sensors and displayed in real time using custom optics and software showing the separate the color video and NIR fluorescence images. A pseudo-colored (lime green) merged image of the color video and fluorescence images is also displayed. The intensities of the light sources could be controlled from the Artemis software. The camera can be attached to a freely moveable arm head. For intraoperative use, the camera and freely moveable arm were wrapped in a sterile shield and drape (Medical Technique Inc., Tucson, AZ).

Statistical and Image Analysis

SPSS statistical software package (Version 20.0, Chicago, IL) was used. Patient characteristics were reported in median, standard deviation (SD), and range. PK parameters (AUC, Cmax, tmax) were statistically summarized including number

of subjects, mean, standard deviation (SD), median, minimum and maximum. Plasma drug concentrations were plotted versus time per individual using both a linear and log y-axis. Additionally, concentration versus time curves were plotted as a spaghetti plot with the median added.

Fluorescent signal in tumor and background was quantified using ImageJ (version 1.49b; a public domain, Java-based image processing program developed at the National Institute of Health). Regions of interest (RoI) were drawn with ImageJ on the stored images to quantify fluorescent signal in arbitrary units [AU]. Tumor to background ratios (TBRs) were calculated by dividing the fluorescent signal of the tumor by fluorescent signal of surrounding tissue. To compare TBR and background signal between malignant and benign lesions independent samples t-test was used. TBR was reported in mean, SD, and range.

ACKNOWLEDGEMENTS

REFERENCES

1. Frangioni JV. In vivo near-infrared fluorescence imaging. *Curr Opin Chem Biol* 2003;7:626-634.

2. Weissleder R, Pittet MJ. Imaging in the era of molecular oncology. *Nature* 2008;452:580-589.

3. Pleijhuis RG, Graafland M, de VJ, Bart J, de jong JS, van Dam GM. Obtaining adequate surgical margins in breast-conserving therapy for patients with early-stage breast cancer: current modalities and future directions. *Ann Surg Oncol* 2009;16:2717-2730.

4. Chang SJ, Bristow RE, Ryu HS. Impact of complete cytoreduction leaving no gross residual disease associated with radical cytoreductive surgical procedures on survival in advanced ovarian cancer. *Ann Surg Oncol* 2012;19:4059-4067.

5. Stummer W, Pichlmeier U, Meinel T, Wiestler OD, Zanella F, Reulen HJ. Fluorescence-guided surgery with 5-aminolevulinic acid for resection of malignant glioma: a randomised controlled multicentre phase III trial. *Lancet Oncol* 2006;7:392-401.

6. Bristow RE, Berek JS. Surgery for ovarian cancer: how to improve survival. *Lancet* 2006;367:1558-1560.

7. Bristow RE, Tomacruz RS, Armstrong DK, Trimble EL, Montz FJ. Survival effect of maximal cytoreductive surgery for advanced ovarian carcinoma during the platinum era: a meta-analysis. *J Clin Oncol* 2002;20:1248-1259.

8. Vergote I, Trope CG, Amant F et al. Neoadjuvant chemotherapy or primary surgery in stage IIIC or IV ovarian cancer. *N Engl J Med* 2010;363:943-953.

9. Hoskins WJ, McGuire WP, Brady MF et al. The effect of diameter of largest residual disease on survival after primary cytoreductive surgery in patients with suboptimal residual epithelial ovarian carcinoma. *Am J Obstet Gynecol* 1994;170:974-979.

10. Handgraaf HJ, Verbeek FP, Tummers QR et al. Real-time near-infrared fluorescence guided surgery in gynecologic oncology: a review of the current state of the art. *Gynecol Oncol* 2014;135:606-613.

11. Vahrmeijer AL, Hutteman M, van der Vorst JR, van de Velde CJ, Frangioni JV. Image-guided cancer surgery using near-infrared fluorescence. *Nat Rev Clin Oncol* 2013;10:507-518.

12. Patterson MS, Chance B, Wilson BC. Time resolved reflectance and transmittance for the non-invasive measurement of tissue optical properties. *Appl Opt* 1989;28:2331-2336.

13. Weissleder R, Ntziachristos V. Shedding light onto live molecular targets. *Nat Med* 2003;9:123-128.

14. Monici M. Cell and tissue autofluorescence research and diagnostic applications. *Biotechnol Annu Rev* 2005;11:227-256.

15. van Dam GM, Themelis G, Crane LM et al. Intraoperative tumor-specific fluorescence imaging in ovarian cancer by folate receptor-alpha targeting: first in-human results. *Nat Med* 2011;17:1315-1319.

16. Burggraaf J, Kamerling IM, Gordon PB et al. Detection of colorectal polyps in humans using an intravenously administered fluorescent peptide targeted against c-Met. *Nat Med* 2015;21:955-961.

17. Tummers QR, Verbeek FP, Schaafsma BE et al. Real-time intraoperative detection of breast cancer using near-infrared fluorescence imaging and Methylene Blue. *Eur J Surg Oncol* 2014;40:850-858.

18. Tummers QR, Hoogstins CE, Peters AA et al. The Value of Intraoperative Near-Infrared Fluorescence Imaging Based on Enhanced Permeability and Retention of Indocyanine Green: Feasibility and False-Positives in Ovarian Cancer. *PLoS One* 2015;10:e0129766.

19. Maeda H, Wu J, Sawa T, Matsumura Y, Hori K. Tumor vascular permeability and the EPR effect in macromolecular therapeutics: a review. *J Control Release* 2000;65:271-284.

20. Matsumura Y, Maeda H. A new concept for macromolecular therapeutics in cancer chemotherapy: mechanism of tumoritropic accumulation of proteins and the antitumor agent smancs. *Cancer Res* 1986;46:6387-6392.

21. low PS, Henne WA, Doorneweerd DD. Discovery and development of folic-acid-based receptor targeting for imaging and therapy of cancer and inflammatory diseases. *Acc Chem Res* 2008;41:120-129.

22. Vergote IB, Marth C, Coleman RL. Role of the folate receptor in ovarian cancer treatment: evidence, mechanism, and clinical implications. *Cancer Metastasis Rev* 2015.

23. Kalli KR, Oberg AL, Keeney GL et al. Folate receptor alpha as a tumor target in epithelial ovarian cancer. *Gynecol Oncol* 2008;108:619-626.

24. O'Shannessy DJ, Somers EB, Smale R, Fu YS. Expression of folate receptor-alpha (FRA) in gynecologic malignancies and its relationship to the tumor type. *Int J Gynecol Pathol* 2013;32:258-268.

25. Parker N, Turk MJ, Westrick E, Lewis JD, low PS, Leamon CP. Folate receptor expression in carcinomas and normal tissues determined by a quantitative radioligand binding assay. *Anal Biochem* 2005;338:284-293.

26. Crane LM, Arts HJ, van OM et al. The effect of chemotherapy on expression of folate receptor-alpha in ovarian cancer. *Cell Oncol (Dordr)* 2012;35:9-18.

27. Despierre E, Lambrechts S, Leunen K et al. Folate receptor alpha (FRA) expression remains unchanged in epithelial ovarian and endometrial cancer after chemotherapy. *Gynecol Oncol* 2013;130:192-199.

28. O'Shannessy DJ, Somers EB, Maltzman J, Smale R, Fu YS. Folate receptor alpha (FRA) expression in breast cancer: identification of a new molecular subtype and association with triple negative disease. *Springerplus* 2012;1:22.

29. Liu TW, Stewart JM, Macdonald TD et al. Biologically-targeted detection of primary and micro-metastatic ovarian cancer. *Theranostics* 2013;3:420-427.

30. Vaitilingam B, Chelvam V, Kularatne SA, Poh S, Ayala-Lopez W, low PS. A folate receptor-alpha-specific ligand that targets cancer tissue and not sites of inflammation. *J Nucl Med* 2012;53:1127-1134.

31. Kennedy MD, Jallad KN, Thompson DH, Ben-Amotz D, low PS. Optical imaging of metastatic tumors using a folate-targeted fluorescent probe. *J Biomed Opt* 2003;8:636-641.

32. Altintas I, Kok RJ, Schiffelers RM. Targeting epidermal growth factor receptor in tumors: from conventional monoclonal antibodies via heavy chain-only antibodies to nanobodies. *Eur J Pharm Sci* 2012;45:399-407.

33. Choi HS, Gibbs SL, Lee JH et al. Targeted zwitterionic near-infrared fluorophores for improved optical imaging. *Nat Biotechnol* 2013;31:148-153.

34. Hyun H, Park MH, Owens EA et al. Structure-inherent targeting of near-infrared fluorophores for parathyroid and thyroid gland imaging. *Nat Med* 2015;21:192-197.

35. Oliveira S, Heukers R, Sornkom J, Kok RJ, van Bergen En Henegouwen PM. Targeting tumors with nanobodies for cancer imaging and therapy. *J Control Release* 2013;172:607-617.

36. Rosenthal EL, Warram JM, de BE et al. Safety and Tumor Specificity of Cetuximab-IRDye800 for Surgical Navigation in Head and Neck Cancer. *Clin Cancer Res* 2015;21:3658-3666.

37. Fader AN, Rose PG. Role of surgery in ovarian carcinoma. *J Clin Oncol* 2007;25:2873-2883.

38. Bristow RE, Tomacruz RS, Armstrong DK, Trimble EL, Montz FJ. Survival effect of maximal cytoreductive surgery for advanced ovarian carcinoma during the platinum era: a meta-analysis. *J Clin Oncol* 2002;20:1248-1259.

39. Hoskins WJ, McGuire WP, Brady MF et al. The effect of diameter of largest residual disease on survival after primary cytoreductive surgery in patients with suboptimal residual epithelial ovarian carcinoma. *Am J Obstet Gynecol* 1994;170:974-979.

40. Barranger E, Antomarchi J, Chamorey E et al. Effect of Neoadjuvant Chemotherapy on the Surgical Treatment of Patients With Locally Advanced Breast Cancer Requiring Initial Mastectomy. *Clin Breast Cancer* 2015.

41. Soucy G, Belanger J, Leblanc G et al. Surgical margins in breast-conservation operations for invasive carcinoma: does neoadjuvant chemotherapy have an impact? *J Am Coll Surg* 2008;206:1116-1121.

42. Crane LM, Arts HJ, van OM et al. The effect of chemotherapy on expression of folate receptor-alpha in ovarian cancer. *Cell Oncol (Dordr)* 2012;35:9-18.

43. O'Shannessy DJ, Somers EB, Maltzman J, Smale R, Fu YS. Folate receptor alpha (FRA) expression in breast cancer: identification of a new molecular subtype and association with triple negative disease. *Springerplus* 2012;1:22.

44. van Driel PB, van de Giessen M, Boonstra MC et al. Characterization and evaluation of the artemis camera for fluorescence-guided cancer surgery. *Mol Imaging Biol* 2015;17:413-423.

45. Zhang Z, Wang J, Tacha DE et al. Folate receptor alpha associated with triple-negative breast cancer and poor prognosis. *Arch Pathol Lab Med* 2014;138:890-895.

46. Monici M, Basile V, Romano G et al. Fibroblast autofluorescence in connective tissue disorders: a future tool for clinical and differential diagnosis? *J Biomed Opt* 2008;13:054025.

47. Weissleder R, Ntziachristos V. Shedding light onto live molecular targets. *Nat Med* 2003;9:123-128.

48. De Jesus JE, Keating JJ, Kularatne SA et al. Comparison of Folate Receptor Targeted Optical Contrast Agents for Intraoperative Molecular Imaging. *Int J Mol Imaging* 2015;2015:469047.

49. O'Shannessy DJ, Yu G, Smale R et al. Folate receptor alpha expression in lung cancer: diagnostic and prognostic significance. *Oncotarget* 2012;3:414-425.

Chapter 10

A novel tumor-specific agent for intraoperative near-infrared fluorescence imaging: a translational study in healthy volunteers and patients with ovarian cancer

Charlotte E.S. Hoogstins[1,5*], Quirijn R.J.G. Tummers[1,5*],
Katja N. Gaarenstroom[2], Cor D. de Kroon[2], J. Baptist M.Z. Trimbos[2],
Tjalling Bosse[3], Vincent T.H.B.M. Smit[3], Jaap Vuyk[4],
Cornelis J.H. van de Velde[1], Adam F. Cohen[5], Philip S. Low[6],
Jacobus Burggraaf[5] and Alexander L. Vahrmeijer[1]

* C.E.S. Hoogstins and Q.R.J.G. Tummers share first authorship.

[1] Department of Surgery, Leiden University Medical Center
[2] Department of Gynecology, Leiden University Medical Center
[3] Department of Pathology, Leiden University Medical Center
[4] Department of Anesthesiology, Leiden University Medical Center
[5] Centre for Human Drug Research, Leiden, the Netherlands.
[6] Department of Chemistry, Purdue University, West Lafayette, USA.

ABSTRACT

Purpose: Completeness of cytoreductive surgery is a key prognostic factor for survival in patients with ovarian cancer. The ability to differentiate clearly between malignant and healthy tissue is essential for achieving complete cytoreduction. Using current approaches, this differentiation is often difficult and can lead to incomplete tumor removal. Near-infrared fluorescence imaging has the potential to improve the detection of malignant tissue during surgery, significantly improving outcome. Here, we report the use of OTL38, a near-infrared (796 nm) fluorescent agent that binds folate receptor alpha, that is expressed in >90% of epithelial ovarian cancers.

Experimental design: We first performed a randomized, placebo-controlled study in 30 healthy volunteers. Four single increasing doses of OTL38 were delivered intravenously. At fixed times following drug delivery, tolerability and blood/skin pharmacokinetics were assessed. Next, using the results of the first study, three doses were selected and administered to 12 patients who had epithelial ovarian cancer and were scheduled for cytoreductive surgery. We measured tolerability and blood pharmacokinetics, as well as the ability to detect the tumor using intraoperative fluorescence imaging.

Results: Intravenous infusion of OTL38 in 30 healthy volunteers yielded an optimal dosage range and time window for intraoperative imaging. In 12 patients with ovarian cancer, OTL38 accumulated in folate receptor alpha-positive tumors and metastases, enabling the surgeon to resect an additional 29% of malignant lesions that were not identified previously using inspection and/or palpation.

Conclusions: This study demonstrates that performing real-time intraoperative near-infrared fluorescence imaging using a tumor-specific agent is feasible and potentially clinically beneficial.

INTRODUCTION

The completeness of surgical tumor removal is an important factor for determining the survival of patients with a solid tumor. Despite advances in preoperative imaging techniques, during surgery the surgical oncologist must rely primarily upon inspection and/or palpation to identify the tumor tissue; however, these methods are often inadequate[1-3].

Ovarian cancer has the highest mortality rate of all gynecological cancers[4]. The surgical treatment of advanced-stage ovarian cancer (i.e., International Federation of Gynecology and Obstetrics stage IIb through stage IV) typically consists of cytoreductive surgery combined with systemic chemotherapy. Several studies have shown that the amount of residual tumor that remains following cytoreductive surgery is the most important prognostic indicator of survival[5-9]. Thus, because imaging modalities that improve tumor identification during surgery can increase the number and thoroughness of metastatic lesions resected during cytoreductive surgery, they can significantly improve patient outcome.

Near-infrared (NIR) fluorescence imaging is an innovative technique that can be used to detect tumor lesions during surgery[10]. NIR fluorescence is invisible to the human eye, but can be detected in the millisecond range using a dedicated imaging system. Because the imaging system can be toggled on and off rapidly, this approach allows the surgeon to identify malignant tissue in real time without altering the surgical field. In addition, NIR light can penetrate tissue on the order of centimeters, allowing the surgeon to delineate targets underneath the tissue surface[11;12]. Despite its high potential in clinical applications, NIR fluorescence in surgical oncology has been used primarily with nonspecific agents previously available for clinical use. For example, indocyanine green is retained either in or around tumor tissue due to impaired secretion or increased vascular permeability and decreased lymphatic drainage; however, indocyanine green does not bind specifically to cancer tissue[13;14]. This lack of specificity results in a high rate of intraoperative false positive images in patients with ovarian cancer[15]. Thus, fluorescent agents that specifically target cancer-specific targets are highly desired.

Folate receptor alpha (FRα) is a promising target, as it is robustly expressed on a variety of cancers of epithelial origin, including >90% of epithelial ovarian cancers[16-18]. Moreover, FRα is expressed at relatively low levels in healthy tissue,

where it is expressed primarily at the apical membrane of polarized epithelial cells, including fallopian tube and endometrial tissue[16;19;20]. Thus, when targeted with a fluorescent agent, background fluorescence will be low in healthy tissue, making this protein an ideal candidate target for fluorescence-guided ovarian cancer surgery. Importantly, because chemotherapy does not affect the expression of FRα, this protein can be targeted in both primary and interval cytoreductive surgical procedures[21;22].

The potential of using a folate analog coupled to a dye that fluoresces outside of the NIR spectrum (e.g., folate-FITC) was demonstrated previously in a small patient series, yielding a positive fluorescence signal in three out of four patients with ovarian cancer[23]. Although this study showed the feasibility of detecting fluorescently labeled tumor deposits in real time, the approach did not allow the surgeon to detect lesions beneath the tissue surface. In addition, we found that using folate-FITC in both ovarian cancer and breast cancer produces high autofluorescence in healthy tissue (data not shown). This finding underscores the need for agents that fluoresce in the NIR spectrum.

OTL38 is a folate analog conjugated to a NIR fluorescent dye (excitation at 776 nm, emission at 796 nm); OTL38 has high specificity and affinity for FRα. Here, we first examined the tolerability, pharmacokinetics, and tissue and blood distribution of increasing doses of OTL38 in healthy volunteers. Based upon these results, we then determined the optimal dosage range and the imaging time window. We then used these parameters in a study in patients with epithelial ovarian cancer in order to determine the correlation between fluorescence detection and histopathology of the resected lesions. We also determined whether the detection of tumors using the traditional surgical view was improved with the addition of fluorescence imaging.

MATERIALS AND METHODS

Study design
The primary objective of the study in healthy volunteers was to assess the tolerability and pharmacokinetics (in plasma and skin) of a single intravenous doses of OTL38; in addition, the results were used to determine the optimal dosage range and time window for performing intraoperative imaging in the subsequent study in patients with ovarian cancer. For the patient study, the

objectives were to assess the tolerability and pharmacokinetics of OTL38, the efficacy with respect to intraoperative detection of ovarian cancer lesions, and the practical feasibility of the technique. The results were used to determine the optimal dose for intraoperative imaging. Because both studies were exploratory in nature, sample size was not based on a formal calculation of statistical power. In the first study, tolerability and pharmacokinetics of a single intravenous dose of OTL38 were used as the endpoints. These same endpoints were used in the patient study; in addition, we also measured the efficacy of OTL38 in the intraoperative detection of ovarian cancer by measuring the following endpoints: TBR (tumor-to-background ratio), defined as the ratio between the fluorescent signal in the tumor tissue and the fluorescent signal in the tissue surrounding the tumor; concordance between the pathology results with respect to the presence of cancer and the imaging assessment; the number and location of FRα-positive, cancerous lesions identified the usual visual and/or tactile approaches with or without fluorescence imaging; and the surgeons' evaluation of the practical application of the technique. Data of all subjects participating in the studies was included in the analyses if the data could meaningfully contribute to the objectives of the studies.

For the study in healthy volunteers, we included 30 subjects who were 18-65 years of age and were considered healthy based on medical screening. For the patient study, we included twelve patients who had a high suspicion of epithelial ovarian cancer or a tissue-based diagnosis of epithelial ovarian cancer and were scheduled for primary or interval cytoreductive surgery. The main exclusion criteria were current pregnancy, history of anaphylactic reactions, impaired renal function (defined as eGFR <50 ml/min/1.73 m^2), and impaired liver function (defined as ALT, AST, or total bilirubin levels that exceeded 3X the established upper limit of normal).

The study in healthy volunteers was a randomized, placebo-controlled design in which subjects were randomized to receive a single intravenous dose of 0.025, 0.05, 0.1, or 0.2 mg/kg OTL38 or placebo. The randomization code was generated by a study-independent statistician using SAS 9.1.3 for Windows (SAS Institute Inc., Cary, NC). The randomization code was made available for data analysis only after the study was completed. At fixed time points following administration, blood samples were collected and used to measure pharmacokinetics and to perform routine laboratory tests. Adverse events, ECG, and vital signs were recorded. The fluorescent signal in superficial skin

was measured using the Artemis imaging system at fixed time points following intravenous administration of OTL38 or placebo (Figure 1). After a dose cohort was completed, all data collected up to 24 hours following each dose were reviewed prior to increasing the dose. In the event of an unacceptable tolerability profile (based on the nature, frequency, and intensity of adverse events, as judged by the investigator), the dose was not increased. Subjects were assigned to a dosing group based on the order in which they enrolled in the study. The study was performed in a double-blind fashion; thus, the investigator, staff, subjects, sponsor, and monitor were blinded with respect to the treatment until the end of the study. The placebo and OTL38 were formulated and packaged identically. The randomization list was made available only to the pharmacist who prepared the study drug, the individual who was responsible for sample bioanalysis, and the statisticians and programmers who prepared the blinded summaries, graphs, and listings to support the dosing decisions.

The patient study was a single ascending dose, open label exploratory study. The patient study was not randomized, and all patients received the active drug. Assignment to the dosage groups was based on the order in which the patients enrolled in the study. The patients received a one-hour intravenous infusion of OTL38 2-3 hours prior to the start of surgery. A dose-escalating scheme with planned doses of 0.025, 0.05, and 0.1 mg/kg (and the possibility to decrease the dose to 0.0125 mg/kg) was used. Dose escalation was terminated in the event of an unacceptable tolerability profile. Tolerability assessment (blood pressure, pulse, peripheral oxygen saturation, respiratory rate, ECG, temperature, and skin assessments) and blood collection for pharmacokinetics and routine laboratory tests were performed at regular intervals starting just prior to administration and lasting until 24 hours post-dosing. Adverse events and the concomitant use of other medications were recorded. Cytoreductive surgery generally included the removal of the uterine adnexa, uterus, and infracolic omentum, as well as resection of all macroscopic tumors, where possible. All surgical procedures were open procedures performed by an experienced gynecological oncologist using a midline abdominal incision. First, the primary tumor and metastases were identified in the surgical field using standard visual and tactile methods. Thereafter, the Artemis imaging system was used to identify NIR-fluorescent lesions. All tumor tissue identified by visual/tactile methods and/NIR fluorescence was resected, provided it was both surgically feasible and clinically useful. Each resected lesion was marked on a case report

form as being either fluorescent or non-fluorescent and as being either clinically suspected of malignancy or not (Figure S1, online available). All resected lesions were examined for tumor status by an experienced pathologist. A positive tumor that was fluorescent was considered a true positive; a negative lesion that was fluorescent was considered a false positive; and a positive tumor that was non-fluorescent was considered a false negative. In addition, we performed immunohistochemistry to demonstrate FRα and FRβ expression coupled with fluorescence microscopy in order to evaluate OTL38 binding (Supplementary Materials and Methods, online available).
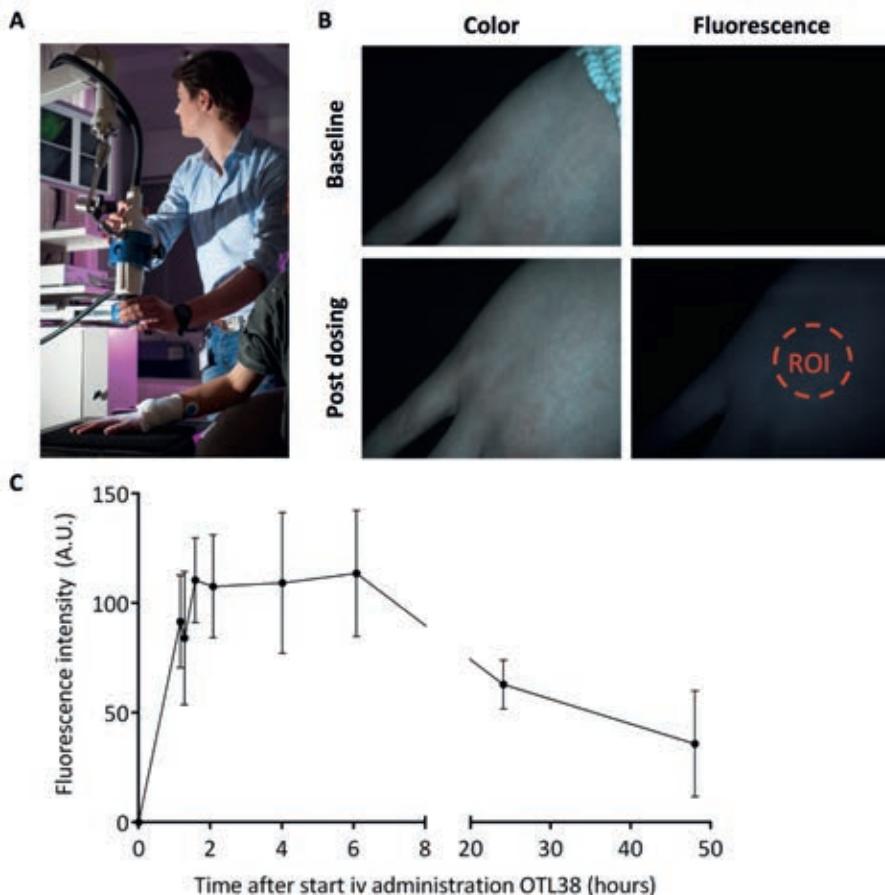

Figure 1. Fluorescence measurements in the skin of healthy volunteers

A. A researcher measuring skin fluorescence using the Artemis imaging system. **B.** Color (left column) and fluorescence (right column) images of a healthy volunteer at baseline (upper row) and after receiving a dose of OTL38 (lower row). Note that a bright fluorescent signal is detected after dosing, and fluorescence intensity can be measured within a region of interest (ROI) (dashed circle). **C.** Fluorescence intensity (measured in arbitrary units) in an ROI over time (in hours). The fluorescence signal reached peak levels at approximately 2 hours and was stable for up to 6 hours, then decreased over the following 48 hours.

Investigational product

OTL38 (chemical formula: $C_{61}H_{63}N_9Na_4O_{17}S_4$; molecular weight: 1414.42 Da) consists of a folate analog conjugated to an NIR fluorescent dye. OTL38 (>96% purity) was obtained from On Target Laboratories (West Lafayette, IN). The drug was synthesized and manufactured at Aptuit (Harrisonville, MO) in compliance with Good Manufacturing Practices (Figure S2, online available). OTL38 was stored in frozen form at -20°C in vials containing 6 mg OTL38 free acid in 3 ml water. Before administration, the frozen vials were thawed, vortexed, and then diluted with 0.9% NaCl or 5% dextrose for intravenous infusion. OTL38 was diluted in either 20 ml or 220 ml and was infused over 10 or 60 minutes. Placebo consisted of a similar volume of 0.9% NaCl or 5% dextrose.

Intraoperative near-infrared fluorescence imaging system

Imaging was performed using the Artemis fluorescence imaging system (Quest Medical Imaging, Middenmeer, the Netherlands)[24]. The system consists of three wavelength-isolated light sources, including a "white" light source and two separate near-infrared light sources. For this study, the camera and light engine where optimized for use with OTL38; specifically, they were designed to generate 7.5 mW/cm^2 at 760-nm light. Color video and fluorescence images were acquired simultaneously using separate sensors and were displayed in real time using custom-built optics and software, thereby displaying color video and NIR fluorescence images separately. A pseudo-colored (lime green) merged image of the color video and fluorescence images was also generated. The intensity of the light source was controlled using the Artemis software. The camera was attached to a freely moveable arm. During surgery, the camera and moveable arm were enclosed in a sterile shield and drape (Medical Technique Inc., Tucson, AZ).

Ethics committee approval

Both studies were performed in accordance with the tenets established by the Helsinki Declaration of 1975 (as amended in Tokyo, Venice, Hong Kong, Somerset West, Edinburgh, Washington, and Seoul), ICH-GCP guidelines, and the laws and regulations of the Netherlands. In addition, both studies were approved by a certified medical ethics review board. All subjects provided written informed consent prior to the start of any study-related procedures. The healthy volunteer study and ovarian cancer patient study were registered

in the European Clinical Trials Database under numbers 2013-004774-10 and 2014-002352-12, respectively; publicly accessible via the CCMO register (https://www.toetsingonline.nl/to/ccmo_search.nsf/Searchform?OpenForm).

Practical evaluation

Directly following the surgical procedure, the surgeon was asked to complete a questionnaire regarding the practical application of the technique during the surgical procedure (Supplementary Materials and Methods, online available).

Visual detection

Color and fluorescence images of seven representative surgical views of patients with confirmed ovarian cancer were captured from the videos recorded using the Artemis imaging system. Intra-observer variability was assessed by including a matching color and fluorescence image set twice (one set was a horizontal mirror image of the original), resulting in a total of eight sets of matching color and fluorescence images that were printed in full color; representative images are shown in Figure 2. Three experienced gynecological oncologists were asked to mark clinically suspected lesions directly on the color images; they were then asked to mark clinically suspected lesions on the matching fluorescence images. Visual detection was performed *ex vivo* because intraoperative assessment of the number of lesions was not feasible.

Pharmacokinetics analysis

The bioanalysis was performed using validated methodologies in compliance with good clinical laboratory practices at Analytical Biochemical Laboratory (Assen, the Netherlands). In brief, OTL38 was extracted from human K2EDTA plasma samples and urine samples using off-line solid-phase extraction, followed by analysis using liquid chromatography-mass spectrometry (APL-4000, Attodyne Inc., Toronto, Ontario, Canada). The assay's lower limit of quantification (LLOQ) and upper limit of quantification (ULOQ) were 2.00 and 500 ng/ml, respectively. The coefficient of variability for intra-day and inter-day plasma LLOQ and urine LLOQ was 8.2% and 13.3%, respectively.
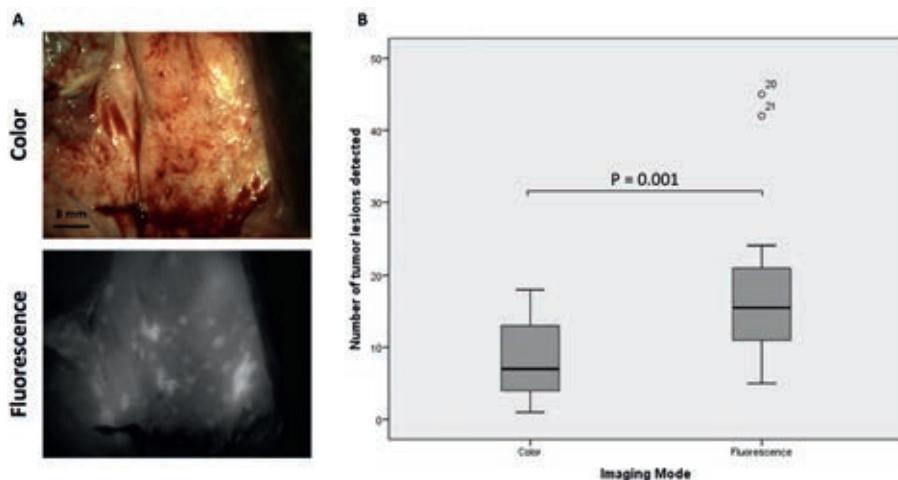
Figure 2. Visual detection of tumor deposits ex vivo

A. Representative color (upper panel) and fluorescence (lower panel) images used to quantify the visual detection of tumor deposits. **B.** Box plot summarizing the number of tumor lesions detected based on the matched color and fluorescence images.

Statistical analysis

SPSS statistical software package (version 20.0, IBM Corp., Armonk, NY) was used for statistical analyses. The individual OTL38 concentration-time profiles were analyzed using non-compartmental methods. The obtained PK parameters (i.e., AUC, Cmax, and tmax) were summarized per treatment group, including the number of subjects, mean values, standard deviation (SD), median values, and minimum and maximum values. The fluorescence signal in the skin (healthy volunteers) or tumor and background tissue (patients) was quantified using ImageJ (version 1.49b, National Institutes of Health, Bethesda, MD; http://imagej.nih.gov/ij/). Using ImageJ, a region of interest (ROI) was drawn on the images and used to quantify the fluorescence signal in arbitrary units (AU). TBR was calculated by dividing the fluorescence signal of the tumor by the fluorescence signal of the surrounding tissue. To compare the TBR values and fluorescence background signals between malignant and benign (i.e., false positive) lesions and between different dose groups, an independent samples Student's t-test was performed. TBR is reported as the mean, SD, and range. Patient characteristics are reported as the median, SD, and range. Tumor deposits that were marked on the color and fluorescence images were counted. To compare the number of deposits between the color and fluorescence images, a paired Student's t-test was performed.

RESULTS

Clinical trial in healthy volunteers
This study included a total of 30 subjects (18 females and 12 males), 18-64 years of age with a BMI of 18-30 kg/m^2 (see Fig. S3 for the CONSORT flow diagram, online available).

Tolerability
OTL38 at 0.025mg/kg diluted in 20 ml 0.9% NaCl infused for 10 or 60 minutes caused moderate hypersensitivity in two out of the four subjects receiving this dose. These reactions were not classic allergic reactions, as they were not accompanied by an increase in tryptase or IgE, nor did they involve the complement system (see Data File S1, online available). Subsequent studies using dynamic light scattering and scanning electron microscopy revealed that these reactions may have been due to aggregation of the OTL38 compound in the 0.9% NaCl solution. This aggregation was reduced considerably when OTL38 was diluted in 5% dextrose and when the infusion volume was increased. Because OTL38 did not aggregate measurably when diluted to 7.5 μM in 5% dextrose, the study was restarted at the lowest dose with OTL38 dissolved in 220 ml 5% dextrose; this volume was infused for a period of 60 minutes.

Infusion of 0.025, 0.05, and 0.1 mg/kg OTL38 diluted in 5% dextrose was associated with mild adverse events that disappeared gradually during and/or after the infusion. These adverse events were dose-dependent and suggestive of hypersensitivity (e.g., abdominal discomfort, nausea, and pruritus), but did not require intervention. All adverse events are listed in Table S1 (online available). At the 0.2 mg/kg dose, some subjects developed adverse events of moderate severity, which required the temporary interruption of the infusion or the administration of an antihistamine (e.g., 1-2 mg clemastine intravenously). Overall, more than 80% of these adverse events were mild in severity, and all other adverse events were moderate in severity. Despite the development of adverse events, the infusion of OTL38 at 0.025-0.2 mg/kg did not cause clinically meaningful changes relative to baseline with respect to laboratory values, ECG, or vital signs.

Pharmacokinetics

The maximum blood plasma concentration was achieved with each dose immediately at the end of the infusion and declined thereafter with a half-life of 2-3 hours (Figure S4, online available). Table S2 summarizes the most important pharmacokinetics (PK) parameters in each treatment group (online available) OTL38 excreted in the urine (expressed as a percentage of the dose administered) increased with increasing dose, and the highest level was approximately 11% for the highest dose (0.2 mg/kg). It is therefore reasonable to assume that the relatively low recovery is due in part to the lower limit of detection for OTL38 in urine.

Pharmacokinetics in superficial tissue

Figure 1 shows example images obtained using the Artemis imaging system. Although OTL38 was cleared from the plasma 2-3 hours after intravenous infusion, our analysis of the fluorescence signal in the skin revealed that fluorescence increased initially, remained increased for six hours, and then decreased with a half-life of approximately 15 hours (Figure 1).

Clinical trial in patients with ovarian cancer

Fourteen patients initially enrolled in this study. However, because the study drug was temporary unavailable, one patient could not participate, another patient withdrew from the study. Thus, a total of 12 patients, 49 to 77 years of age with a BMI of 20-41 kg/m^2 received OTL38 (see Figure S5 for the CONSORT flow diagram, online available). The surgical procedure, histology, differentiation grade, and International Federation of Gynecology and Obstetrics (FIGO) stages are summarized in Table 1.

Dose escalation

Patients 1, 2, and 3 received a starting dose of 0.025 mg/kg. After we reviewed the safety and efficacy data, the dose was increased to 0.05 mg/kg in the next three patients. However, when the 3 patients 4, 5, and 6 received this higher dose, the number and severity of symptoms (primarily consisting of abdominal discomfort, nausea, and pruritus) increased. In addition, TBR appeared to decrease. Therefore, the dose was decreased to 0.0125 mg/kg for the next three patients (patients 7, 8, and 9), yielding fewer, less severe symptoms, as well as an increase in TBR. Nevertheless, even at this lowest dose, mild, self-limiting

Table 1. Surgery and tumor characteristics of ovarian cancer patients

Patient ID	Surgical procedure	Diagnosis	FIGO stage	Grade	Metastases identified	Tumor FRα positive	Fluorescence imaging successful
1	Interval debulking	Serous adenocarcinoma	4	III	Yes	Yes	Yes
2	Interval debulking	Serous adenocarcinoma	4	III	Yes	Yes	Yes
3	Interval debulking	Serous adenocarcinoma	3c	III	Yes	Yes	Yes
4	Interval debulking	Serous adenocarcinoma	4	III	Yes	Yes	Yes
5	Interval debulking	Serous adenocarcinoma	3c	III	Yes	Yes	Yes
6	Primary debulking	Mucinous adenocarcinoma	3b	Unknown	Yes	Yes	Yes
7	Debulking recurrent disease	Endometrioid carcinoma	3b	II	Yes	Yes	Yes
8	Primary debulking	Serous adenocarcinoma	3c	III	Yes	Yes	Yes
9	Debulking recurrent disease	Clear cell carcinoma	3	I	Yes	Yes	Yes
10	Interval debulking	Mucinous adenocarcinoma	3c	Unknown	Yes	Yes	Yes
11	Debulking recurrent disease	Endometrioid carcinoma	3c	III	Yes	Yes	Yes
12	Interval debulking	Adenocarcinoma†	3c	III	Yes	Yes	Yes

FIGO, International Federation of Gynecology and Obstetrics; FRα, folate receptor alpha
† Further classification was not possible due to prior chemotherapy

adverse events were reported. After reviewing the safety and efficacy data collected using all three doses, 0.0125 mg/kg was chosen as the optimal dose for the expansion cohort (patients 10, 11, and 12). In retrospect, this lower dose was a good choice, as adverse symptoms were minimal and TBR was maximal. Table S3 and Figure S6 summarize the TBR results (online available).

Other adverse events

One patient who received a dose of 0.0125 mg/kg OTL38 developed a case of post-operative hospital-acquired pneumonia and coughing-induced wound dehiscence. These complications were considered unrelated to OTL38 administration. The complete list of all adverse events recorded in the patients is provided in Table S4 (online available). Administration of OTL38 itself did not lead to any obvious changes in laboratory values, ECG, vital signs, or temperature.

Pharmacokinetics

The PK profile of OTL38 in patient blood was similar to the profile measured in the healthy volunteers. Specifically, with each dose, the maximum concentration was achieved at the end of the infusion. After stopping the infusion, plasma concentration decreased with a half-life of 2-3 hours (Figure S4).

Intraoperative near-infrared fluorescence imaging

Lesions could be detected clearly after OTL38 administration. The optimal camera exposure time was dependent on OTL38 dose, with lower doses requiring longer exposure times. At higher doses, the longer exposure time led to saturated images; however, in all cases it was possible to use a sufficiently brief exposure time in order to obtain real-time images.

Figure 3 shows an example of fluorescent lesions that were subsequently confirmed as ovarian cancer metastases on histopathology. A total of 83 fluorescent lesions were resected during the surgeries; 62 of these lesions were confirmed as malignant on histopathology (i.e., true positives). Strikingly, 18 (29%) of these true positive lesions were not detected using standard inspection and/or palpation methods. Mean TBR was 4.4 (SD: 1.46, range: 1.7-9.8), and TBR generally decreased with increasing doses, likely due to increased background signal. TBR was constant throughout the surgical procedure, and fluorescence could be detected for at least six hours after infusion. Importantly, using NIR fluorescence enabled us to detect malignant lesions up to 8 mm

below the tissue surface, showing the added value of using light in the NIR spectrum (Movie S1, online available).
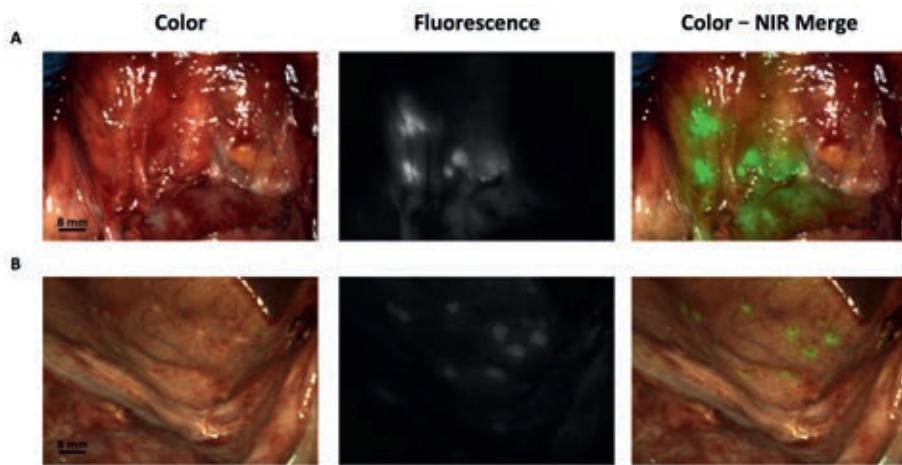

Figure 3. Intraoperative detection of ovarian cancer metastases using fluorescence-based imaging

A-B. Color (left column), fluorescence (middle column), and merged (right column) images of retroperitoneal lymph nodes containing metastases of ovarian cancer (**A**) and superficial peritoneal metastases of ovarian cancer (**B**).

Histopathology of resected lesions

No malignant disease was found in 21 of the 83 fluorescent lesions, corresponding to a false positive rate of 23%. These false positive lesions were observed primarily in lymph nodes, representing 52% of all false positive lesions (Table S5, online available). Additional staining experiments and a closer examination of these lymph nodes revealed that activated macrophages, accumulated in the sinuses of the lymph node, express folate receptor beta (FRβ), which is also a binding target for OTL38. Our immunofluorescence experiments revealed that the fluorescence signal co-localized with FRβ staining (Figure 4).

Other false positive results arose due to the expression of FRα on the apical membrane of non-cancerous epithelial cells in the uterus and fallopian tubes, which are routinely resected during cytoreductive surgery. The mean TBR of the false positive lesions was 5.4 (SD: 2.0, range: 1.8-9.3), which did not differ sufficiently from true positive lesions (mean: 4.4, range: 1.7-9.8) to allow us to differentiate between false positive and true positive lesions based solely on TBR. We observed only two false negative lesions. Finally, fluorescence microscopy revealed the accumulation of OTL38 in the membrane and cytoplasm of FRα-expressing tumor cells (for representative images, see Figure 5).
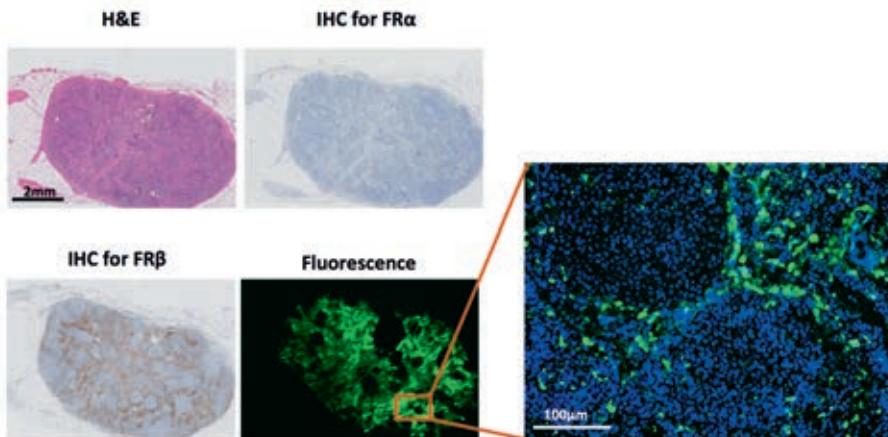
Figure 4. Histopathological evaluation and fluorescence signal of a false positive lymph node

The images show a fluorescent lymph node (bottom right panel) that did not contain ovarian cancer metastases on hematoxylin and eosin (H&E) staining (upper left panel) and was negative for FRα immuno staining (upper right panel). Immunostaining for FRβ showed positive staining in the sinuses, but not in the follicles (lower left panel). The magnified image at the right shows that the fluorescence pattern was localized to the sinuses, consistent with FRβ staining.
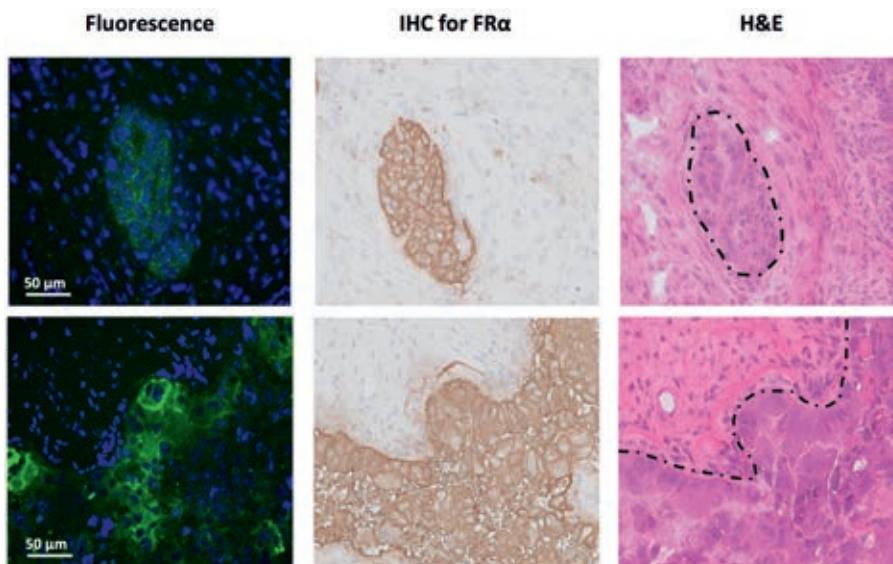

Figure 5. Histopathological evaluation and fluorescence signal in ovarian cancer

Representative samples from two different patients. Fluorescence microscopy (left column) shows clear membranous and cytoplasmic accumulation of OTL38 in tumor cells. The fluorescence signal is indicated in green, and the nuclei were counterstained with DAPI (blue). The fluorescence pattern is consistent with FRα expression measured using immunohistochemistry (middle column), which corresponds to the anatomical site containing a serous ovarian adenocarcinoma metastasis visible on hematoxylin and eosin (H&E) staining (right column, dashed outline).

Visual detection

The examination of tumor deposits based on color images obtained from the intraoperative videos allowed us to identify an average of 8.3 (SD: 5.4, range: 1-18) lesions per image. In contrast, performing the same assessment using the matching NIR fluorescence images allowed us to identify an average of 17.6 (SD: 10.8, range: 5-45) lesions per image, reflecting a more than two-fold improvement in our ability to detect tumor lesions (Figure 2).

Practical evaluation

The use of fluorescence imaging did not interfere with the surgeon's ability to perform cytoreductive surgery, and the majority of participating surgeons reported that they found the technique to be useful (Supplementary Materials and Methods).

DISCUSSION

Here, we report the successful use of the first tumor-specific NIR fluorescence-based imaging agent to target FRα in ovarian cancer, significantly increasing removal of tumor lesions.

In healthy volunteers, OTL38 caused moderate hypersensitivity; however, these reactions were easily managed. Given their symptomology, these reactions were likely pseudoallergic, a finding that has been described previously by Szebeni with respect to radiocontrast media[25]. Moreover, investigating the cause of this hypersensitivity led to the development of procedures designed to minimize or eliminate this reaction in our subsequent study with cancer patients. This was likely related to aggregation of OTL38 rather than a classic allergic response to the drug, suggesting that the severity may be reduced further by modifying the drug's formulation. Regardless, even these reactions were not severe enough to preclude the administration of a single dose of OTL38.

In healthy volunteers, the agent was essentially cleared from the plasma within 2-3 hours of intravenous delivery; however, a stable signal remained visible in the skin for at least six hours after dosing. This information was extremely valuable for determining the optimal time window for intraoperative imaging in patients, in which a favorable TBR was required during the surgical

procedure. Our assessment of TBR at all doses revealed that the TBR of fluorescent lesions was maintained throughout the surgical procedure (i.e., 2-6 hours after dosing). However, because the fluorescent lesions were resected during surgery, we were unable to track the TBR of individual lesions over time.

A sufficiently high TBR is needed in order to optimally detect the tumor; in our study, a TBR of approximately 4.4 allowed the clear detection of tumor deposits. Higher doses (non-quenched) of OTL38 may translate into higher TBR, assuming linear binding of the agent to the tumor and background tissue. However, because the tumor contains a fixed number of receptors, it is conceivable that even with a low dose, the majority of FRα molecules in the tumor tissue will be bound by the agent. Therefore, higher doses will not necessarily increase the tumor-specific signal but might lead to increased nonsaturable, nonspecific background binding, resulting in a less favorable TBR at higher doses. Indeed, the highest dose used in this study (0.05 mg/kg) resulted in a high background signal and lower TBR value, whereas the lowest dose tested (0.0125 mg/kg) yielded the highest TBR and—most importantly—the mildest symptoms. To obtain the best imaging results, the exposure times differed between the different dosing groups; thus, the lowest dose (0.0125 mg/kg) required the longest exposure time (75 ms). Nevertheless, even this relatively longer exposure time enabled us to perform real-time imaging.

When translated to our patient cohort, the optimal dose of OTL38 (i.e., 0.0125 mg/kg) enabled the surgeons to successful identify malignant lesions with reasonably high sensitivity and specificity. Moreover, 29% of all resected malignant lesions would have gone undetected without the aid of fluorescence-based imaging. Unfortunately, the relatively low number of patients precluded our ability to calculate the specificity and sensitivity of the technique. Moreover, our inability to study true negatives precluded a clear assessment of specificity. Nevertheless, both the *in situ* and *ex vivo* visual detection of lesions were clearly improved by the use of fluorescence-based imaging. With respect to *in situ* detection, 29% more lesions were resected. However, even this increase may underestimate the total number of lesions that could be detected during surgery, as resection is dependent upon several factors other than detection. Lastly, our *ex vivo* visual detection was performed using still images, as it was not feasible to count lesions during surgery. Although this approach is commonly used and yields useful information, it may be considered suboptimal, as three-dimensional and tactile information is lost.

Although epithelial ovarian cancer cells overexpress FRα, this receptor is also expressed—albeit it to a lesser extent—at the apical membrane of various non-cancerous epithelial cells. During surgery, we noted mild, homogenous fluorescence of the uterus and the fallopian tubes, and biopsy revealed FRα expression in these non-malignant tissues, consistent with previous reports[17;26]. The fluorescence signal in these tissues was homogenous and was clearly distinguishable from the fluorescence measured in the tumor deposits.

In the majority of our patients, we detected brightly fluorescent lymph nodes, and only a small number of these lymph nodes actually contained ovarian cancer metastases. The fluorescence measured in the non-cancerous lymph nodes was likely due to OTL38 binding to activated macrophages, which express FRβ[27-30]. On the other hand, the formation of OTL38 aggregates and nonspecific uptake by lymph nodes is unlikely, as dissolving the agent at 7.5 µM in 5% dextrose did not lead to the formation of measurable aggregates. Indeed, given that only three of the 12 patients received the highest dose (0.05 mg/kg), corresponding to a molarity slightly higher than 7.5 µM (9.5-11.8 µM OTL38), the presence of aggregates in the infusion solution is highly unlikely. In addition, to further minimize the likelihood of aggregate formation in the circulation, the solution was infused for 60 minutes. Although this apparent false positive fluorescence in the lymph nodes could be considered a drawback of this imaging agent, activated macrophages may actually be tumor-associated macrophages that play a role in preparing the tumor environment for metastasis[31-33]. This notion is supported by our finding that FRβ-expressing macrophages were also found in primary tumors as well as in lymph nodes that did contain metastasized tumor cells (Figure S7, online available). Until the precise role of FRβ-expressing macrophages in the lymph nodes is determined, lymph nodes should be resected solely on the basis of standard clinical assessments.

The use of fluorescent light in the near-infrared spectrum allowed us to detect lesions beneath the tissue surface, which is a major improvement over agents that use light outside the NIR spectrum[23;34;35]. For example, in our study malignant lesions were visible up to ~1 cm below the tissue surface. In addition, most biological tissues have extremely low autofluorescence when excited by light in the NIR spectrum[36;37]. OTL38 also has several advantageous pharmacokinetic properties, including long residence time in the tumor and relatively rapid clearance from plasma; these properties provide the surgeon

with a long window of time in which the tumor lesions can be detected. Unlike fluorescent antibodies—which have a much longer terminal half-life—OTL38 can be administered shortly before surgery [38].

Although more tumor deposits can be visualized and resected using intraoperative fluorescence imaging with OTL38 compared to conventional methods, more prospective research is necessary to establish the effect on overall survival. In addition, the diagnostic accuracy of fluorescence imaging with OTL38 should be further assessed in a larger patient group.

In conclusion, we provide the first evidence that a specific intraoperative NIR imaging agent can be used to increase the efficacy of tumor removal in patients with ovarian cancer. Our approach to clinical translation using both healthy subjects and patients in the same Phase I protocol allowed us to rapidly determine the optimal dose, formulation, and time window for intraoperative imaging, thereby greatly increasing the level of cytoreduction achieved in patients with ovarian cancer.

ACKNOWLEDGEMENTS

REFERENCES

1. Frangioni JV. In vivo near-infrared fluorescence imaging. *Curr Opin Chem Biol* 2003;7:626-634.

2. Weissleder R, Pittet MJ. Imaging in the era of molecular oncology. *Nature* 2008;452:580-589.

3. Lim MC, Seo SS, Kang S et al. Intraoperative image-guided surgery for ovarian cancer. *Quant Imaging Med Surg* 2012;2:114-117.

4. Ferlay J, Soerjomataram I, Dikshit R et al. Cancer incidence and mortality worldwide: sources, methods and major patterns in GLOBOCAN 2012. *Int J Cancer* 2015;136:E359-E386.

5. Chang SJ, Bristow RE, Ryu HS. Impact of complete cytoreduction leaving no gross residual disease associated with radical cytoreductive surgical procedures on survival in advanced ovarian cancer. *Ann Surg Oncol* 2012;19:4059-4067.

6. Vergote I, Trope CG, Amant F et al. Neoadjuvant chemotherapy or primary surgery in stage IIIC or IV ovarian cancer. *N Engl J Med* 2010;363:943-953.

7. Bristow RE, Tomacruz RS, Armstrong DK, Trimble EL, Montz FJ. Survival effect of maximal cytoreductive surgery for advanced ovarian carcinoma during the platinum era: a meta-analysis. *J Clin Oncol* 2002;20:1248-1259.

8. Hoskins WJ, McGuire WP, Brady MF et al. The effect of diameter of largest residual disease on survival after primary cytoreductive surgery in patients with suboptimal residual epithelial ovarian carcinoma. *Am J Obstet Gynecol* 1994;170:974-979.

9. Bristow RE, Berek JS. Surgery for ovarian cancer: how to improve survival. *Lancet* 2006;367:1558-1560.

10. Vahrmeijer AL, Hutteman M, van der Vorst JR, van de Velde CJ, Frangioni JV. Image-guided cancer surgery using near-infrared fluorescence. *Nat Rev Clin Oncol* 2013;10:507-518.

11. Frangioni JV. In vivo near-infrared fluorescence imaging. *Curr Opin Chem Biol* 2003;7:626-634.

12. Chance B. Near-infrared (NIR) optical spectroscopy characterizes breast tissue hormonal and age status. *Acad Radiol* 2001;8:209-210.

13. Maeda H, Wu J, Sawa T, Matsumura Y, Hori K. Tumor vascular permeability and the EPR effect in macromolecular therapeutics: a review. *J Control Release* 2000;65:271-284.

14. Matsumura Y, Maeda H. A new concept for macromolecular therapeutics in cancer chemotherapy: mechanism of tumoritropic accumulation of proteins and the antitumor agent smancs. *Cancer Res* 1986;46:6387-6392.

15. Tummers QR, Hoogstins CE, Peters AA et al. The Value of Intraoperative Near-Infrared Fluorescence Imaging Based on Enhanced Permeability and Retention of Indocyanine Green: Feasibility and False-Positives in Ovarian Cancer. *PLoS One* 2015;10:e0129766.

16. O'Shannessy DJ, Somers EB, Smale R, Fu YS. Expression of folate receptor-alpha (FRA) in gynecologic malignancies and its relationship to the tumor type. *Int J Gynecol Pathol* 2013;32:258-268.

17. Parker N, Turk MJ, Westrick E, Lewis JD, Low PS, Leamon CP. Folate receptor expression in carcinomas and normal tissues determined by a quantitative radioligand binding assay. *Anal Biochem* 2005;338:284-293.

18. Kalli KR, Oberg AL, Keeney GL et al. Folate receptor alpha as a tumor target in epithelial ovarian cancer. *Gynecol Oncol* 2008;108:619-626.

19. Vergote IB, Marth C, Coleman RL. Role of the folate receptor in ovarian cancer treatment: evidence, mechanism, and clinical implications. *Cancer Metastasis Rev* 2015;34:41-52.

20. Low PS, Henne WA, Doorneweerd DD. Discovery and development of folic-acid-based receptor targeting for imaging and therapy of cancer and inflammatory diseases. *Acc Chem Res* 2008;41:120-129.

21. Crane LM, Arts HJ, van OM et al. The effect of chemotherapy on expression of folate receptor-alpha in ovarian cancer. *Cell Oncol (Dordr)* 2012;35:9-18.

22. Despierre E, Lambrechts S, Leunen K et al. Folate receptor alpha (FRA) expression remains unchanged in epithelial ovarian and endometrial cancer after chemotherapy. *Gynecol Oncol* 2013;130:192-199.

23. van Dam GM, Themelis G, Crane LM et al. Intraoperative tumor-specific fluorescence imaging in ovarian cancer by folate receptor-alpha targeting: first in-human results. *Nat Med* 2011;17:1315-1319.

24. van Driel PB, van de Giessen M, Boonstra MC et al. Characterization and evaluation of the artemis camera for fluorescence-guided cancer surgery. *Mol Imaging Biol* 2015;17:413-423.

25. Szebeni J. Complement activation-related pseudoallergy: a new class of drug-induced acute immune toxicity. *Toxicology* 2005;216:106-121.

26. Wu M, Gunning W, Ratnam M. Expression of folate receptor type alpha in relation to cell type, malignancy, and differentiation in ovary, uterus, and cervix. *Cancer Epidemiol Biomarkers Prev* 1999;8:775-782.

27. Shen J, Hilgenbrink AR, Xia W et al. Folate receptor-beta constitutes a marker for human proinflammatory monocytes. *J Leukoc Biol* 2014;96:563-570.

28. O'Shannessy DJ, Somers EB, Wang LC, Wang H, Hsu R. Expression of folate receptors alpha and beta in normal and cancerous gynecologic tissues: correlation of expression of the beta isoform with macrophage markers. *J Ovarian Res* 2015;8:29.

29. Puig-Kroger A, Sierra-Filardi E, Dominguez-Soto A et al. Folate receptor beta is expressed by tumor-associated macrophages and constitutes a marker for M2 anti-inflammatory/regulatory macrophages. *Cancer Res* 2009;69:9395-9403.

30. Kurahara H, Takao S, Kuwahata T et al. Clinical significance of folate receptor beta-expressing tumor-associated macrophages in pancreatic cancer. *Ann Surg Oncol* 2012;19:2264-2271.

31. Smith HA, Kang Y. The metastasis-promoting roles of tumor-associated immune cells. *J Mol Med (Berl)* 2013;91:411-429.

32. Joyce JA, Pollard JW. Microenvironmental regulation of metastasis. *Nat Rev Cancer* 2009;9:239-252.

33. Lewis CE, Pollard JW. Distinct role of macrophages in different tumor microenvironments. *Cancer Res* 2006;66:605-612.

34. Keereweer S, van Driel PB, Snoeks TJ et al. Optical image-guided cancer surgery: challenges and limitations. *Clin Cancer Res* 2013;19:3745-3754.

35. Weissleder R, Ntziachristos V. Shedding light onto live molecular targets. *Nat Med* 2003;9:123-128.

36. Monici M. Cell and tissue autofluorescence research and diagnostic applications. *Biotechnol Annu Rev* 2005;11:227-256.

37. Monici M, Basile V, Romano G et al. Fibroblast autofluorescence in connective tissue disorders: a future tool for clinical and differential diagnosis? *J Biomed Opt* 2008;13:054025.

38. Rosenthal EL, Warram JM, de BE et al. Safety and Tumor Specificity of Cetuximab-IRDye800 for Surgical Navigation in Head and Neck Cancer. *Clin Cancer Res* 2015;21:3658-3666.
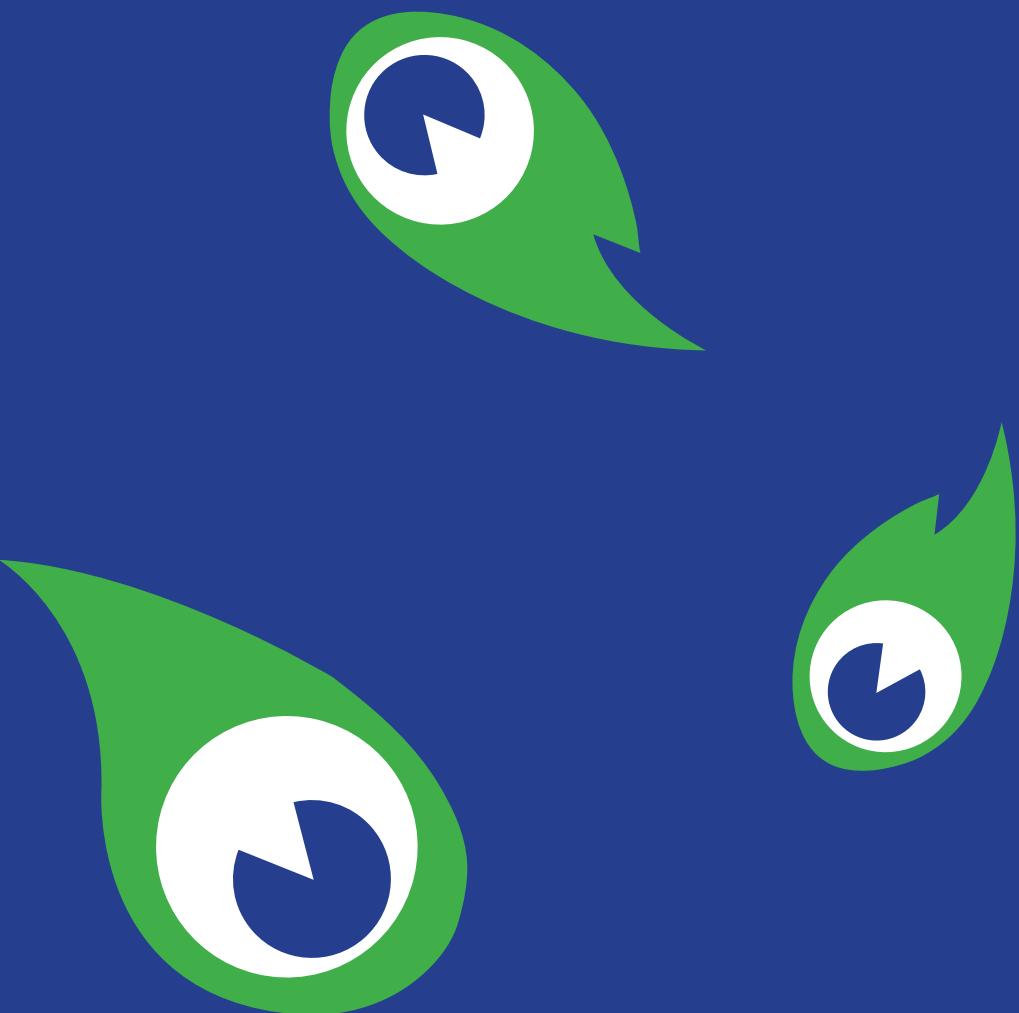
Part III

Chapter 11

Summary and future perspectives

SUMMARY

The quality of cancer surgery can be improved by assisting the surgeon with better and more objective, real time visual information during the procedure. Fluorescence-guided surgery can play a pivotal role in the intraoperative detection of tumor tissue, lymph nodes and vital structures.

This thesis focuses on a number of important indications in cancer surgery where clinically available near-infrared (NIR) fluorescence contrast agents can be used to improve surgical practice (Part 1) and the clinical translation (first in human study) of newly developed tumor-specific fluorescent contrast agents to improve the real time detection of tumor tissue (Part 2).

Part 1: **Exploring clinical available fluorescent contrast agents in cancer surgery**

In **chapter 2**, the detection of sentinel lymph nodes in gastric cancer is demonstrated. The lymph drainage pattern in gastric cancer is difficult to predict. Therefore, a total or partial gastrectomy is often combined with extensive lymphadenectomy. In the present study, indocyanine green (ICG) was adsorbed to nanocolloid to increase its hydrodynamic diameter and to improve retention in first draining lymph nodes. Subsequently, the ICG-Nanocolloid complex was then subserosally injected around the tumor, followed by detection of lymphatic vessels and lymph nodes. In 21 of 22 patients, at least 1 sentinel lymph node was identified using this technique. Interestingly, in 8 of the 21 patients, SLNs outside the standard plane of resection were identified, and tumor involvement was found in 2 of these nodes (in two patients).

Chapter 3 focused on the intraoperative detection of breast cancer using methylene blue (MB). Although the exact mechanism is not exactly clear, we hypothesized that breast cancer could be visualized using MB, based on physicochemical similarities of MB and 99mTc-MIBI. 99mTc-MIBI is a SPECT radiodiagnostic agent with a sensitivity of 83 - 90% to detect breast cancer preoperatively. In 20 out of 24 patients, we successfully identified breast cancer lesions in the resection specimen. And in 2 patients breast cancer tissue was identified in the wound bed using fluorescence imaging. Although MB is a promising agent for breast cancer detection, tumor-ligand specific contrast agents could further improve the accuracy of intra-operative breast cancer imaging.

Chapter 4 described the identification of hepatic metastases from uveal melanoma during laparoscopic liver surgery. ICG was administered 24 hours before surgery. The dye gets excreted by healthy liver into bile, but is trapped in the transition zone between healthy liver and metastatic lesions. At the day of surgery, a clear fluorescent rim around the tumor was seen. Even lesions not detected by pre-operative CT-scan, intraoperative inspection or laparoscopic ultrasound were identified. Therefore, NIR fluorescence imaging during laparoscopic liver surgery is a minimal invasive way to determine whether patients could potentially benefit from a metastasectomy. Moreover, it might help to obtain clear resection margins.

In **chapter 5**, ICG was administered to patients suffering from a pituitary gland adenoma. We hypothesized that ICG could improve distinction between normal and abnormal pituitary gland tissue during transnasal transsphenoidal selective adenomectomy, based on differences in tissue vascularization. In nine out of 10 patients with a histologically proven pituitary adenoma, the normal pituitary gland showed a stronger fluorescent signal than the adenoma. In two patients, adenoma resection actually took place under direct NIR fluorescence guidance. The available endoscopic imaging system didn't allow simultaneous imaging of color video and fluorescence, which limited the additional value of fluorescence imaging. Introduction of ligand-specific contrast agents and improved imaging systems could further improve fluorescence-guided pituitary gland surgery.

Chapter 6 described a clinical case in which MB was used to identify a paraganglioma, a rare neuro-endocrine tumor. It even allowed the detection of a local metastasis, which was not detected by preoperative imaging and intraoperative inspection.

Based on the principle of comparable biodistribution of MB and the 99mTc-MIBI tracer, **chapter 7** elaborated on the intraoperative fluorescence guidance during parathyroid surgery. MB allowed not only identification of parathyroid adenomas, but also identified normal parathyroid glands that were otherwise not detectable. Although promising results with newly developed structure inherent contrast agents are reported, MB can play a vital role in parathyroid surgery until newer probes enter the clinic.

In **chapter 8**, the enhanced permeability and retention (EPR) effect in ovarian cancer was explored. This effect is based on the fact that macromolecules, such as protein bound ICG, accumulate in tumor tissue due to increased vascular

permeability and reduced drainage. In the current study, several malignant lesions were identified using fluorescence imaging. However, also 13 non-malignant lesions were fluorescent, resulting in a false-positive ratio of 62%. This lack of specificity of the EPR effect shows that it is not suitable for daily clinical practice. A more tumor-specific accumulation profile or ligand-binding mechanism could overcome this limitation.

Part 2: Clinical translation of innovative tumor-specific fluorescent contrast agents

Chapter 9 described the use of EC17, a folate analogue coupled to fluorescein, for the identification of folate receptor alpha (FRα) positive ovarian and breast cancer. Intravenous administration of EC17, 2-3 hours before surgery, resulted in clear, bright fluorescent metastatic lesions of ovarian cancer. It resulted in an increased resection of 16% more malignant lesions, and a 70% increase in detection of metastatic lesions on post-operative analyzed images. In breast cancer, the overexpression of FRα is lower than in ovarian cancer. Therefore, preoperative obtained biopsies were stained for receptor expression. This personalized approach guarantees that only patients that can potentially benefit from fluorescence-guided surgery are included in trials using a tumor-specific contrast agent. Also in breast cancer, a clear fluorescent signal was seen in the tumor. Notwithstanding, autofluorescence signal of healthy tissue at 500nm caused false-positive lesions in breast cancer. In addition, this autofluorescence made it difficult to discriminate breast cancer-specific fluorescence from background fluorescence. Imaging in the NIR fluorescence light spectrum could solve this problem.

In **chapter 10,** we used a newly developed FRα specific contrast agent. This agent, OTL38, consists of a folate analogue coupled to a NIR fluorescent contrast agent (fluorescent at 800nm). First, tolerability and pharmacokinetics in blood and skin were assessed in a randomized, placebo-controlled, dose-ascending trial in healthy subjects. Hereafter three intravenous doses, selected based on the results from the healthy subject study, were administered to 12 patients with epithelial ovarian cancer, and scheduled for cytoreductive surgery. Clear accumulation of OTL38 in FRα positive tumors and metastases was seen, leading to the resection of 29% additional malignant lesions that were not identified by inspection and palpation. Almost no background fluorescence was seen.

GENERAL CONCLUSION

Intraoperative NIR fluorescence imaging using ICG and MB was explored in multiple important indications in cancer surgery. Imaging using ICG resulted in accurate tumor imaging of liver metastases and SLN detection in gastric cancer, with high TBRs and a prolonged fluorescent signal. For these indications, our data suggests that fluorescence imaging should be implemented in the clinic to improve patient care. MB allowed successful imaging of parathyroid adenomas, neuro-endocrine tumors and breast cancer lesions, but accuracy and imaging characteristics can probably be improved by the introduction of more tumor-specific contrast agents. However, in the meantime MB can be used for intraoperative guidance in for instance difficult cases.

Intraoperative imaging of ovarian cancer using the FRα specific EC17 and OTL38 showed highly specific and accurate tumor imaging with a high TBR and prolonged fluorescent signal in malignant lesions. Administration of these low molecular weight contrast agents resulted in rapid accumulation in tumor tissue and fast clearance from the rest of the body. Moreover, with the NIR fluorescent contrast agent OTL38 almost no background signal or autofluorescence was seen. Clinical translation using both healthy subjects and patients allowed a rapid determination of the optimal dose, formulation, and time window for intraoperative imaging, facilitating a fast clinical introduction of newly developed contrast agents in clinical trials.

FUTURE PERSPECTIVES

Over the past years several indications are identified to use clinical available contrast agents for image-guided surgery. ICG and MB have the potential to improve cancer surgery by identifying more malignant lesions, speed up time of surgery, and avoid iatrogenic injury due to better identification of vital structures. Although the number of indications is limited due to the intrinsic characteristics of these contrast agents, fluorescence-guided surgery can directly be implemented in daily clinical care in for example liver surgery, SLN imaging and expected difficult bile duct surgeries. Until newly developed ligand-binding, tumor-specific contrast agents have been developed and introduced in the clinic, tumor identification can be improved in for example breast cancer surgery, parathyroid surgery and paraganglioma surgery, as discussed in this thesis.

The introduction of ligand-binding, tumor-specific contrast agents have opened new possibilities for more accurate intraoperative tumor imaging. As long as appropriate tumor or tissue specific ligands will be discovered, it will be possible to identify almost any structure a surgeon wants to identify during surgery. As shown in our studies, investigating EC17 and OTL38, both folate analogues coupled to fluorescent contrast agents resulted in highly specific tumor imaging, within 2-3 hours after administration. Moreover, the fluorescent signal and TBR remained excellent for up to at least 6 hours.

Contrast agents

To achieve accurate tumor detection, it is important to optimize binding capacity, biodistribution and pharmacokinetics of a contrast agent. Multiple compounds as monoclonal antibodies, antibody fragments, such as single-chain antibody fragments and small peptides are therefore being investigated[1-5].

These different compounds all have their own pharmacokinetic profiles, and thereby different intervals for imaging based on the half-life of the agent. Rosenthal et al.[5] reported the imaging of head and neck cancer using cetuximab-IRDye800. Surgery was scheduled 3 days after administration of the compound because of the pharmacokinetic profile of this monoclonal antibody based contrast agent (half life 24 – 32 hours; molecular weight 150 kDa)[6]. Moreover, relatively high dosages were needed to achieve sufficient TBRs (up to 25% of therapeutic dose; 62,5 mg/m^2).

Administration of the folate analogue OTL38 (half life 2-3 hours; molecular weight 1.4 kDa) showed a high fluorescent signal in malignant lesions after only 2-3 hours, which prolonged for at least 6 hours (optimal dose 0.0125 mg/kg). Due to the fast clearance of the agent, low background signals were observed. It seems that these properties are ideal for accurate tumor imaging. Future studies will show which compounds are favorable, and this may even differ for different surgical indications.

One would ideally develop one contrast agent that targets almost all solid tumors. It remains however challenging to develop a contrast agent that is highly specific for cancer tissue, while gets excreted from the rest of the body. Receptor expression profiles in tumors can thereby differ. In ovarian cancer for example, over 90% of patients are positive for the FRα, and almost all patients are likely to benefit from treatment with an FRα specific contrast agent. In cancers where expression profiles are more divers, other strategies must be applied. Preoperative obtained biopsies could be used to explore the receptor expression profile of a specific tumor, introducing personalized medicine for precision surgery. This was for example done for the breast cancer patients in our EC17 study. Besides, cocktails with multiple ligand-binding agents can be administered based on biomarker profiles, or so-called multi-headed tumor-specific contrast agents can be developed. These are compounds that have multiple ligands bound to one fluorophore to enlarge the number of receptors that can be bound. A very important hurdle for the design of these agents is that all changes to such molecules can influence binding capacity and fluorescent properties.

One of the main limitations of fluorescence imaging is related to tissue penetration. In the visible light spectrum this is in the order of micrometers, improving to approximately 10 mm in the NIR spectrum. To overcome this limitation, contrast agents that combine fluorescence imaging with other diagnostic imaging modalities are being developed (multimodal imaging, combined optical positron emission tomography (PET) or single-photon emission computed tomography (SPECT) agents)[7]. These types of agents allow pre-operative surgical planning, intraoperative guidance towards deeper located targets and real-time visual discrimination of tumors from healthy tissue. In literature, combinations with photoacoustic imaging, magnetic resonance imaging, PET, SPECT and even triple-modal imaging are described[8]. However, most of these agents are still in a pre-clinical phase of development.

Imaging systems

Successful fluorescence-guided surgery depends on the combination of both contrast agents and imaging systems. Therefore, the development of imaging systems is crucial for the wide acceptance of fluorescence-guided surgery. Over the last years, multiple companies and institutes have launched imaging systems, all with their pros and cons[9]. Especially in endoscopic imaging there is much to gain, as suggested in chapter 4 and 5 of this thesis. Moreover, a more standardized approach to compare systems could assist in the development of new improved systems[10].

Clinical implementation

To provide guidance in the clinical implementation of image-guided surgery, cooperation is necessary, and international society's, like the International Society of Image Guided Surgery, are formed to discuss regulatory pathways and clinical trial design[11;12]. Endpoints in phase 1 studies should focus not only on safety, but also on imaging endpoints.

There is a promising role for the development of pharmacokinetic and pharmacodynamic models[13-15]. These models could give more insight in all the different variables that play a role in the mechanism of action in tumor imaging. Information on compound size, half-life, clearance, receptor density, tumor volume, binding constant, protein binding and so on could be combined in a model. Even imaging characteristics as quantum yield and wavelength can be added. This could potentially predict safety and imaging outcomes of newly designed compounds and could provide information on the optimal dose of a drug. The information obtained from these models could lead to exposure of less healthy subject and patients in first in human studies. It could even predict which imaging system performs best for a specific indication with a specific compound. This would make phase 1 studies more efficient, and lower the hurdle for promising compounds to enter the clinic.

New clinical indications

Cancer treatment requires a multidisciplinary approach where surgery, systemic chemotherapy or immunotherapy and radiotherapy all play a significant role[16;17]. Recent developments in neoadjuvant chemo-radiation therapy have resulted in an increase in the number of complete pathological response in for example rectal and oesophageal cancer[18-20]. These patients won't benefit

from a surgical resection, while no vital tumor tissue is present at pathological examination. On the contrary, these surgical resections are associated with morbidity and mortality, and safely avoiding such procedures would have a major impact on quality of life. This has resulted in a paradigm swift toward omitting surgery in patients with a complete clinical response and facilitating organ-preservation. Hereby it's essential to select patients with a complete clinical response after neoadjuvant therapy and to monitor them. There are several studies reporting on this "Watch and Wait" policy in rectal cancer[21], and an international database was recently established to monitor the results of this strategy[22]. Molecular imaging could have major impact on the selection and monitoring of a patient, because it could give more precise and objective information on the presence of vital tumor tissue in for example the scar tissue after chemo-radiation therapy.

CONCLUSIONS

Fluorescence-guided surgery has shown its potential in visualizing tumor tissue and increasing the number of detected malignant lesions that are otherwise undetectable. Besides, it assists in the identification of lymph nodes and vitals structures. Further studies, preferably randomized controlled trials, should validate whether improved tumor detection results in better patient outcomes by means of improved survival and reduced morbidity. Combined efforts in the rapidly expanding field of fluorescence-guided surgery hopefully leads to clinical implementation and determining its place in standard of care treatment of cancer patients in the near future.

REFERENCES

1. Kelderhouse LE, Chelvam V, Wayua C et al. Development of tumor-targeted near infrared probes for fluorescence guided surgery. *Bioconjug Chem* 2013;24:1075-1080.

2. Altintas I, Kok RJ, Schiffelers RM. Targeting epidermal growth factor receptor in tumors: from conventional monoclonal antibodies via heavy chain-only antibodies to nanobodies. *Eur J Pharm Sci* 2012;45:399-407.

3. Choi HS, Gibbs SL, Lee JH et al. Targeted zwitterionic near-infrared fluorophores for improved optical imaging. *Nat Biotechnol* 2013;31:148-153.

4. Oliveira S, Heukers R, Sornkom J, Kok RJ, van Bergen En Henegouwen PM. Targeting tumors with nanobodies for cancer imaging and therapy. *J Control Release* 2013;172:607-617.

5. Rosenthal EL, Warram JM, de BE et al. Safety and Tumor Specificity of Cetuximab-IRDye800 for Surgical Navigation in Head and Neck Cancer. *Clin Cancer Res* 2015;21:3658-3666.

6. Zinn KR, Korb M, Samuel S et al. IND-directed safety and biodistribution study of intravenously injected cetuximab-IRDye800 in cynomolgus macaques. *Mol Imaging Biol* 2015;17:49-57.

7. Chi C, Du Y, Ye J et al. Intraoperative imaging-guided cancer surgery: from current fluorescence molecular imaging methods to future multi-modality imaging technology. *Theranostics* 2014;4:1072-1084.

8. Bai J, Wang JT, Rubio N et al. Triple-Modal Imaging of Magnetically-Targeted Nanocapsules in Solid Tumours In Vivo. *Theranostics* 2016;6:342-356.

9. Zhu B, Sevick-Muraca EM. A review of performance of near-infrared fluorescence imaging devices used in clinical studies. *Br J Radiol* 2015;88:20140547.

10. Pleijhuis R, Timmermans A, De JJ, de BE, Ntziachristos V, Van DG. Tissue-simulating phantoms for assessing potential near-infrared fluorescence imaging applications in breast cancer surgery. *J Vis Exp* 2014;51776.

11. Rosenthal EL, Warram JM, de BE et al. Successful Translation of Fluorescence Navigation During Oncologic Surgery: A Consensus Report. *J Nucl Med* 2016;57:144-150.

12. Snoeks TJ, van Driel PB, Keereweer S et al. Towards a successful clinical implementation of fluorescence-guided surgery. *Mol Imaging Biol* 2014;16:147-151.

13. Cohen A. Pharmacokinetic and pharmacodynamic data to be derived from early-phase drug development: designing informative human pharmacology studies. *Clin Pharmacokinet* 2008;47:373-381.

14. Danhof M, Alvan G, Dahl SG, Kuhlmann J, Paintaud G. Mechanism-based pharmacokinetic-pharmacodynamic modeling-a new classification of biomarkers. *Pharm Res* 2005;22:1432-1437.

15. Wittrup KD, Thurber GM, Schmidt MM, Rhoden JJ. Practical theoretic guidance for the design of tumor-targeting agents. *Methods Enzymol* 2012;503:255-268.

16. Kapiteijn E, Marijnen CA, Nagtegaal ID et al. Preoperative radiotherapy combined with total mesorectal excision for resectable rectal cancer. *N Engl J Med* 2001;345:638-646.

17. Mieog JS, van der Hage JA, van de Velde CJ. Preoperative chemotherapy for women with operable breast cancer. *Cochrane Database Syst Rev* 2007;CD005002.

18. Glynne-Jones R, Wallace M, Livingstone JI, Meyrick-Thomas J. Complete clinical response after preoperative chemoradiation in rectal cancer: is a "wait and see" policy justified? *Dis Colon Rectum* 2008;51:10-19.

19. Jin HL, Zhu H, Ling TS, Zhang HJ, Shi RH. Neoadjuvant chemoradiotherapy for resectable esophageal carcinoma: a meta-analysis. *World J Gastroenterol* 2009;15:5983-5991.

20. O'Neill BD, Brown G, Heald RJ, Cunningham D, Tait DM. Non-operative treatment after neoadjuvant chemoradiotherapy for rectal cancer. *Lancet Oncol* 2007;8:625-633.

21. Pozo ME, Fang SH. Watch and wait approach to rectal cancer: A review. *World J Gastrointest Surg* 2015;7:306-312.

22. Beets GL, Figueiredo NL, Habr-Gama A, van de Velde CJ. A new paradigm for rectal cancer: Organ preservation: Introducing the International Watch & Wait Database (IWWD). *Eur J Surg Oncol* 2015;41:1562-1564.

Appendices

Nederlandse samenvatting en
toekomstperspectieven

List of publications

Curriculum vitae

Dankwoord

NEDERLANDSE SAMENVATTING EN TOEKOMSTPERSPECTIEVEN

Wanneer de chirurg tijdens het opereren wordt voorzien van betere en meer objectieve visuele informatie, kan dit de kwaliteit van de oncologische chirurgie verbeteren. Fluorescentie-geleide chirurgie kan hierbij een belangrijke rol spelen, doordat het tijdens operaties tumor weefsel, lymfklieren en vitale structuren kan identificeren.

Dit proefschrift bespreekt een aantal belangrijke indicaties binnen de oncologie chirurgie, waarbij klinisch beschikbare nabij-infrarode (NIR) fluorescente contrastmiddelen gebruikt kunnen worden om operaties te optimaliseren (Deel 1). Daarnaast wordt de klinische translatie besproken van nieuw ontwikkelde tumor-specifieke, fluorescente contrastmiddelen, die de intra-operatieve tumordetectie verbeteren (Deel 2).

Deel 1: **Toepassingen van klinisch beschikbare fluorescente contrastmiddelen in de oncologische chirurgie**

Hoofdstuk 2 beschrijft de detectie van de schildwachtklier tijdens maagkanker operaties. Het lymfedrainagepatroon bij maagkanker laat zich lastig voorspellen. Daarom wordt naast een totale of partiële gastrectomie vaak een uitgebreide lymfadenectomie uitgevoerd. In onze studie werd indocyanine groen (ICG) gekoppeld aan een nanocolloid. Hierdoor wordt de hydrodynamische diameter vergroot, en verbetert de opname in de schildwachtklier. ICG-Nanocoll werd vervolgens subserosaal geïnjecteerd rond de tumor, waarna beeldvorming van lymfvaten en –klieren plaatsvond. In 21 van de 22 patiënten werd op zijn minst één schildwachtklier gevonden. Daarbij viel het op dat in 8 van de 21 patiënten schildwachtklieren buiten het geplande resectievlak gevonden werden, waarvan er bij twee patiënten tumorcellen bevatten.

In **hoofdstuk 3** wordt de intra-operatieve beeldvorming van borstkanker met behulp van methyleen blauw (MB) beschreven. Alhoewel het exacte mechanisme van accumulatie van MB niet geheel duidelijk is, werd op basis van preklinisch onderzoek de hypothese gevormd dat het met behulp van MB mogelijk zou kunnen zijn om borstkanker te identificeren. Methyleen blauw heeft dezelfde fysisch-chemische eigenschappen als 99mTc-MIBI, een SPECT radiodiagnosticum dat met een sensitiviteit van 83 - 90% borstkanker kan identificeren in preoperatieve setting. In onze studie werd bij 20 van de 24 patiënten met succes de borstkanker laesie geïdentificeerd in het resectie preparaat. Daarbij werd bij 2 patiënten fluorescent borstkanker weefsel in het

wondbed gezien. En hoewel MB een veelbelovend middel is om borstkanker zichtbaar te maken, kan de introductie van nieuwe stoffen die specifiek aan een bepaalde tumorreceptor binden de intra-operatieve beeldvorming van borstkanker nog nauwkeuriger maken.

In **hoofdstuk 4** wordt de identificatie van levermetastasen van oogmelanoom tijdens laparoscopische leverchirurgie beschreven. Door ICG 24 uur voor operatie toe te dienen, vormt zich een fluorescente ring rondom een maligne laesie. Dit komt doordat ICG uitgescheiden wordt door gezonde levercellen, maar gevangen raakt in de overgangszone tussen gezonde lever en metastase. Zelfs afwijkingen die onzichtbaar waren voor het menselijk oog, en die niet gevonden werden met preoperatieve CT of intra-operatieve echografie konden worden geïdentificeerd. Op deze manier maakte fluorescente beeldvorming het mogelijk om op een minimaal-invasieve manier patiënten te identificeren, die potentieel baat hebben bij een resectie, en hielp het bij het verkrijgen van tumorvrije resectie marges.

Hoofdstuk 5 beschrijft de studie waarbij ICG werd gebruikt om hypofyse adenomen te identificeren tijdens transnasale transsfenoïdale selectieve adenomectomie. Gezonde hypofyse en hypofyse adenoom verschillen van elkaar in vascularisatie, wat mogelijk tot identificatie met ICG zou kunnen leiden. Bij 9 van de 10 patiënten met een microscopisch bewezen hypofyse adenoom werd een sterker fluorescent signaal gezien in de gezonde hypofyse dan in het adenoom. Bij twee patiënten kon de daadwerkelijke resectie van het adenoom onder fluorescentie-geleide plaatsvinden. Een van de beperkingen bij deze studie was dat de beschikbare endoscoop nog geen gelijktijdige weergave van kleur en fluorescentie beelden kon laten zien. Verdere optimalisatie van contrastmiddelen en camerasystemen kan de toegevoegde waarde van fluorescente beeldvorming tijdens hypofyse chirurgie nog verder verbeteren.

In **hoofdstuk 6** wordt een klinische casus gepresenteerd waarbij MB gebruikt werd om een paraganglioom, een zeldzame neuro-endocriene tumor, te detecteren. Tijdens operatie bleek het zelfs mogelijk een lokale metastase te identificeren, die niet zichtbaar was voor het menselijk oog.

Voortgaand op de vergelijkbare biodistributie van MB en 99mTc-MIBI, wordt in **hoofdstuk 7** de fluorescente beeldvorming tijdens bijschildklierchirurgie beschreven. Het bleek niet alleen mogelijk om bijschildklier adenomen te detecteren, maar ook normale schildklieren van slechts een millimeter groot werden gevonden. En hoewel recente ontwikkelingen met nieuwe

contrastmiddelen veelbelovend zijn, kan fluorescente beeldvorming met MB een belangrijke rol spelen tijdens bijschildklierchirurgie, totdat deze nieuwe stoffen daadwerkelijk klinisch gebruikt kunnen worden.

Hoofdstuk 8 beschrijft het enhanced permeability and retention (EPR) effect, en de mogelijkheden hiervan bij de detectie van ovarium carcinoom. Het EPR effect is gebaseerd op het principe dat macromoleculen, zoals eiwitgebonden ICG, zich ophopen in tumor weefsel. Dit komt omdat tumor weefsel zich vaak kenmerkt door een toegenomen vasculaire permeabiliteit en verminderde lymfdrainage. Meerdere maligne laesies werden succesvol geïdentificeerd in onze studie. Het probleem daarentegen was dat er ook 13 niet-maligne laesies fluorescent werden. Dit resulteerde in een fout-positieve ratio van 62%. Door dit gebrek aan specificiteit is fluorescente tumor beeldvorming gebaseerd op het EPR effect niet toepasbaar in de kliniek. Stoffen die specifiek tumorweefsel binden, bijvoorbeeld door een bepaalde tumor-receptor te binden, kunnen dit probleem oplossen.

Deel 2: Klinische translatie van innovatieve tumor-specifieke fluorescente contrastmiddelen

Hoofdstuk 9 beschrijft het gebruik van EC17, een folaat analoog gekoppeld aan fluoresceïne, voor de intra-operatieve detectie van folaat receptor alfa (FRα) positieve ovarium- en mammacarcinomen. EC17 werd 2 tot 3 uur voor operatie intraveneus toegediend, wat resulteerde in helder fluorescent ovariumcarcinoom weefsel tijdens operatie. Hierdoor konden 16% meer maligne laesies gereseceerd worden, en konden zelfs 70% meer laesies gedetecteerd worden op postoperatieve beeldanalyse. Bij mammacarcinoom is de over-expressie van de FRα lager dan bij ovariumcarcinoom. Daarom werd op preoperatief verkregen biopten eerst het expressie profiel van de FRα bepaald, alvorens patiënten definitief te includeren. Deze aanpak, waarbij de specifieke eigenschappen van de tumor van een individuele patiënt centraal staan, garandeert dat alleen patiënten geïncludeerd worden die potentieel baat hebben bij het gebruik van het tumor-specifieke contrastmiddel. Net als bij ovariumcarcinoom werd bij mammacarcinoom een duidelijk fluorescent signaal in de tumor gezien. Er werd echter ook autofluorescentie van gezond weefsel gezien op een golflengte van 500nm, wat resulteerde in fout-

positieve laesies. Daarnaast bemoeilijkte de autofluorescentie het maken van onderscheid tussen maligne weefsel en gezond weefsel. Dit probleem zou opgelost kunnen worden door fluorescente beeldvorming in het nabij-infrarode lichtspectrum te doen.

In **hoofdstuk 10** wordt daarom het gebruik van een nieuw ontwikkeld FRα specifiek contrastmiddel beschreven. OTL38 bestaat uit een folaat analoog, maar nu gekoppeld aan een NIR fluorescente stof (fluorescent op 800nm). Eerst werden verdraagbaarheid en farmacokinetiek in huid en bloed onderzocht in een gerandomiseerde, placebo-gecontroleerde studie in gezonde vrijwilligers, waarbij oplopende doseringen getest werden. Op basis van dit onderzoek werden 3 doseringen geselecteerd en vervolgens toegediend aan 12 patiënten met ovariumcarcinoom, die gepland stonden voor debulking chirurgie. Er werden duidelijke fluorescente FRα positieve ovariumcarcinomen en metastasen gezien. Dit resulteerde in de resectie van 29% meer maligne laesies, die niet met het blote oog gezien of gevoeld konden worden. Bij het gebruik van OTL38 werd nauwelijks achtergrondfluorescentie gezien.

ALGEMENE CONCLUSIE

Het gebruik van ICG en MB bij intra-operatieve fluorescente beeldvorming werd onderzocht voor een aantal belangrijke indicaties binnen de oncologische chirurgie. Beeldvorming met behulp van ICG resulteerde in accurate detectie van lever tumoren, en identificatie van schildwachtklieren bij maagkanker met hoge contrastratio's en langdurig fluorescent signaal. Op basis van onze gegevens zou fluorescente beeldvorming moeten worden toegepast in de kliniek voor deze indicaties om de kwaliteit van zorg voor kankerpatiënten te verbeteren. Met het gebruik van MB konden bijschildklier adenomen, neuro-endocrine tumoren en borstkanker laesies succesvol geïdentificeerd worden. De introductie van meer tumor-specifieke contrastmiddelen kan de nauwkeurigheid en beeldvorming waarschijnlijk verder verbeteren, maar tot die tijd kan MB gebruikt worden als ondersteuning bij bijvoorbeeld lastige casuïstiek.

Het gebruik van EC17 en OTL38 zorgde voor nauwkeurige en zeer specifieke intra-operatieve beeldvorming van ovariumcarcinoom. Daarbij werden hoge contrastratio's gezien, en bleef het fluorescente signaal langdurig aanwezig.

Het gebruik van deze contrastmiddelen van laagmoleculair gewicht zorgde voor snelle ophoping in tumorweefsel, terwijl het snel werd uitgescheiden uit de rest van het lichaam. Daarnaast werd bij beeldvorming in het nabij-infrarode spectrum nauwelijks achtergrond signaal of autofluorescentie gezien. Wanneer binnen nieuwe studies zowel gezonde personen als patiënten betrokken worden, kan op snelle en efficiënte manier onderzoek gedaan worden naar de optimale dosis, bereiding van het contrastmiddel en tijdsspanne van beeldvorming. Dit bespoedigt de introductie van nieuw ontwikkelde contrastmiddelen in klinische studies.

TOEKOMSTPERSPECTIEVEN

De afgelopen jaren zijn er meerdere indicaties vastgesteld waarbij klinisch beschikbare fluorescente contrastmiddelen gebruikt kunnen worden. ICG en MB hebben de potentie om de kwaliteit van oncologische operaties te verbeteren, doordat meer maligne laesies gevonden kunnen worden, de operatietijd verkort kan worden en iatrogeen letsel voorkomen zou kunnen worden door betere identificatie van vitale structuren. En hoewel het aantal indicaties beperkt is door de intrinsieke eigenschappen van deze reeds beschikbare contrastmiddelen, kan de techniek wel direct worden toegepast bij bijvoorbeeld leverchirurgie, schildwachtklierprocedures of lastige operaties aan de galwegen. Totdat nieuw ontwikkelde ligand-bindende, tumor-specifieke stoffen ontwikkeld zijn en gebruikt mogen worden in patiënten, kan tumor identificatie verbeterd worden bij bijvoorbeeld borstkanker-, bijschildklier- en paraganglioom chirurgie, zoals beschreven in dit proefschrift.

De introductie van ligand-bindende, tumor-specifieke contrastmiddelen heeft de deur geopend naar nog preciezere intra-operatieve tumor identificatie. Zolang de juiste tumor- of weefsel specifieke liganden maar gevonden worden, kan zo mogelijk elke structuur zichtbaar gemaakt worden die een chirurg wil zien tijdens een operatie. Zoals beschreven in onze EC17 en OTL38 studies, waarbij een folaat analoog gekoppeld werd aan een fluorofoor, bleek het mogelijk zeer specifieke tumor imaging te verzorgen, binnen 2 tot 3 uur na toediening. Bovendien bleef het fluorescente signaal en de contrastratio voor minstens 6 uur van zeer goede kwaliteit.

Contrast middelen

Wanneer men nauwkeurige tumor detectie wil verkrijgen, is het belangrijk om bindingscapaciteit, biodistributie en de farmacokinetiek van een contrastmiddel te optimaliseren. Daarom worden veel verschillende soorten stoffen onderzocht, zoals monoclonale antilichamen, antilichaam fragmenten zoals enkel-stengs antilichaam fragmenten en peptiden[1-5].

Al deze stoffen hebben hun eigen farmacokinetische profiel en half-waarde tijd, en daarmee verschillende optimale momenten voor beeldvorming. Rosenthal et al.[5] hebben het gebruik van cetuximab-IRDye800 bij hoofd-hals tumoren beschreven, waarbij de operatie 3 dagen na toediening van de stof moest plaatsvinden vanwege de lange half-waarde tijd van deze op een monoklonaal antilichaam gebaseerde stof (half-waarde tijd 24 – 32 uur, moleculair gewicht 150 kDa)[6]. Daarbij moesten relatief hoge doseringen gebruikt worden om een adequate contrastratio te krijgen (tot wel 25% van de therapeutische dosis; 62,5 mg/m^2).

Toediening van het folaat analoog OTL38 (half-waarde tijd 2 – 3 uur, moleculair gewicht 1.4 kDa) resulteerde in een sterk fluorescent signaal na slechts 2 tot 3 uur, wat aanhield voor minstens 6 uur (optimale dosis 0,0125 mg/kg). En vanwege de snelle klaring van de stof werd een laag achtergrond signaal gezien. Het lijkt dat deze eigenschappen ideaal zijn voor nauwkeurige tumor imaging. Toekomstige studies zullen moeten uitwijzen welk soort stof optimaal is, en mogelijk verschilt dit ook per chirurgische indicatie.

Idealiter zou men één stof ontwikkelen die bijna alle tumoren bindt. Het blijft echter een enorme uitdaging om een stof te ontwikkelen die zeer specifiek kankerweefsel bindt, en daarnaast uitgescheiden wordt uit de rest van het lichaam. Bovendien kunnen de expressie profielen van receptoren sterk wisselen. Bij ovarium carcinoom bijvoorbeeld, is meer dan 90% van alle tumoren FRα positief. Het voordeel hiervan is dat bijna alle patiënten baat hebben bij het gebruik van een FRα bindend contrastmiddel. Bij tumoren waarbij het expressie profiel meer divers is, moet een andere benadering worden gekozen. Zo kunnen preoperatief verkregen biopten gebruikt worden voor het bepalen van het expressie profiel, wat resulteert in een zeer precieze benadering per individuele patiënt. Dit werd bijvoorbeeld gedaan bij de borstkanker patiënten in onze EC17 studie. Daarnaast kunnen cocktails van verschillende contrastmiddelen gebruikt worden, of stoffen ontwikkeld worden die tegelijkertijd meerdere receptoren kunnen binden, doordat ze

multipele liganden hebben gekoppeld aan één fluorofoor. Dit zijn interessante ontwikkelingen, waarbij bedacht moet worden dat elke verandering aan een stof consequenties voor bindingscapaciteit en fluorescente eigenschappen heeft.

Een van de belangrijkste beperkingen van fluorescente beeldvorming heeft betrekking op de dieptepenetratie. In het zichtbare licht bedraagt deze enkele micrometers, en dit verbetert tot ongeveer een centimeter in het NIR lichtspectrum. Om deze beperking te overwinnen zijn er ontwikkelingen gaande waarbij fluorescente beeldvorming gecombineerd wordt met andere diagnostische modaliteiten, de zogenaamde multimodale beeldvorming (beeldvorming gecombineerd met bijvoorbeeld positron emission tomography (PET) of single-photon emission computed tomography (SPECT) stoffen)[7]. Door deze combinaties wordt het mogelijk om zowel preoperatieve chirurgische planning te verzorgen, als tijdens operaties naar dieper gelegen laesies te navigeren, terwijl daarbij real-time onderscheid gemaakt wordt tussen tumor en gezond weefsel. In de literatuur zijn inmiddels combinaties beschreven met foto-acoustische beeldvorming, magnetic resonance imaging, PET, SPECT en zelf tri-modale beeldvorming[8]. De meeste van deze stoffen bevinden zich momenteel echter nog in preklinische fase van ontwikkeling.

Camerasystemen

Succesvolle fluorescente beeldvorming is afhankelijk van de combinatie van zowel contrastmiddel als camerasysteem. Daarom is de ontwikkeling van camerasystemen essentieel voor de algemene acceptatie en introductie van fluorescentie-geleide chirurgie. De afgelopen jaren zijn door meerdere bedrijven en instituten camerasystemen ontwikkeld, allemaal met hun eigen voor- en nadelen[9]. Vooral in de endoscopische beeldvorming is nog veel te verbeteren, zoals aangegeven in hoofdstuk 4 en 5 van dit proefschrift. Bovendien kan het ontwikkelen van een meer gestandaardiseerde manier om camera's te vergelijken bijdragen aan het maken van nieuwe, verbeterde camerasystemen[10].

Klinische implementatie

Om de klinische implementatie van fluorescentie-geleide chirurgie te stroomlijnen is samenwerking essentieel. Daarom worden internationale verenigingen opgericht, zoals de International Society of Image Guided

Surgery, om wet- en regelgeving omtrent klinisch onderzoek en studieontwerp te bespreken en optimaliseren[11;12]. Zo moeten eindpunten in fase 1 studies bijvoorbeeld niet alleen focussen op veiligheid, maar ook op kwaliteit en eigenschappen van de beeldvorming.

Er is daarnaast een veelbelovende rol weggelegd voor de ontwikkeling van farmacokinetische en farmacodynamische modellen[13-15]. Deze modellen kunnen ons meer inzicht geven in alle verschillende variabelen die een rol spelen bij optimale tumor beeldvorming. Door informatie over grootte, halfwaardetijd en klaring van een stof, receptor dichtheid, tumorgrootte, bindingsconstante en eiwitbinding te combineren in een model, eventueel aangevuld met beeldvorming-specifieke eigenschappen als quantum yield en golflengte, kunnen mogelijk voorspellingen gedaan worden over de veiligheid en mogelijkheid tot tumor beeldvorming van een nieuw ontwikkelde stof. Ook zou eventueel een optimale dosis voorspeld kunnen worden. Hierdoor kunnen mogelijk fase 1 studies gedaan worden, waarbij minder gezonde vrijwilligers en patiënten nodig zijn. Ook zouden er misschien voorspellingen gedaan kunnen worden over welk camerasysteem het meest geschikt is voor een specifieke indicatie met een specifiek contrastmiddel. Op deze manier worden fase 1 studies veel efficiënter, en wordt de drempel om veelbelovende stoffen naar de kliniek te brengen lager.

Nieuwe klinische indicaties

De behandeling van kanker vraagt om een multidisciplinaire aanpak waarbij chirurgie, systemische chemotherapie of immunotherapie en radiotherapie allemaal een belangrijke rol spelen[16;17]. Constant verbeterende neoadjuvante chemo- en radiotherapie hebben ertoe geleid dat er een toenemend aantal complete pathologische responses wordt gezien, in bijvoorbeeld rectum en slokdarm kanker[18-20]. Bij deze patiënten is geen vitaal tumor weefsel meer aanwezig, en zij hebben dus ook geen baat meer bij chirurgische resectie, terwijl deze procedures wel geassocieerd zijn met morbiditeit en mortaliteit. Wanneer een resectie bij de juiste patiënten achterwege kan blijven, heeft dit grote impact op de kwaliteit van leven van deze mensen.

Dit heeft geleid tot een cultuurverandering binnen de behandeling van kanker, waarbij ernaar gestreefd wordt om chirurgie achterwege te laten bij patiënten met een complete klinische respons, en zo orgaan-sparende behandeling mogelijk te maken. Hiervoor is het echter wel essentieel om

patiënten adequaat te selecteren, die een complete klinische respons hebben, en om ze te vervolgen. Meerdere studies beschrijven deze "Watch and Wait" policy bij rectum kanker[21], en recent werd een internationale database opgericht om de resultaten van dit beleid te monitoren[22]. Moleculaire beeldvorming kan een grote rol spelen bij het selecteren en monitoren van patiënten, omdat het nog preciezere en objectievere informatie kan geven over de aanwezigheid van vitaal tumorweefsel in bijvoorbeeld littekenweefsel na chemoradiatie.

CONCLUSIES

Met behulp van fluorescentie-geleide chirurgie kan tumorweefsel zichtbaar gemaakt worden, en kunnen meer maligne laesies gevonden worden, die anders onzichtbaar waren gebleven. Daarnaast ondersteunt de techniek de identificatie van lymfeklieren en vitale structuren. Nu moeten aanvullende studies, bij voorkeur gerandomiseerde onderzoeken, uitwijzen of deze verbeterde tumordetectie ook daadwerkelijk leidt tot verbeterde overleving en verminderde morbiditeit. Fluorescentie-geleide chirurgie wint snel aan populariteit, en hopelijk leidt een gezamenlijke aanpak tot verdere klinische implementatie en het verwerven van een standaard plek binnen de behandeling van kanker op korte termijn.

REFERENTIES

1. Kelderhouse LE, Chelvam V, Wayua C et al. Development of tumor-targeted near infrared probes for fluorescence guided surgery. *Bioconjug Chem* 2013;24:1075-1080.

2. Altintas I, Kok RJ, Schiffelers RM. Targeting epidermal growth factor receptor in tumors: from conventional monoclonal antibodies via heavy chain-only antibodies to nanobodies. *Eur J Pharm Sci* 2012;45:399-407.

3. Choi HS, Gibbs SL, Lee JH et al. Targeted zwitterionic near-infrared fluorophores for improved optical imaging. *Nat Biotechnol* 2013;31:148-153.

4. Oliveira S, Heukers R, Sornkom J, Kok RJ, van Bergen En Henegouwen PM. Targeting tumors with nanobodies for cancer imaging and therapy. *J Control Release* 2013;172:607-617.

5. Rosenthal EL, Warram JM, de BE et al. Safety and Tumor Specificity of Cetuximab-IRDye800 for Surgical Navigation in Head and Neck Cancer. *Clin Cancer Res* 2015;21:3658-3666.

6. Zinn KR, Korb M, Samuel S et al. IND-directed safety and biodistribution study of intravenously injected cetuximab-IRDye800 in cynomolgus macaques. *Mol Imaging Biol* 2015;17:49-57.

7. Chi C, Du Y, Ye J et al. Intraoperative imaging-guided cancer surgery: from current fluorescence molecular imaging methods to future multi-modality imaging technology. *Theranostics* 2014;4:1072-1084.

8. Bai J, Wang JT, Rubio N et al. Triple-Modal Imaging of Magnetically-Targeted Nanocapsules in Solid Tumours In Vivo. *Theranostics* 2016;6:342-356.

9. Zhu B, Sevick-Muraca EM. A review of performance of near-infrared fluorescence imaging devices used in clinical studies. *Br J Radiol* 2015;88:20140547.

10. Pleijhuis R, Timmermans A, De JJ, de BE, Ntziachristos V, Van DG. Tissue-simulating phantoms for assessing potential near-infrared fluorescence imaging applications in breast cancer surgery. *J Vis Exp* 2014;51776.

11. Rosenthal EL, Warram JM, de BE et al. Successful Translation of Fluorescence Navigation During Oncologic Surgery: A Consensus Report. *J Nucl Med* 2016;57:144-150.

12. Snoeks TJ, van Driel PB, Keereweer S et al. Towards a successful clinical implementation of fluorescence-guided surgery. *Mol Imaging Biol* 2014;16:147-151.

13. Cohen A. Pharmacokinetic and pharmacodynamic data to be derived from early-phase drug development: designing informative human pharmacology studies. *Clin Pharmacokinet* 2008;47:373-381.

14. Danhof M, Alvan G, Dahl SG, Kuhlmann J, Paintaud G. Mechanism-based pharmacokinetic-pharmacodynamic modeling-a new classification of biomarkers. *Pharm Res* 2005;22:1432-1437.

15. Wittrup KD, Thurber GM, Schmidt MM, Rhoden JJ. Practical theoretic guidance for the design of tumor-targeting agents. *Methods Enzymol* 2012;503:255-268.

16. Kapiteijn E, Marijnen CA, Nagtegaal ID et al. Preoperative radiotherapy combined with total mesorectal excision for resectable rectal cancer. *N Engl J Med* 2001;345:638-646.

17. Mieog JS, van der Hage JA, van de Velde CJ. Preoperative chemotherapy for women with operable breast cancer. *Cochrane Database Syst Rev* 2007;CD005002.

18. Glynne-Jones R, Wallace M, Livingstone JI, Meyrick-Thomas J. Complete clinical response after preoperative chemoradiation in rectal cancer: is a "wait and see" policy justified? *Dis Colon Rectum* 2008;51:10-19.

19. Jin HL, Zhu H, Ling TS, Zhang HJ, Shi RH. Neoadjuvant chemoradiotherapy for resectable esophageal carcinoma: a meta-analysis. *World J Gastroenterol* 2009;15:5983-5991.

20. O'Neill BD, Brown G, Heald RJ, Cunningham D, Tait DM. Non-operative treatment after neoadjuvant chemoradiotherapy for rectal cancer. *Lancet Oncol* 2007;8:625-633.

21. Pozo ME, Fang SH. Watch and wait approach to rectal cancer: A review. *World J Gastrointest Surg* 2015;7:306-312.

22. Beets GL, Figueiredo NL, Habr-Gama A, van de Velde CJ. A new paradigm for rectal cancer: Organ preservation: Introducing the International Watch & Wait Database (IWWD). *Eur J Surg Oncol* 2015;41:1562-1564.

LIST OF PUBLICATIONS

1. Van Driel PB, Boonstra MC, Prevoo HA, van de Giessen M, Snoeks TJ, **Tummers QR**, Keereweer S, Cordfunke RA, Fish A, van Eendenburg JD, Lelieveldt BP, Dijkstra J, van de Velde CJ, Kuppen PJ, Vahrmeijer AL, Löwik CW, Sier CF. EpCAM as multi-tumour target for near-infrared fluorescence guided surgery. *BMC Cancer* 2016; 16(1):884

2. Hoogstins CE, **Tummers QR**, Gaarenstroom KN, de Kroon CD, Trimbos JB, Bosse T, Smit VT, Vuyk J, van de Velde CJ, Cohen AF, Low PS, Burggraaf J, Vahrmeijer AL. A Novel Tumor-Specific Agent for Intraoperative Near-Infrared Fluorescence Imaging: A Translational Study in Healthy Volunteers and Patients with Ovarian Cancer. *Clin Cancer Res* 2016;22(12):2929-38.

3. **Tummers QR**, Hoogstins CE, Gaarenstroom KN, de Kroon CD, van Poelgeest MI, Vuyk J, Bosse T, Smit VT, van de Velde CJ, Cohen AF, Low PS, Burggraaf J, Vahrmeijer AL. Intraoperative imaging of folate receptor alpha positive ovarian and breast cancer using the tumor specific agent EC17. *Oncotarget* 2016;7(22):32144-55.

4. Verstegen MJ, **Tummers QR**, Schutte PJ, Pereira AM, van Furth WR, van de Velde CJ, Malessy MJ, Vahrmeijer AL. Intraoperative Identification of Normal Pituitary Gland and Adenoma using Near-Infrared Fluorescence Imaging and Low-dose Indocyanine Green. *Operative Neurosurgery* 2016;12(3):260-268.

5. **Tummers QR**, Boogerd, LS, De Steur WO, Verbeek FP, Boonstra MC, Handgraaf HJ, Frangioni JV, van de Velde CJ, Hartgrink HH, Vahrmeijer AL. Near-infrared fluorescence sentinel lymph node detection in gastric cancer: A pilot study. *World J Gastroenterol* 2016;22(13):3644-51.

6. **Tummers QR**, Hoogstins CE, Peters AA, de Kroon CD, Trimbos JB, van de Velde CJ, Frangioni JV, Vahrmeijer AL, Gaarenstroom KN. The value of intraoperative near-infrared fluorescence imaging based on enhanced permeability and retention of indocyanine green: feasibility and false-positives in ovarian cancer. *PlosONE* 2015;10(6)

7.   **Tummers QR**, Schepers A., Hamming JF, Kievit J, Frangioni JV, van de Velde CJ, Vahrmeijer AL. Intraoperative Guidance in Parathyroid Surgery using Near-Infrared Fluorescence Imaging and Low-Dose Methylene Blue. *Surgery* 2015;158(5):1323-30.

8.   **Tummers QR**, Boonstra MC, Frangioni JV, van de Velde CJ, Vahrmeijer AL, Bonsing BA. Intraoperative Near-Infrared Fluorescence Imaging of a Paraganglioma using Methylene Blue: a case report. *Int J Surg Case Rep* 2015;6C:150-3.

9.   Handgraaf HJ, Boogerd LS, Verbeek FP, **Tummers QR**, Hardwick JC, Baeten CI, Frangioni JV, van de Velde CJ, Vahrmeijer AL. Intraoperative fluorescence imaging to localize tumors and sentinel lymph nodes in rectal cancer. *Minim Invasive Ther Allied Technol* 2016;25(1):48-53.

10. Verbeek FP, **Tummers QR**, Rietbergen DD, Peters AA, Schaafsma BE, Van de Velde CJ, Frangioni JV, Van Leeuwen FW, Gaarenstroom KN, Vahrmeijer KN. Sentinel lymph node biopsy in vulvar cancer using combined radioactive and fluorescence guidance. *Int J Gyn Cancer* 2015;25(6):1086-93.

11. Boonstra MC, Van Driel PB, Van Willigen DM, Stammes MA, Prevoo HA, **Tummers QR**, Mazar A, Beekman F, Kuppen PJ, Van de Velde CJ, Lowik CW, Frangioni JV, Van Leeuwen FW, Sier CF, Vahrmeijer AL. uPAR-targeted multimodal tracer for pre- and intraoperative imaging in cancer surgery. *Oncotarget* 2015;6(16):14260-73.

12. Handgraaf HJ, Verbeek FP, **Tummers QR**, Boogerd LS, van de Velde CJ, Vahrmeijer AL, Gaarenstroom KN. Real-time near-infrared fluorescence guided surgery in gynecologic oncology: A review of the current state of the art. *Gynecol Oncol* 2014;135(3):606-13.

13. Schaafsma BE, Verbeek FP, Elzevier HW, **Tummers QR**, van der Vorst JR, Frangioni JV, van de Velde CJ, Pelger RC, Vahrmeijer AL. Optimization of sentinel lymph node mapping in bladder cancer using near-infrared fluorescence imaging. *J Surg Oncol* 2014; 110(7):845-50.

14. **Tummers QR**, Verbeek FP, Prevoo HA, Braat AE, Baeten CI, Frangioni JV, van de Velde CJ, Vahrmeijer AL. First Experience on Laparoscopic Near-Infrared Fluorescence Imaging of Hepatic Uveal Melanoma Metastases Using Indocyanine Green. *Surg Innov* 2015;22(1):20-5.

15. **Tummers QR**, Verbeek FP, Schaafsma BE, Boonstra MC, van der Vorst JR, Liefers GJ, van de Velde CJ, Frangioni JV, Vahrmeijer AL. Real-time intraoperative detection of breast cancer using near-infrared fluorescence imaging and Methylene Blue. *Eur J Surg Oncol* 2014;40(7):850-8.

16. Verbeek FP, van der Vorst JR, **Tummers QR**, Boonstra MC, de Rooij KE, Löwik CW, Valentijn AR, van de Velde CJ, Choi HS, Frangioni JV, Vahrmeijer AL. Near-Infrared Fluorescence Imaging of Both Colorectal Cancer and Ureters Using a Low-Dose Integrin Targeted Probe. *Ann Surg Oncol* 2014;21 Suppl 4:S528-37.

17. Verbeek FP, Schaafsma BE, **Tummers QR**, vd Vorst JR, vd Made WJ, Baeten CI, Bonsing BA, Frangioni JV, van de Velde CJ, Vahrmeijer AL, Swijnenberg RJ. Optimization of near-infrared fluorescence cholangiography for open and laparoscopic surgery. *Surg End* 2014;28(4):1076-82.

18. vd Vorst JR, Schaafsma BE, Verbeek FPR, Swijnenberg RJ, **Tummers QR**, Hutteman M, Hamming JF, Kievit J, Frangioni JV, van de Velde CJ, Vahrmeijer AL. Intraoperative near-fluorescence imaging of parathyroid adenomas using low-dose methylene blue. *Head Neck* 2014;36(6):853-8.

19 de Kruijf EM, van Nes JG, Sajet A, **Tummers QR**, Putter H, Osanto S, Speetjens FM, Smit VT, Liefers GJ, van de Velde CJ, Kuppen PJ. The predictive value of HLA class I tumor cell expression and presence of intratumoral Tregs for chemotherapy in patients with early breast cancer. *Clin Cancer Res* 2010;16(4):1272-80.

20. Ray A, Huisman MV, Tamsma JT; Research and Writing-group, van Asten J, Bingen BO, Broeders EA, Hoogeveen ES, van Hout F, Kwee VA, Laman B, Malgo F, Mohammadi M, Nijenhuis M, Rijkée M, van Tellingen MM, Tromp M, **Tummers QR**, de Vries L. The role of inflammation on atherosclerosis, intermediate and clinical cardiovascular endpoints in type 2 diabetes mellitus. *Eur J Intern Med* 2009;20(3):253-60.

CURRICULUM VITAE

Quirijn Tummers werd op 30 april 1986 geboren te Leiden. In 2004 behaalde hij cum laude zijn eindexamen aan het Gymnasium van het Bonhoeffer College te Enschede, waarna hij Geneeskunde ging studeren aan de Universiteit Leiden. Gedurende zijn studie was hij onder andere werkzaam als allocatie medewerker bij Eurotransplant International Foundation. Daarnaast was hij actief lid van de Leidse Studenten Vereniging 'Minerva'.

Voorafgaand aan zijn co-schappen deed hij een klinische stage in het Mangochi District Hospital in Malawi. Tijdens zijn wetenschapsstage naar de rol van lymfocyten infiltraat bij borstkanker onder leiding van prof. dr. C.J.H. van de Velde en dr. P.J.K Kuppen, kwam hij voor het eerst in contact met het 'Greenlight' onderzoek in het LUMC. Op 30 maart 2012 behaalde Quirijn cum laude zijn artsexamen. Daarna begon hij als arts-onderzoeker in de Image-Guided Surgery onderzoeksgroep onder leiding van dr. A.L. Vahrmeijer en prof. dr. C.J.H. van de Velde, waarvan de resultaten beschreven zijn in dit proefschrift. Tijdens deze periode kreeg hij onder andere een Fellowship Grant van de European Society of Surgical Oncology voor de ECCO-AACR-EORTC-ESMO workshop 'Methods in Clinical Cancer Research' in Flims, Zwitserland. Daarnaast won hij de Best Poster Award tijdens het World Molecular Imaging Congress 2013 in Savannah, USA.

In 2015 startte hij als ANIOS Heelkunde in het Medisch Centrum Haaglanden-Bronovo te Den Haag. Daarnaast was hij dat jaar als voorzitter betrokken bij de organisatie van het Symposium Experimenteel Onderzoek voor Heelkundige Specialismen te Leiden. Op 1-1-2016 begon hij met de opleiding Heelkunde in het Haaglanden Medisch Centrum te Den Haag (opleiders dr. H.J. Smeets en dr. S.A.G. Meylaerts).

Momenteel woont Quirijn samen met zijn vriendin Maxime Slooter in Amsterdam.

DANKWOORD

Om te beginnen wil ik alle patiënten en gezonde vrijwilligers die deelgenomen hebben aan de verschillende studies hartelijk bedanken. Zonder deelname was dit proefschrift er niet geweest. Voor alle patiënten in het bijzonder gold dat zij niet wisten of onze onderzoekstechnieken zouden bijdragen aan hun eigen behandeling. Ik heb diep respect voor de bereidheid om in deze vaak zeer moeilijke levensfase deel te nemen aan wetenschappelijk onderzoek.

Promoveren is teamsport, maar er zijn een aantal mensen die ik in het bijzonder heel hartelijk wil bedanken voor de totstandkoming van dit proefschrift.

Prof. Van de Velde, beste Professor; ik beschouw het als een zeer grote eer dat ik onder uw leiding mijn promotieonderzoek heb mogen doen. Ik heb veel bewondering voor uw staat van dienst, heb genoten van al uw bijzondere anekdotes, en vond het mooi om te zien dat u ondanks al uw prestaties uit het verleden, altijd uw blik op de toekomst hield.
Beste Xandra, heel veel dank voor jouw hulp bij het uitspelen van Converis, en eigenlijk bij alles wat geregeld moest worden rond mijn promotie.

Dr. Vahrmeijer, allerbeste Lex; als pater familias gaf jij op onnavolgbare wijze leiding aan onze onderzoeksgroep. Altijd op de hoogte van wat er speelde, en vooral heel goed op de hoogte van wat er nog meer uitgezocht kon worden. Jouw vermogen om 100 balletjes tegelijk hoog te houden is zeer bewonderenswaardig. Dank voor het vertrouwen, voor de begeleiding, en voor alles wat je teruggaf als beloning voor onze inspanningen.

Prof. Burggraaf, beste Koos; met de samenwerking tussen de Heelkunde van het LUMC en het CHDR is het niveau van onze onderzoeken nog verder gestegen. Ik wil je bedanken voor deze fantastische samenwerking en de begeleiding.
Prof. Cohen, beste Adam; ook jou wil ik bedanken voor alle mogelijkheden die mij geboden zijn door samen met het CHDR onderzoek te doen.

Professor Frangioni, dear John; thank you for your introduction and guidance in the NIR fluorescence imaging research world. Your motivating, sharp, positive and visionary view on science has been a great inspiration to me.

Dear Marty, thanks for choosing our research group for the cooperation with On Target. Your ability to look beyond On Targets interests, and allowing us to perform extensive research, next to bringing OTL38 to the clinic, was absolutely amazing.

Green Team, dank voor de fantastische promotietijd! De groep is inmiddels te groot om iedereen persoonlijk te bedanken, maar ik heb genoten, veel van jullie geleerd, en ik heb veel vertrouwen in de toekomst van onze groep. Mark, ik wil jou in het bijzonder bedanken voor de fantastische tijd die we samen hebben meegemaakt. En Charlotte, voor de schitterende samenwerking die we tot stand hebben gebracht tussen LUMC en CHDR.

Matthijs en Joost, mijn paranimfen, dank voor jullie hulp en steun in de eindfase van mijn promotie. Ik vind het mooi dat wij in 2004 samen begonnen aan onze studie, en nu als goede vrienden dit mogen meemaken.

Tom, Bram, Wouter en Erik, ik voel me vereerd dat ik al mijn hele leven met jullie bevriend ben. We hebben het er vaak over gehad, maar mooi dat jullie nu eindelijk in het echt een Leidse promotie meemaken!

Tom, Kaa, Ruud en Luc, naast Matthijs en Joost als harde kern van Kanon Select wil ik jullie bedanken voor al jullie steun, het informeren naar en meeleven met mijn promotietraject. Mooi dat we dit feest met zijn allen kunnen vieren.

Lieve mam en pap, dank voor jullie onvoorwaardelijke steun en trots bij mijn promotietraject (en alles daarbuiten). Jullie hebben de basis gelegd voor alles wat ik bereikt heb, zonder jullie was dit nooit gelukt.
Lieve Johanneke, Willemieke en Fokkedien, dank voor al jullie steun en medeleven. Ik ben trots op jullie.

Lieve Maxime, jij bent zonder twijfel de allermooiste beloning voor mijn promotie. Dank voor alle liefde, steun, betrokkenheid en levensvreugde die ik van je krijg. Ik hoop dat we samen nog heel veel moois gaan meemaken, en kijk uit naar onze toekomst!